Raman Imaging to Assess the Risk of Disease Using a Targeted Nanoparticle-DNA Reporter System

Kirsty Callan

June 2020

A thesis submitted to the Department of Pure and Applied Chemistry, University of Strathclyde, in part fulfilment of the requirements for the degree of Doctor of Philosophy

This thesis is the result of the author's original research. It has been composed by the author and has not been previously submitted for examination which has led to the award of a degree.

The copyright of this thesis belongs to the author under the terms of the United Kingdom Copyright Acts as qualified by University of Strathclyde Regulation 3.50. Due acknowledgement must always be made of the use of any material contained in, or derived from, this thesis.

Signed: ⟶
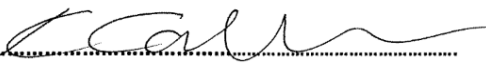
Date: 26th June 2020

Abstract

The aim of this work was to develop a novel method for detecting mRNA in cells using gold nanoparticles and surface enhanced Raman spectroscopy (SERS), with the ultimate goal of early detection of cardiovascular disease. Three different methods to detect mRNA in cells using Raman spectroscopy were investigated.

The first approach used a method analogous to fluorescence *in situ* hybridisation (FISH), named Raman *in situ* hybridisation. An oligonucleotide complementary to the mRNA target was attached to gold nanoparticles and labelled with a Raman reporter. When incubated with cells it was hoped that the probe would hybridise to the target mRNA and allow visualisation using Raman mapping. Despite utilisation of various probe designs, no significant discrimination could be seen between the target oligonucleotide and a random control oligonucleotide.

The second approach made use of a molecular beacon. Gold nanoparticles were functionalised with a dye and a dye-labelled hairpin loop oligonucleotide. In the closed position SERS signal was obtained from both dyes due to close proximity with the nanoparticles. In the presence of the target oligonucleotide, a change in the spectra was observed due to an increase in distance between the oligonucleotide dye and the nanoparticle. This allowed ratiometric detection of the target.

For the final approach nanoparticles were coated with a Raman active dye and an oligonucleotide. Two batches of nanoparticles were prepared, each with oligonucleotides complementary to half of the target sequence. When combined with the target sequence, the oligonucleotides should both hybridise, bringing the nanoparticles closer together and enhancing the Raman signal. These probes could be detected in cells, however it was not possible to determine whether or not they were hybridised to the target mRNA meaning further work is required.

Overall, each method had its own limitations and further development would be required to create a feasible assay.

Acknowledgements

Firstly, I would like to thank my supervisors; Professor Duncan Graham, Professor John Mullins and Professor Karen Faulds for their guidance and support throughout my PhD. I would also like to thank OPTIMA, and everyone involved, for this opportunity.

Thanks to everyone in the group for generally making the whole experience more enjoyable and helping with any issues I had (there were a lot). A special thanks to Corrina Wetherill for helping me with all things cells, and Sian Sloan-Dennison, Stacey Laing and William Tipping for their help with my thesis.

My experience would have been a lot less enjoyable if it wasn't for Iceland; aka Anastasia Kapara, Amy Morrison and Daniel McDonald. From listening to me rant about *another* failed experiment, general chat or helping me with science – it wouldn't have been the same without you. Anastasia – I definitely wouldn't have made it through this whole thing if it wasn't for you, so thanks for that.

I would also like to thank my fellow OPTIMA-ers; Rachael Cameron, Gillian Craig and Hazel Stewart, for helping keep me sane – usually in the form of pizza and cookie dough.

Thanks to my family for continuing to support me – despite having absolutely no idea what I do. Finally, and most importantly, thanks to my Isabella for keeping me company during looong thesis writing days.

Abbreviations

AgNP	Silver nanoparticle
AuNP	Gold nanoparticle
DLS	Dynamic light scattering
DNA	Deoxyribonucleic acid
ds	Double-stranded
EdU	5-ethynyl-2'-deoxyuridine
FBS	Fetal bovine serum
FISH	Fluorescence *in situ* hybridisation
LSPR	Localised surface plasmon resonance
MBA	4-mercaptobenzoic acid
MGITC	Malachite green isothiocyanate
MTT	3-(4,5-dimethylthiazol-2-yl)-2,5-diphenyl tetrazolium bromide
PB	Phosphate buffer
PBS	Phosphate buffered saline
RISH	Raman *in situ* hybridisation
RNA	Ribonucleic acid
RR	Resonance Raman
SERRS	Surface enhanced resonance Raman spectroscopy
SERS	Surface enhance Raman spectroscopy
SRS	Stimulated Raman spectroscopy
ss	Single-stranded
T_m	Melting temperature
UV	Ultraviolet

Table of Contents

1. Introduction

1.1 Cardiovascular Disease

Cardiovascular disease (CVD) is a circulatory disease which covers multiple diseases, including coronary artery disease, stroke, peripheral artery disease and aortic disease. It manifests itself as a blockage of the heart or arteries known as atheroma. Atheroma is a build-up of fatty material, the presence of which causes the blood vessel to decrease in diameter or become completely blocked, preventing blood flow. The main risk factors for CVD are high cholesterol and hypertension. Other risk factors include obesity, diet, lack of exercise, alcohol, smoking, diabetes, stress, increased age, sex (men are at higher risk), ethnicity (African Caribbean and South Asian ethnicities have a higher risk) and family history. Instances of CVD also tend to be higher in areas of social deprivation. Many risk factors associated with CVD are lifestyle related, meaning that they are avoidable. However, despite this, CVD is a major problem in the United Kingdom with over 167,000 deaths per year. [1,2]

Glucocorticoids, such as cortisol, are steroid hormones responsible for a variety of biological processes. The enzyme 11β-hydroxysteroid dehydrogenase type 2 (HSD2) is responsible for converting glucocorticoids (cortisol in humans) to the inert keto form (cortisone), thus preventing them from activating the mineralocorticoid receptor (MR) as shown in Figure 1.1.
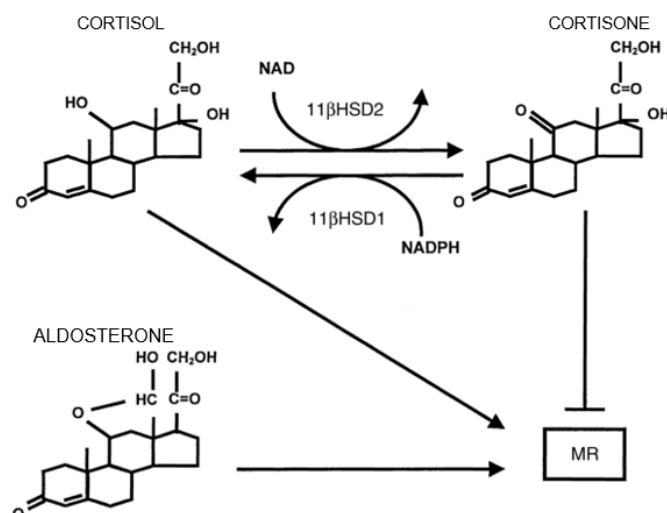
Figure 1.1 - Mineralocorticoid receptor activation. Reproduced with permission from [3].
Copyright © 2000 International Society of Nephrology.

The mineralocorticoid aldosterone plays a key role in sodium transport via the MR. Glucocorticoids and mineralocortcoids have similar affinity for the MR, which can result in overstimulation of the receptor since glucocorticoids are present at much higher levels. This problem is avoided *in vivo* by the presence of HSD2 which deactivates glucocorticoids. However, mutations can cause a lack, or inactivity, of HSD2, whilst glyceyrrhetinic acid (a constituent of liquorice) can inhibit it. [4]

HSD2 is found in sodium-transporting epithelial cells, including the kidney, colon and placenta. The enzyme has two isoforms, HSD type 1 is responsible for the reverse reaction to type 2, i.e. the conversion of cortisone to cortisol (Figure 1.1). A lack of HSD2 results in over activation of the MR by glucocorticoids and a condition known as the syndrome of apparent mineralocorticoid excess (SAME). Patients with SAME exhibit sodium retention, hypertension and hypokalaemia (potassium deficiency). This condition can be partially treated by supressing cortisol but is usually fatal in childhood. [3] [5]

The condition can be diagnosed by assessing the cortisol to cortisone ratio in urine since absence or deficiency of HSD2 increases the ratio. However, there is currently no clinical diagnostic assay for the measurement of HSD2.[5]

Craigie *et al* investigated the effect of low/standard/high-salt diets on wild type and HSD+/- mice. Wild type mice showed a proportional relationship between the amount of sodium ingested and the fractional sodium excreted and no relationship with blood pressure. In heterozygous mice the relationship between salt ingestion and excretion was reduced leading to salt sensitivity and hypertension. [6] From this it can be assumed that humans with HSD2 deficiency, who do not necessarily have SAME, will have an increased sensitivity to salt and tendency to hypertension, increasing their risk of cardiovascular disease (CVD).

1.2 DNA

1.2.1 Introduction to DNA

Dexoyribonucleic acid (DNA) was first discovered in 1869 by Fredrich Miescher. [7] Miescher was trying to characterise proteins found in white blood cells from surgical bandages when he found a substance made up of carbon, hydrogen, oxygen, nitrogen and phosphorus that was not protein. [7]

Found in the nucleus of all cells – except red blood cells – we now know that this substance is responsible for life as we know it. DNA contains the information required for all living things to function on a cellular level, making it the key building block of life.

1.2.2 DNA Structure

The three-dimensional structure of DNA as we know it today was first proposed almost a century after Miescher's discovery in 1953 by Watson and Crick. [8] Following on from x-ray crystallography experiments led by Franklin and Wilkins [9,10], Watson and Crick realised that DNA has a double helix structure with hydrogen bonds holding together two, separate strands (Figure 1.2). [8]
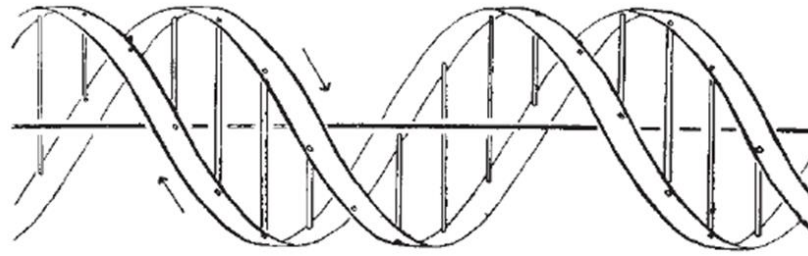
Figure 1.2 - DNA structure as proposed by Watson and Crick. Reproduced from [8].
Copyright © 1953, Springer Nature.

Each strand is a polymer of nucleotides – individual units made up of a sugar, a phosphate and a nitrogenous base (Figure 1.3) – joined together by phosphodiester linkages. The strands run anti-parallel; one strand runs in the 5' to 3' direction, whilst the other runs from 3' to 5' (based on the numbering of the carbon atoms in the sugar).
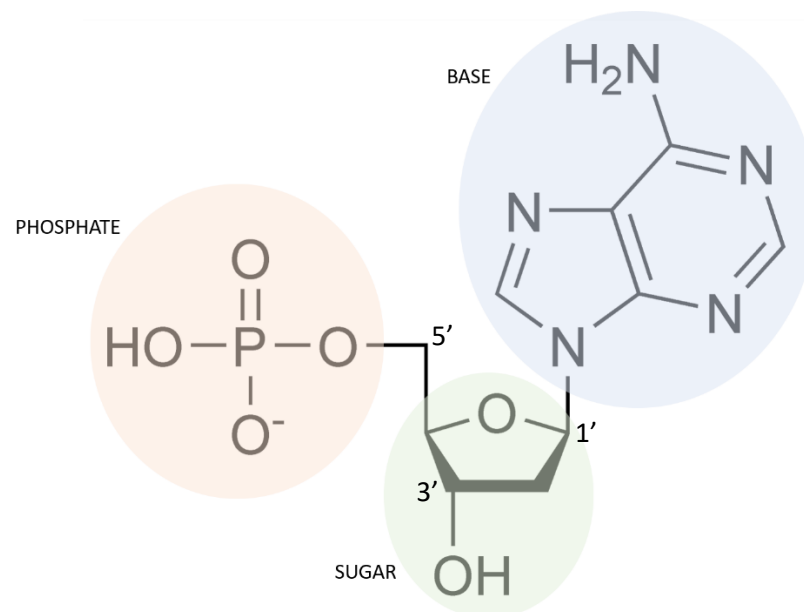
Figure 1.3 - Nucleotide schematic showing a nitrogenous base (adenine shown), pentose sugar and phosphate group. The phosphate group of one nucleotide joins to the 3' carbon of the sugar on the adjacent nucleotide to form an oligonucleotide strand.

In DNA, the sugar is 2'-deoxy-β-D-ribose and this, along with the phosphate group, remains constant throughout the chain forming a sugar-phosphate backbone. At

physiological pH, DNA is negatively charged due to ionisation of the phosphate groups.

There are four possible bases: adenine, guanine, thymine and cytosine (Figure 1.4). It is the order of these bases in the chain which makes up the genetic code. The bases fall into two groups: purines (joined 5- and 6-membered heterocyclic rings; adenine and guanine) and pyrimidines (6-membered heterocyclic rings; cytosine and thymine).
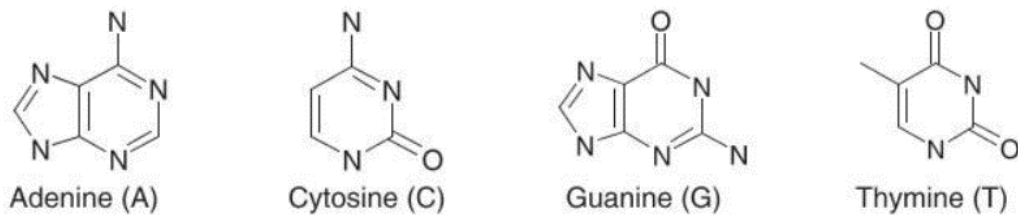
Figure 1.4 - Structure of the four bases present in DNA. Reproduced from [11]. *Copyright © 2010, John Wiley and Sons.*

Hydrogen bonds between the bases hold the two chains together in the double helix structure (Figure 1.5). Purines always bond to pyrimidines in the complementary chain. Chargaff discovered that any given DNA molecule has the same number of adenines and thymines, and the same number of cytosines and guanines. This led to the discovery of Chargaff's rule – that adenine in one chain always binds to thymine in the complementary chain and the same goes for guanine and cytosine. Guanine-cytosine interactions have three hydrogen bonds between them, making them stronger than adenine-thymine interactions, which only have two. [12]
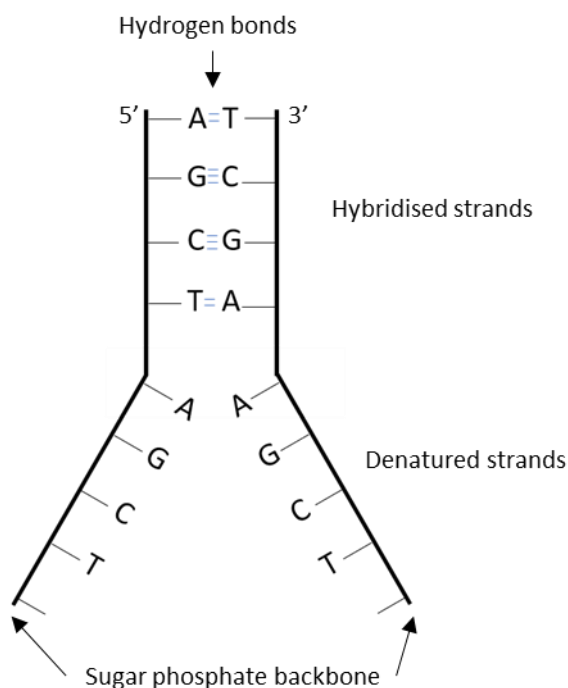
Figure 1.5 - Schematic of two antiparallel strands with hydrogen binding holding the strands together (adapted from reference [13]).

The planar bases form a ladder between the two strands, which then coil around an axis giving the double helix structure. Additionally, van der Waals stacking interactions between adjacent bases adds stability to the structure. This stability is crucial for preservation of the genetic information, which is held in the sequence of the bases. [12]

A vital concept regarding the structure of DNA is that the two strands can be separated. Heating the DNA above its melting temperature breaks the hydrogen bonds between the bases, causing the double-stranded DNA to denature into two single strands. This process is reversible – lowering the temperature will allow the strands to re-hybridise – and can be followed using UV-vis spectroscopy. As DNA denatures its absorbance at 260 nm increases (Figure 1.6). [14–16]

Enzymes called DNA polymerases synthesise DNA by replication of a parent DNA molecule. In order to replicate, the two strands unzip (as shown in Figure 1.5). Each strand is then used as a template; by filling in the complementary bases a new complementary strand is formed, creating two new molecules, each identical to the parent molecule.
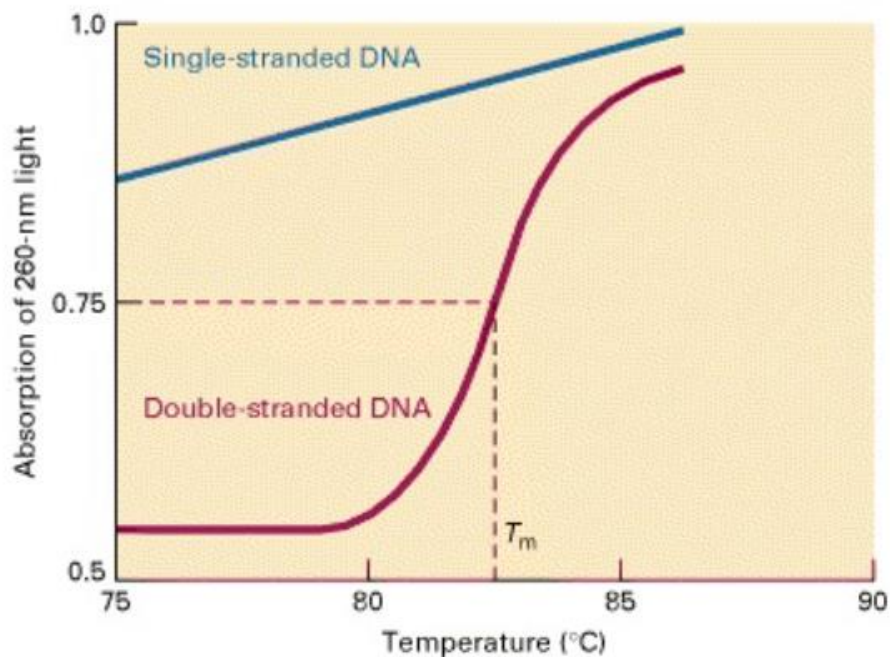
Figure 1.6 - Absorption spectroscopy can be used to follow the transition from double stranded DNA to single stranded DNA as temperature increases. The temperature at which half of the DNA is in its double-stranded state and half is single-stranded is known as the melting temperature (T_m). [16] Copyright © 2000, W. H. Freeman and Company.

In the nucleus, DNA is stored in the form of chromosomes which consist of DNA tightly packed around proteins called histones; the human genome consists of 3.1 billion base pairs held in 23 pairs of chromosomes. It contains the genetic information, stored in the order of the bases. Coding regions (or genes), which contain the information to make proteins, make up approximately 1.5 % of the entire genome. [17]

1.2.3 Gene expression

Different sequences of DNA – genes – encode different proteins, which carry out the various processes required within a cell. This process of gene expression has two main steps; transcription and translation (Figure 1.7).
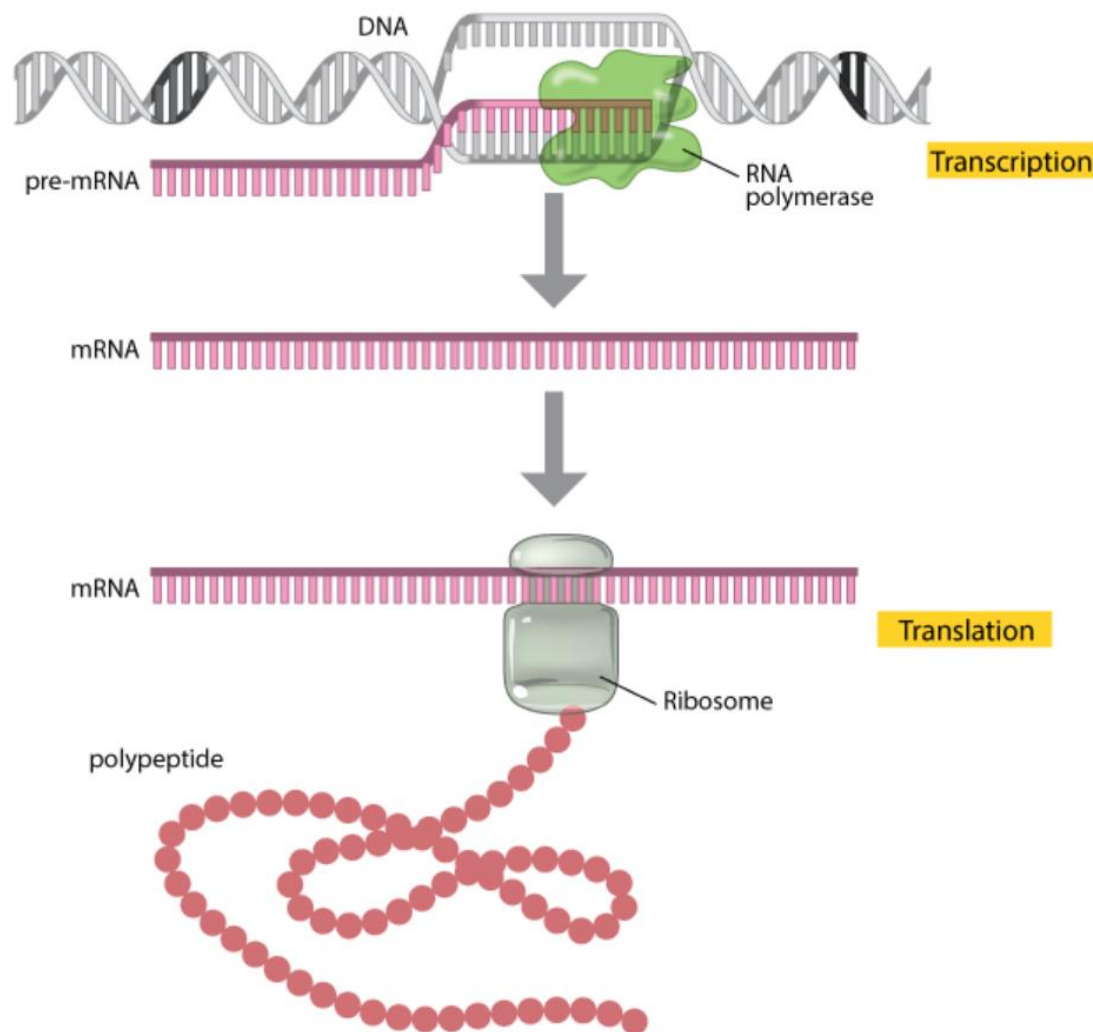
Figure 1.7 - Schematic representing the processes of transcription and translation. Reproduced from [18]. © 2014 Nature Education.

During transcription, a region of DNA is used as a template to create a second molecule – messenger RNA (mRNA). mRNA is the intermediary between DNA and protein. It is created by the enzyme DNA polymerase and is a single stranded molecule complementary to the gene it is responsible for encoding. Due to the nature

of transcription, an mRNA strand is the reverse complement of the corresponding DNA sequences.

During translation, mRNA is used to synthesise the corresponding protein. Every sequence of three nucleotides – a codon – in the mRNA corresponds to a different amino acid. By 'reading' the sequence of the nucleotides, a ribosome assembles the corresponding amino acids to build up the protein.

1.2.4 DNA vs RNA

Despite both being composed of nucleotides, there are key differences between DNA and RNA, summarised in Table 1.1. These differences make RNA a less stable molecule than DNA.

Table 1.1 - Summary of key differences between DNA and RNA

	DNA	RNA
Sugar	Deoxyribose	Ribose
Bases	Adenine	Adenine
	Thymine	Uracil
	Guanine	Guanine
	Cytosine	Cytosine
Structure	Double helix	Complex structures
Stability	Long term stability	Less stable
Location	Nucleus	Throughout the cell

Both molecules contain a pentose sugar, however in RNA the sugar is ribose (Figure 1.8). Ribose has an additional hydroxyl group in the 2' position. This increases the reactivity of RNA and causes the structure of the sugar to twist slightly to decrease repulsions.

In RNA, the base thymine is replaced by uracil (Figure 1.8). Uracil has a similar structure to thymine but is lacking the methyl group on carbon 5. Spontaneous deamination of cytosine converts it to uracil, however, since uracil is not normally present in DNA, the mutation is recognised and re-converted, ensuring long-term stability. Since long term stability is less of an issue with RNA, uracil can remain.
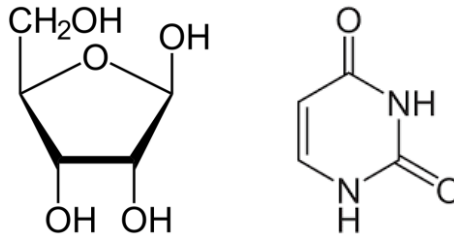
Figure 1.8 – Ribose (left) and uracil (right) structures.

The structure of the two molecules is also different. In cells, DNA is present as a β-type double helix, whereas RNA can take more complex structures. Within these complex structures are single-stranded regions and short α-type double helices, which can occur both within and between molecules. The α-type helices are more compact than the β-type, with bases no longer perpendicular to the backbone. [19]

In cells, DNA is found in the nucleus. Whilst RNA is also formed in the nucleus, it can be found throughout the cytoplasm. Complementary DNA and RNA strands can hybridise to one another – since thymine is not present in RNA, adenine bonds to uracil.

1.2.5 Detection of DNA

Since DNA is usually present at very low levels, amplification is generally required for detection. The polymerase chain reaction (PCR) was developed in 1983 by Kary Mullis. [20] Mullis *et al.* developed a reaction which could be used to specifically copy DNA. Following the extraction of DNA from its sample, PCR can be used to yield billions of copies of the desired sequence. Oligonucleotide primers, a DNA

polymerase enzyme and deoxynucleoside triphosphates are added to the DNA which is to be amplified.

Temperature is used to control the reaction. DNA is firstly denatured by heating the sample to a high temperature. The temperature is then reduced, allowing oligonucleotide primers to hybridise to the edges of the region to be amplified. DNA polymerase enzymes use the deoxynucleoside triphosphate molecules to form a complementary strand, at a slightly higher temperature, resulting in a copy of the original DNA sequence. This reaction is then cycled, with the number of DNA sequences increasing exponentially with each cycle (Figure 1.9). The cycle is repeated 28-34 times. [20]
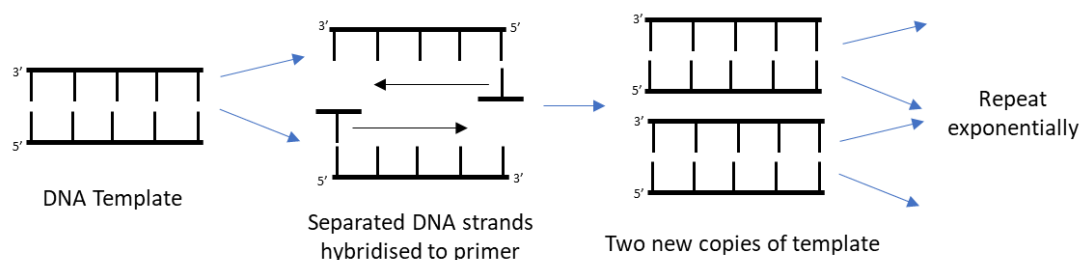
Figure 1.9 - Schematic of a PCR reaction.

Quantitative PCR (qPCR) is the main method used for DNA quantification. The amount of DNA present in a sample is measured by incorporating a fluorophore into the new strand in the PCR reaction. At the end of every cycle the fluorescence is measured, resulting in an amplification plot of fluorescence versus cycle number. Since the amount of fluorescence is proportional the amount of DNA present, this can be used to determine the concentration of DNA in the sample by comparing to an internal standard. [21]

Southern blotting – and its adaptation for RNA; northern blotting – is another method which relies of nucleic acid hybridisation for the detection of specific DNA sequences. It was developed by E. M. Southern in 1975. In this case, an oligonucleotide complementary to the target sequence is chosen and radiolabelled. As with PCR, the DNA must first be extracted from the sample. The separated DNA is digested and

fragments are separated according to size by gel electrophoresis. The DNA is then transferred to a nitrocellulose filter which is incubated with the labelled probe. The probe hybridises to the target DNA, allowing them to be visualised. [14]

In a similar manner, *in situ* hybridisation (ISH) can be used to detect specific DNA/RNA sequences within cells. A labelled oligonucleotide probe complementary to the sequence to be detected is incubated with the cells and, upon hybridisation, the target sequences can be visualised using a microscope. Most commonly, the oligonucleotide is labelled with a fluorophore. [14]

Unlike other methods, which usually involve pooling of cells and DNA/RNA extraction, ISH is useful since individual cells can be analysed and localisation determined. ISH can also be used to visualise the location of specific genes on chromosomes. [22]

ISH was first described in 1969 by Joseph Gall and Mary Lou Pardue. [23,24] They used radio-labelled RNA to detect DNA in toad oocytes. Toad ovaries were squashed, denatured and incubated with tritium-labelled rRNA. Autoradiography was then used to visualise the probes, indicating the location of extrachromosomal rDNA. [23,24] Around the same time John *et al.* and Buongiorno-Nardelli and Amaldi were also developing similar techniques. [25,26]

Approximately 10 years later, with the emergence of fluorescently labelled oligonucleotides and more advanced fluorescence microscopy, fluorescence *in situ* hybridisation (FISH) was developed. FISH had the advantage of improved resolution and shorter exposure times. [24]

In 1977, Rudkin and Stollar reported the first incorporation of fluorescence into the ISH assay, [27] however their method was indirect and included the use of an antibody. A modified antiserum against poly(rA).poly(dT) was incubated with the cells, followed by fluorescently-labelled IgG which binds to the antibody. Fluorescence microscopy was then used for visualisation of the fluorophore. [27,28]

Not long after this, a more direct FISH procedure was reported using fluorescently labelled DNA, making FISH commonplace in cytogenetics with single-molecule detection reported. [29]

Femino *et al.* were able to detect single mRNA molecules using a modified version of FISH by creating probes with five fluorophores per oligonucleotide. [30] Multiple β-actin probes specific to adjacent regions of the mRNA on the 3' untranslated region (UTR) were used. When the probes hybridized the collective fluorescence appeared as a point source, aiding identification. Five probes were used in order to achieve fluorescence that could be reliably measured above the background. It was noted that there was variability in the levels of fluorescence measured with between one to five probes hybridized but detection was possible with as little as one probe. [30] Using a similar method, Raj *et al.* were able to simultaneously detect three different mRNA molecules in single cells. [31] They used oligonucleotide probes labelled at the 3' end with a single fluorophore. In order to validate their method, two different sets of probes were used. 48 probes targeting adjacent regions in the coding region of the gene were labelled with one fluorophore. A region of the 3' UTR which contained 32 tandem repeats 80 nucleotides long was targeted by a second set of probes labelled with a second fluorophore. A computational program was used in order to identify the mRNA based on co-localization of both fluorophores. In order to detect three mRNAs simultaneously, three fluorophores were used with multiple probes for each mRNA, similar to the first set of probes in the validation study. This method provided both quantitative and spatial information on the mRNAs. [31]

In situ hybridisation is discussed further in chapter 3.

1.3 Raman Spectroscopy

1.3.1 Introduction to Raman Spectroscopy

When light interacts with a sample it can be either absorbed, transmitted or scattered. Raman scattering is concerned with the scattering of light by the molecules in a sample.

Raman scattering was first observed in 1928 by C.V. Raman, who went on to win the 1930 Nobel Prize in Physics for his work on light scattering. Raman *et al.* used a telescope to focus sunlight onto a sample and optical filters to show that some of the light scattered by the sample was at a different frequency to the incident light. [32] This inelastically scattered light is what is measured in Raman spectroscopy.

In Raman spectroscopy a single wavelength of light is shone onto a sample. This light causes polarization of the cloud of electrons around the nuclei in the molecule, forming a short-lived, unstable 'virtual state'. Since this state is not stable, the light photon is quickly re-radiated. Scattered light is then collected at an angle to the incident light, allowing a Raman spectrum to be obtained. [33]

1.3.2 Theory of Raman Spectroscopy

Figure 1.10 shows a Jablonski diagram detailing the energy changes associated with Raman spectroscopy. The energy of the virtual states is dependent on the frequency of the incident laser light.

Due to the small size of electrons, electron cloud distortion causes very small changes in the frequency of the scattered light. This is known as elastic, or Rayleigh, scattering and is not used in Raman spectroscopy. Most photons are Rayleigh scattered, making it the dominant process, however since no energy change occurs, no information about the molecule can be obtained.

If nuclear motion occurs, energy can be transferred from the incident light to the molecule or from the molecule to the scattered light. This is Raman, or inelastic, scattering. In Raman scattering the energy of the scattered light is one vibrational unit greater/lower than that of the incident light. Raman scattering is a very weak process – only one in every 10^6-10^8 incident photons are Raman scattered. [33]
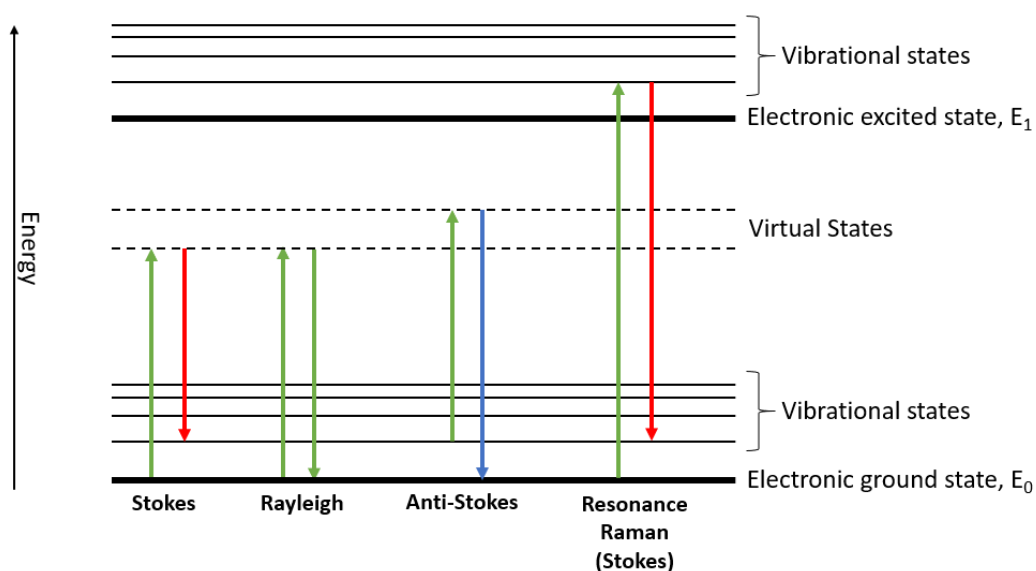
Figure 1.10 - Jablonski diagram showing Raman scattering; Stokes scattering occurs at lower energy, thus higher wavelength, than Rayleigh (inelastic) scattering, whilst anti-Stokes scattering occurs at higher energy. Resonance Raman occurs when the energy of the incident light is close to that of an electronic transition in the molecule.

If the molecule is in the ground state and absorbs energy from the incident light, causing it to be promoted to a higher energy state, this is Stokes scattering. If the molecule is already in an excited vibrational state it can transfer energy to the scattered photon - this is anti-Stokes scattering.

The ratio of Stokes to anti-Stokes scattering can be determined from the Boltzmann equation (equation 1), where n represents the excited vibrational energy level, m represents the ground vibrational energy level, N is the number of molecules in each state, g is the degeneracy o the levels, E is the energy of the energy levels and k is Boltzmanns constant (1.380×10^{-23} J K^{-1}).

$$\frac{N_n}{N_m} = \frac{g_n}{g_m} exp \left[\frac{-(E_n - E_m)}{kT} \right]$$ **Eqn. 1**

Since, at room temperature, most molecules will be in the ground state, Stokes scattering will be stronger than anti-Stokes. [33]

Due to Raman scattering being a weak effect, sensitivity can be poor. High power lasers and microscopes can be used to overcome this but these come with their own problems, such as sample degradation and competitive fluorescence. [33]

The intensity of Raman scattering (I) is given by equation 2, where K is constant, l is the laser power, ω is the frequency of the incident light and α is the polarizability of the electrons in the molecule being analysed.

$$I = Kl\alpha^2\omega^4$$ **Eqn. 2**

Since the polarizability of the electrons in the molecule cannot be altered, the modifiable parameters to increase the scattering intensity are the laser power and frequency. However, this is not always straight forward. Since intensity is proportional to the fourth power of the frequency of the incident light it makes sense that higher frequency, lower wavelength, light (e.g. UV light) would give the best signal. However, high energy UV radiation is absorbed by many compounds and can cause sample degradation. For this reason, the most commonly used lasers are in the visible region.

Intense Raman scattering occurs when the vibration causes a change in the polarizability of the electron cloud surrounding the molecule. This occurs to a greater extent with symmetric vibrations. Infrared spectroscopy, on the other hand, requires a change in the dipole moment of the molecule, making asymmetric vibrations most intense. For this reason, the two techniques can be used to complement each other. The mutual exclusion rules dictates that in a centrosymmetric molecule – one where reflection of any point through the centre will reach an identical point on the other side – no band can be both Raman and infrared active. [33]

1.3.3 Enhanced Raman Scattering

Whilst Raman scattering itself is an inherently weak effect, there are methods available to overcome this. One way of enhancing Raman scattering is by matching the energy of the laser to the energy of an electronic transition within the sample, known as resonance Raman scattering (RR), Figure 1.10. Enhancement of the Raman signal by up to 10^6 can be achieved, however 10^3-10^4 is more common. [33,34]

Another method of enhancing the signals in Raman spectroscopy is to adsorb the molecule onto a roughened metal surface to give surface enhanced Raman scattering (SERS). SERS can give enhancement of up to 10^6 compared with Raman spectroscopy. [33] Albrecht *et al.* reported in 1977 that the Raman spectra of pyridine adsorbed at a silver electrode gave anomalously intense signals, approximately five times greater than expected. This enhancement was attributed to a 'surface effect' increasing the Raman cross-section. [35]

Gold nanoparticles can be used as the metal surface in SERS. These particles have multiple properties which make them useful SERS substrates: i) due to coupling of plasmons, a colour change from red to blue is seen when the particles aggregate, ii) they are generally non-toxic making them biocompatible, and iii) 'hot-spots' occur between adjacent particles which result in enhanced electromagnetic field and, hence, enhanced Raman signal. [36] Furthermore, nanoparticles are known to quench fluorescence, reducing any fluorescent background in the spectrum. [37,38]

Combining both of the above techniques, i.e. adsorbing the molecule onto a roughened metal surface and using a laser frequency close to that of a transition in the sample, will give surface enhanced resonance Raman scattering (SERRS). [33,39]

Compared with fluorescence, SE(R)RS has several advantages which may make its use favourable; i) spectra produced give a molecular fingerprint of the molecule being probed, ii) the bands in the spectrum are narrow, aiding multiplexing potential, iii) SERS spectra are produced on a shorter timescale which can allow shorter integration times to be used, and iv) photobleaching is less of a problem. [39,40] Another benefit of

SERS is its high sensitivity – single-molecule detection using SERS was first reported in 1997. [40–42] In 2004, a comparison of SERRS and fluorescence detection limits for detection of labelled oligonucleotides showed that SERRS outperformed fluorescence by around three orders of magnitude. [43]

1.3.4 Uses of Raman Spectroscopy with Nanoparticles

Gracie *et al.* developed a quantitative multiplex assay for detection of bacterial meningitis causing pathogens using SERS. In this assay, two oligonucleotide probes hybridised to adjacent points on the target pathogen sequence. One contained a biotin moiety at the 3' end, whilst the other had a fluorophore at the 3' end and a phosphate at the 5' end. Streptavidin coated magnetic beads, which bind to biotin, were then added to the solution and re-suspended in exonuclease buffer. Lambda exonuclease, which digests a single strand of phosphate modified DNA, was added next before the solution was added to aggregated silver nanoparticles for SERS analysis. All three pathogens could be detected and quantified simultaneously. In a similar assay, two pathogens were detected simultaneously from clinical samples. [44,45]

Faulds *et al.* developed a molecular beacon for use with SERRS; SERRS Beacons (Figure 1.11). Benzotriazole azo dye maleimide – a SERRS label which complexes to silver nanoparticles – was added to the 5' end of a DNA sequence and fluorescent dye FAM was added to the 3' end. In the hairpin loop configuration, no fluorescence was observed due to nanoparticle quenching and the main SERRS signals were from the FAM label. When the complementary sequence was added fluorescence was emitted and the SERRS signal changed, indicating that the loop had opened separating the fluorophore from the silver surface. [46]
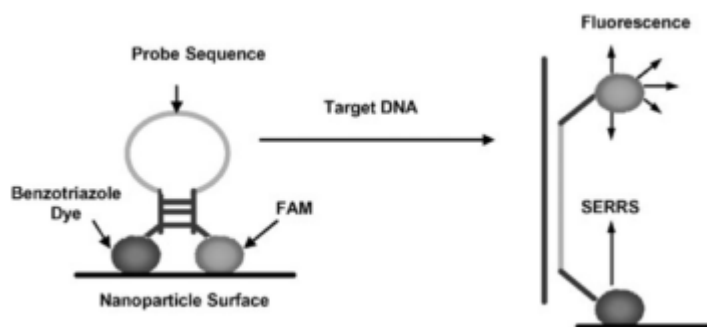
Figure 1.11 - Schematic of SERRS molecular beacon [46]. Reproduced with permission from The Royal Society of Chemistry.

Kneipp *et al.* were able to measure SERS spectra of intrinsic cellular components by adding gold nanoparticles to cells, which caused enhancement of their intrinsic signals. It was clear that the signals improved over time as aggregates of the particles formed. It was shown in TEM images that the longer the nanoparticles were in the cells, larger aggregates grew (Figure 1.12). No signals were observed from areas without the presence of nanoparticles due to sensitivity limitations of Raman. [47]

Figure 1.12 - TEM images of cells containing gold nanoparticles over time. Reproduced with permission from [47]. *Copyright © 2006, American Chemical Society.*

Similarly, Stokes *et al.* used SERRS to map macrophages treated with gold and silver nanoparticles using various excitation wavelengths. The nanoparticles were incubated with the cells for various lengths of time prior to fixation using

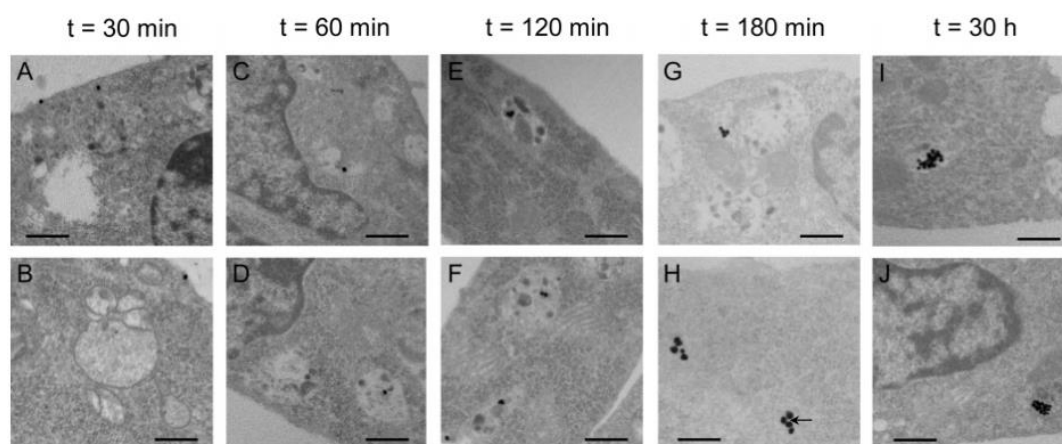paraformaldehyde. The macrophages were then stained. Polarized light microscopy and transmission electron microscopy showed that both types of nanoparticles were taken up by the cells via endocytosis within two hours, however they did not appear to enter the nucleus.

When they compared stained cells which had been incubated with and without nanoparticles, they found that the Raman signals were enhanced in the presence of nanoparticles due to SERRS enhancement. It was found that gold nanoparticles did not give effective enhancement at 514.5nm, however they were effective at 632.8nm, 785nm and 830nm. They were able to use fast line mapping to give efficient, sensitive maps. [48]

Ye *et al.* combined fluorescence and SERS for the quantification of miRNAs in cells by designing a dual-signal switchable nanoprobe. [49] Gold nanoparticles were functionalised with i) fluorescently labelled DNA (H1) hybridised to its complementary strand (H-C) and ii) a hairpin probe (H2). Figure 1.13 shows a schematic. In order to detect miRNAs with both low and high expression, an amplification step was included. In the absence of target, fluorescence can be measured due to the distance between the label and the nanoparticle. In the presence of the target, due to the close proximity between the nanoparticle and the labels, fluorescence is switched off and SERS is switched on. Fluorescence allowed direct intracellular monitoring, whilst SERS allowed high sensitivity and narrow peaks for multiplex detection. They were able to simultaneously quantify miRNAs with vast differences in expression in live cells. [50]
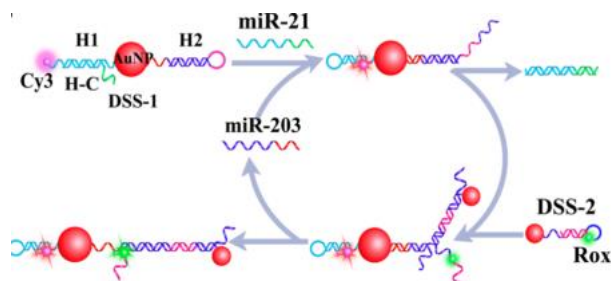

Figure 1.13 - Schematic of dual fluorescence/SERS miRNA probes. Reproduced with permission from [50]. *Copyright © 2017, American Chemical Society.*

1.3.5 Stimulated Raman Spectroscopy

Unlike spontaneous Raman, stimulated Raman spectroscopy (SRS) uses two, co-aligned incident lasers – the pump beam and the Stokes beam – to stimulate a specific transition within a sample. The frequency of these lasers is chosen such that the difference in energy between them is equal to the energy of the chosen molecular vibration within the sample (Figure 1.14), resulting in the corresponding signal being enhanced. Compared with spontaneous Raman spectroscopy, this can result in both improved sensitivity and shorter acquisition times. [51]
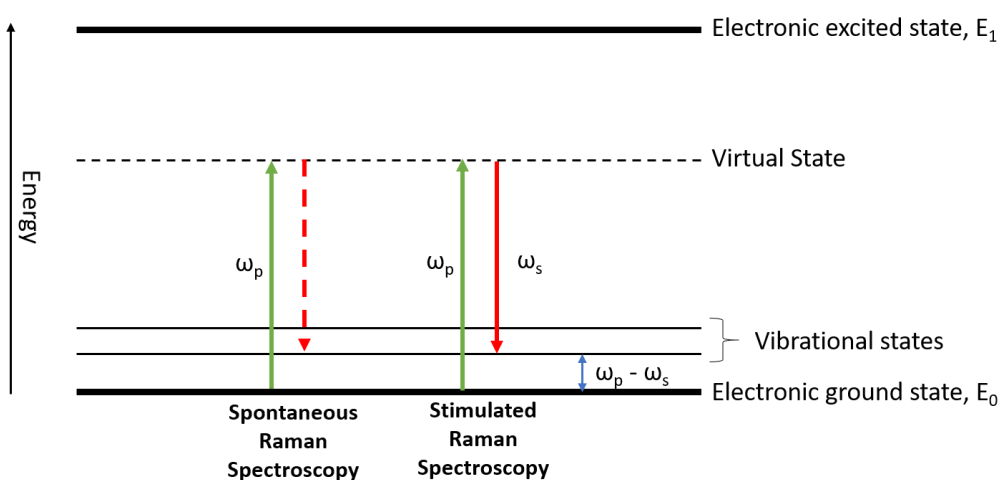
Figure 1.14 - Schematic comparing spontaneous and stimulated Raman spectroscopy. In spontaneous Raman an incident pump beam (ω_p) interacts with the sample resulting in scattered light with one vibrational unit difference. In stimulated Raman, two incident beams (pump beam, ω_p, and Stokes beam, ω_s) interact with the sample, resonantly enhancing the transition with energy ω_p-ω_s.

1.3.6 Raman Spectrometer Set-up

Raman instruments may include microscopes in the setup which can be used for analysis of cells, making it possible to produce both 2D maps of the surface and 3D maps on the entire cell. In order to create a map, a Raman spectrum is collected at an individual point and the sample is then moved to allow the next point to be interrogated. An individual Raman shift can then be chosen and its intensity at each individual point can be plotted. One of the main disadvantages of mapping, as opposed to imaging where the spectrum is only collected at an individual Raman shift,

is that it is relatively time consuming. As well as for analysis of cells, this use of Raman is suitable for mapping the surface of drugs to determine whether they are homogeneous. [33]

The set-up of a Raman spectrometer can vary, however the main components are generally the same. Figure 1.15 shows a schematic of a typical Raman microscope set-up.
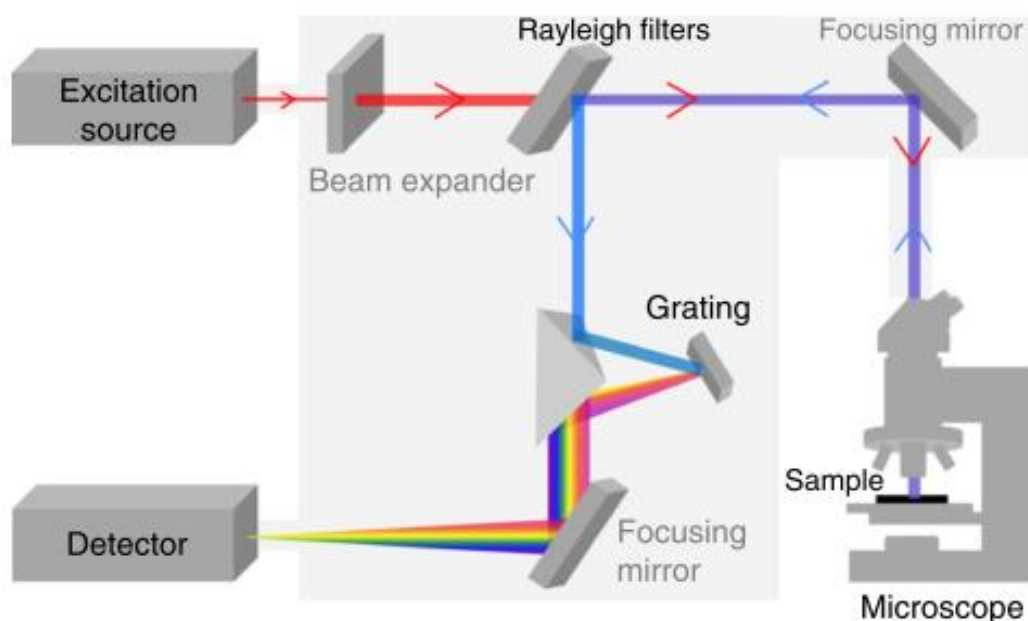
Figure 1.15 - Overview of Raman microscopy setup. Reproduced with permission from [52]**. *Copyright © 2016, Springer Nature.***

First is the excitation source. The laser chosen will depend on the sample to be analysed. From equation 2, it can be seen that the scattering intensity is proportional to the laser power and the laser frequency. This means that lower wavelength lasers will give better intensity. However, the power must be controlled to prevent photodegradation of the sample. The line width of the laser is also important as this will determine the resolution available.

The laser light is shone through a series of filters, mirrors and gratings to reach the sample and carry information back to the detector. Most commonly, the detector is a charge-coupled device (CCD). CCDs detect photons *via* thousands of pixels arranged

in multichannel arrays. Each pixel can collect charge, which is proportional to the Raman scattering intensity, from the scattered photons. The charge is passed from pixel to pixel until it reaches the end of the detector chip where it is converted to voltage and a read-out is provided. [52]

1.4 Metallic Nanoparticles

1.4.1 Introduction to Metallic Nanoparticles

Nanoparticles are particles with at least one dimension less than 100 nm. Metallic nanoparticles can be formed from pure metals (e.g. gold[53], silver[54], platinum[55]) or compounds containing metals (e.g. Fe_3O_4[56]). This work will focus on pure gold and silver nanoparticles; AuNP and AgNP, respectively.

Metallic nanoparticles have been used for many years due to their characteristic optical properties. The Lycurgus cup (Figure 1.16) is a Roman cup which dates back to the 4th century. In reflected light the cup appears green, whilst in transmitted light it is red. This dichroism is a result of colloidal gold and silver particles 50-100 nm present in the glass. [57] More recently, metallic nanoparticles have been shown to have uses in applications from pregnancy tests to drug delivery to cancer detection, owing to their unique optical properties and propensity for conjugation to other molecules. [58–60]

Figure 1.16 - The Lycurgus Cup shown green in reflected light (left) and red in transmitted light (right) [57]**. © The Trustees of the British Museum.**

Nanoparticles behave differently to their bulk material, exemplified by the red colour of gold nanoparticles compared to gold metal. Their optical properties depend on both the size and shape of the particles, both of which influence the electric field density on the particle surface. The dielectric constant of their adjacent medium will also influence their properties. [61]

Small gold nanospheres (~ 20 nm) are ruby red in colour with a maximum absorbance of approximately 520 nm. As the size of the spheres is increased the maximum absorbance is red-shifted, resulting in a transition to a more red-purple colour. Silver nanoparticles are yellow in colour (with a maximum absorbance ~ 400 nm) and become orange as their size increases.

1.4.2 Nanoparticle Synthesis

Nanoparticles can be synthesised *via* bottom up or top down approaches. The former uses reducing agents to generate metal atoms which can form nanoparticles whilst the latter involves etching a bulk material. Bottom up methods are preferred as they allow synthesis of smaller, more monodisperse particles.

The first recorded synthesis of gold nanoparticles was in 1857 by Faraday. He described how gold solution could be reduced with phosphorus, resulting in a ruby red solution. [62] There are now many methods of metal nanoparticle synthesis, generally involving reduction of a metal salt. [53,63,64]

One of the most common methods of synthesizing gold nanoparticles is the modified Turkevich method which uses a citrate reduction. Sodium citrate solution is added to hot chlorauric acid with stirring. The pale yellow solution turns blue during nucleation before becoming a ruby red colour, as described by Faraday. The size of the particles depends on the amount of reducing agent added – increasing the amount of reducing agent will decrease the final size of the particles. In this method citrate acts as both a reducing agent and a capping agent, forming a coating layer on the nanoparticles and, hence, enhancing their stability.

Figure 1.17 shows a schematic illustration of the proposed mechanism for gold nanoparticle growth *via* the Turkevich method. Initially, small nuclei are formed as Au^{3+} is reduced to gold atoms (step 1) which coalesce (step 2) and grow into small particles (step 3). These continue to grow as the gold salt continues to be reduced until it is used up (step 4). [65]
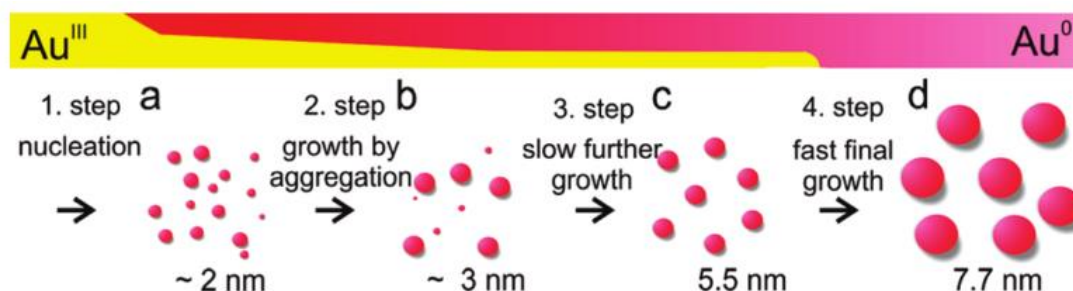
Figure 1.17 - Schematic of AuNP growth. Reprinted with permission from [65]. Copyright (2010) American Chemical Society.

1.4.3 Localised Surface Plasmon Resonance

The characteristic colour of AuNP (and AgNP) is a result of the absorption and scattering of light.

In 1908, Mie solved Maxwell's equation for nanoparticles interacting with an electromagnetic field, concluding that the plasmon band in the extinction spectrum was a result of dipole oscillations of free electrons in the conductance band. [66,67]

The wavelength of visible light is larger than the diameter of a nanoparticle and, as a result, it causes free outer electrons in the metal to oscillate. This causes polarisation of the metal electron cloud in resonance with the light (Figure 1.18).

Figure 1.18 - Schematic representation of LSPR showing the oscillation of the outer electrons in gold nanoparticles induced by an electromagnetic field.

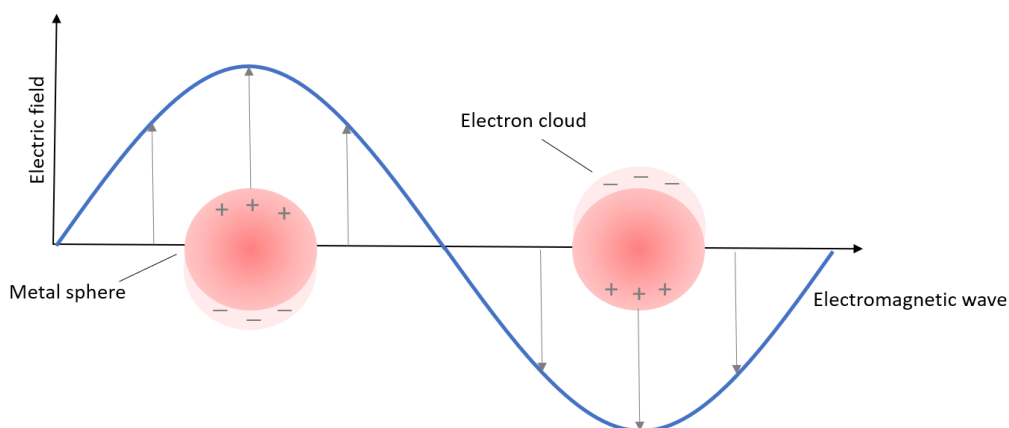For gold nanoparticles, this collective oscillation of the outer electrons – localised surface plasmon resonance (LSPR) – is in the visible region as can be seen in the extinction spectrum. [61] Each nanoparticle has a characteristic frequency where LSPR is maximised, for gold nanoparticles (20 nm) this is 520 nm. This changes depending on the size, shape or medium of the particles – gold nanorods, for example, have their LSPR in the near-IR region (~ 800 nm). [60,68]

It is this plasmon resonance absorption which gives gold nanoparticles extinction coefficients an order of magnitude larger than strongly absorbing dyes allowing lower for more sensitive detection. [61]

1.4.4 Uses of Metallic Nanoparticles and Oligonucleotides

In 1996, Mirkin *et al.* published a method for the assembly of DNA-functionalised nanoparticles which paved the way for the use of DNA-functionalised nanoparticles for the detection of specific DNA sequences. [69]

Thiol-modified oligonucleotides were incubated with gold nanoparticles for 24 hours. These DNA-functionalised nanoparticles showed increased stability to both high temperature and salt conditions compared to bare nanoparticles, indicating that the

DNA had coated the nanoparticle surface. To achieve assembly of the nanoparticles, two batches were separately functionalised with non-complementary oligonucleotides. A DNA sequence with 'sticky ends' was then added – the ends of the DNA sequence were complementary to the oligonucleotides attached to the particles. When the conditions were altered in favour of DNA hybridisation, the particles self-assembled causing aggregation (Figure 1.19). This aggregation was reversible on heating. [69]
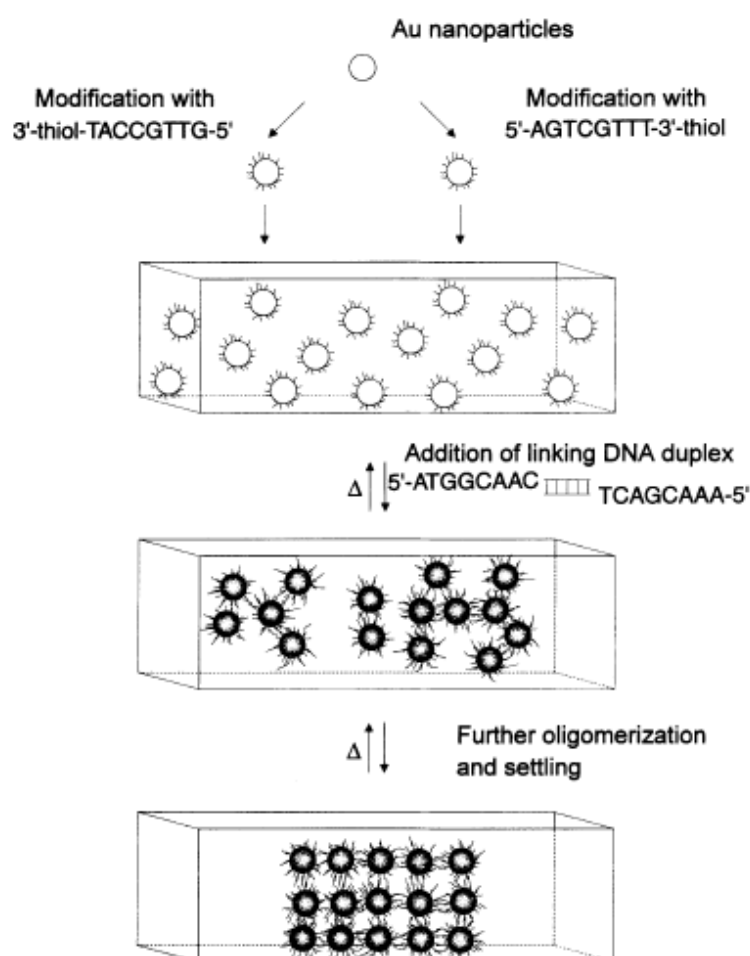

Figure 1.19 - Schematic of DNA induced nanoparticle assembly. Reprinted with permission from [69]. Copyright © 1996, Springer Nature.

In the same year, Alivisatos *et al.* also reported self-assembly of nanocrystals using DNA. By attaching the DNA to the nanocrystals at either the 5' or 3' end, they were able to create different orientations; head-to-tail, head-to-head, and trimers. [70]

Following on from this, Graham *et al.* reported that this specific self-assembly of DNA-functionalised nanoparticles could be used to 'turn on' SERRS. This method exploited the enhancement of Raman signals that occurs when nanoparticles aggregate. [71]

By functionalising two batches of nanoparticles with oligonucleotides that are each complementary to half of the target sequence, upon addition of the target sequence DNA hybridisation will cause the nanoparticles to self-assemble into aggregates. This results in a shift in the extinction spectrum λ_{max} from approximately 520 nm to approximately 600 nm, as well as an increase in the intensity of specific Raman signals due to surface enhancement effects (Figure 1.20).

Target DNA

SERRS 'off'
λ_{max} ~ 520nm

SERRS 'on'
λ_{max} ~ 600nm
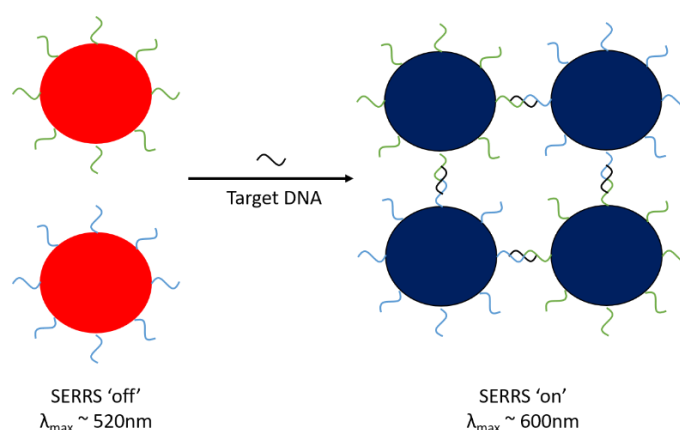
Figure 1.20 - Schematic of DNA induced nanoparticle aggregation showing unaggregated nanoparticles before the addition of the complementary target DNA which causes aggregation of the particles resulting in a red-shift in the λ_{max} of the particles and a 'turning on' of SERS.

Graham *et al.* used SERRS to detect DNA at low concentrations by mixing dye-labelled DNA with the polyamine spermine for attachment to silver nanoparticles. Spermine worked both to prevent the negative-negative charge repulsion of the DNA and nanoparticle surface, allowing the DNA to come into proximity with the particles, and

to cause aggregation of the particles, providing areas of high electric field for SERRS. They were able to detect DNA down to 0.8 pM. [72]

Molecular beacons, used for DNA detection, consist of a DNA sequence arranged in a hairpin loop structure with a fluorophore on one end and a quencher on the other. When the loop is closed, fluorescence is quenched due to the proximity between the fluorophore and the quencher. However, when a strand of DNA complementary to the loop sequence is added the beacon opens up, increasing the distance between the fluorophore and quencher, resulting in emission of fluorescence.

One problem with molecular beacons is inefficient quenching of fluorescence in the closed position. In order to overcome this, and improve sensitivity, Dubertret *et al.* hybridised molecular beacons to gold nanoparticles to replace the quencher. The beacon consisted of an oligonucleotide, which was self-complementary at the ends, functionalised with a fluorescent dye on the 3' end and a small gold nanoparticle on the 5' end. Various dyes were assessed (rhodamine 6g, fluorescein, Texas red and cy5) and all showed better quenching efficiency when used with gold nanoparticles compared to a traditional quencher molecule. [37]

Pan *et al.* used a similar method for mRNA detection in cells for cancer detection. A multiplex probe consisting of a gold nanoparticle functionalised with molecular beacons was used. Four different molecular beacons were used, each labelled with a separate dye, in order to detect four different mRNA sequences. The levels of fluorescence were shown to correlate with mRNA expression levels determined by RT-PCR and the probe was demonstrated to be non-toxic to the cells. [73]

An alternative to the nano-beacon approach is a nanoflare. Prigodich *et al.* developed a method of mRNA detection in live cells using nanoflares – Figure 1.21. [74] Gold nanoparticles were functionalised with oligonucleotides complementary to the target mRNA. These oligonucleotide sequences were hybridised to second, fluorescently labelled oligonucleotides. When the second oligonucleotide was hybridised, fluorescence was quenched due to the proximity of the nanoparticle and

the fluorophore. Cells were treated with the nanoflares for 24 hours. In the presence of the mRNA, the labelled oligonucleotide was displaced, resulting in emission of fluorescence. Having multiple oligonucleotide sequences on the nanoparticle allowed simultaneous detection of multiple targets. [75]
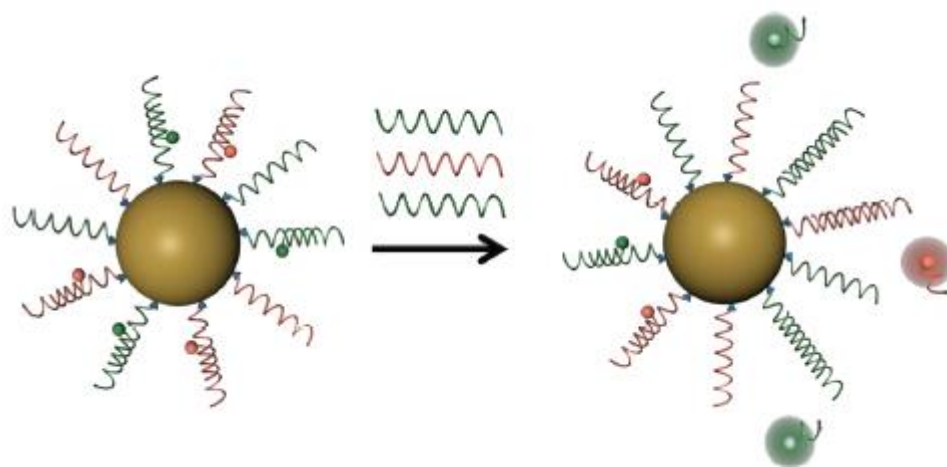

Figure 1.21 - Nanoflare schematic. Reprinted with permission from [75]**. *Copyright © 2009, American Chemical Society.***

Prigodich *et al.* also showed how nanoflares could be used for detection and regulation of mRNA. They wanted a probe which was i) cell permeable and stable in the cell environment, ii) able to hybridise with nucleic acids and iii) had a switchable signal for detection. They used the nanoflare approach described above. In this assay they used a combination of DNA and LNA to increase the hybridisation efficiency. The nanoflares were first tested with a synthetic target, it was demonstrated that it took approximately 10 minutes for the nanoflares to be removed in the presence of the target. The probes were shown to be sensitive to base mismatches; a one base mismatch showed 50 % of the signal compared to an exact match, whilst two, three or four base mismatches showed little fluorescence signal.

In cells, target specific probes showed almost double the fluorescence as controls. When the probes were incubated with cells for four days at a high concentration, target levels were found to decrease by 92 %. This indicates that high concentrations of the probes can control mRNA levels – something which must be considered when

using such probes in live cells as the effect of mRNA inhibition may have detrimental effects on the cells. [76]

It is worth noting, however, that there has been some controversy regarding the reliability of nanoflare approaches. Czarnek and Bereta found that the fluorescence of such probes did not correlate with RNA levels assessed using qPCR. [77]

1.4.5 Interaction of Nanoparticles with Cells

Bulk gold is known for its inherent inertness and gold nanoparticles are generally considered to be non-toxic and more cell compatible than silver. However, there is some conflicting evidence regarding the toxicity of nanoparticles.

Multiple studies have assessed gold nanoparticles of different size, with different capping agents, and in different cell lines and found them to be non-toxic. However, there are also reports of gold nanoparticles causing toxicity in cells. Positively charged gold nanoparticles seem to be of particular concern, as do nanoparticles less than 2 nm in diameter. [78] Cellular uptake also appears to depend on the size and shape of the particles. [79]

The conflicting toxicity data may be a result of the complex nature of the experiments. There are many factors which may influence toxicity effects such as cell type, nanoparticle physicochemical properties and media used. For example, 13 nm citrate-capped gold nanoparticles were found to be non-toxic in human liver carcinoma cells but were toxic in human lung carcinoma cells. For this reason, it is important to carry out individual toxicity assays using the relevant conditions. [78]

Arnida *et al.* studied the uptake and toxicity of bare and PEGlyated AuNP in PC-3 cells. Neither bare nor PEGylated AuNP (30 nm, 50 nm and 90 nm) particles were found to interfere with cell proliferation when assessed using an MTT toxicity assay at 1.5 nM particle concentration.

It was determined that uptake into cells was size dependent, with 90 nm particles taken up to a lesser extent than the smaller particles. Figure 1.22 shows TEM images of bare 30 nm AuNP entering PC-3 cells by endocytosis. They found that bare particles had higher levels of uptake compared to PEGylated particles. This was attributed to formation of a hydrophilic stealth coating causing less interaction with the cells. The particles appeared to enter the cells in clusters via vesicles, before being released from the vesicles into the cytoplasm. Some particles were also found to enter the nucleus. [80]
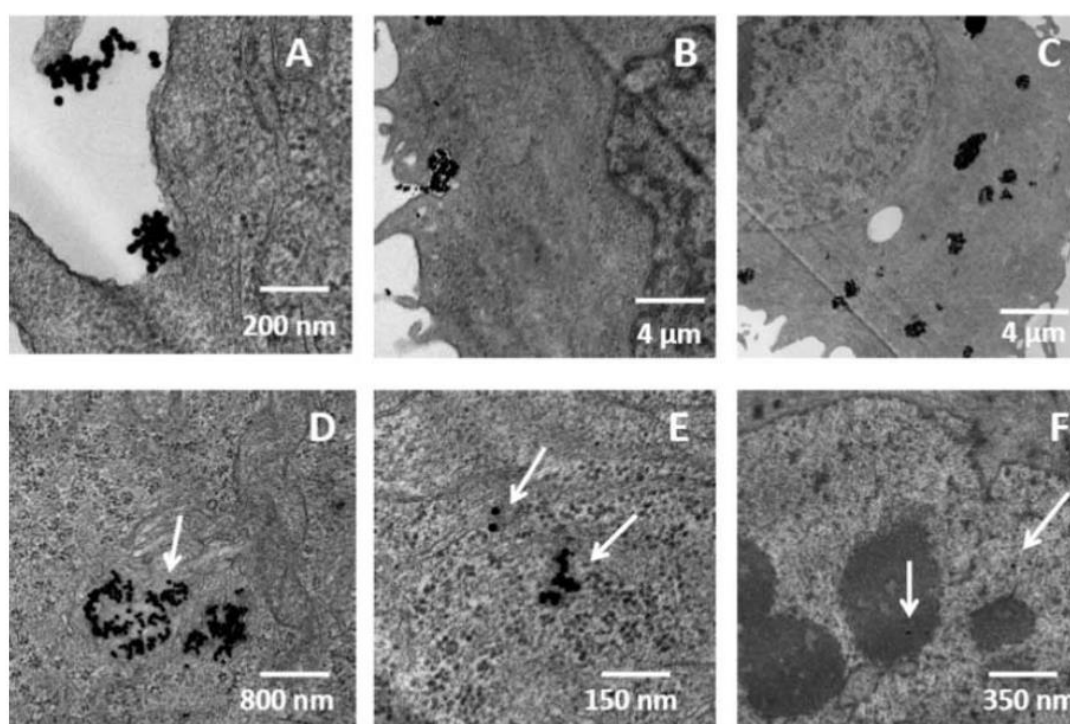

Figure 1.22 - TEM images showing AuNP incubated with PC-3 cells (A) AuNP on cell surface, (B) AuNP being internalised, (C) intracellularr distribution, (D) release into cytosol from vesicle, (E) AuNP in cytoplasm, (F) AuNP in nucleus). Reprinted with permission from [80]. Copyright © 2009 John Wiley & Sons, Ltd.

Rosi *et al.* showed that despite being negatively charged, oligonucleotide-coated gold nanoparticles readily entered a range of cell types with no effect on cellular morphology or viability. They also showed that the duplexoligonucleotides bound to the AuNP degraded slower than those without AuNP and that higher packing densities resulted in higher binding constants. [81]

1.5 Project Aims

The overall goal of this project was to investigate the use of Raman spectroscopy and functionalised gold nanoparticles for the detection of specific mRNA molecules, with the aim of developing an assay that can be used as a biological tool and, ultimately, for the detection of disease.

More specifically, the goal of this project was to develop an assay for the measurement of HSD2. In order to do this, mRNA which codes for the enzyme was targeted with an oligonucleotide probe. By choosing a probe which is complementary to a region of the mRNA it should hybridise according to Watson-Crick base pairing rules.

The project was split into two main parts; firstly, a proof of concept study using Raman spectroscopy for *in situ* hybridisation using a housekeeping gene and, secondly, developing this method for the detection of HSD2. By using SERRS with nanoparticles it was hoped high sensitivity would be achieved, whilst the sharp peaks would facilitate a multiplex measurement if required. Ideally, the measurement would be dynamic allowing for changes in expression in response to stimulus in cells to be measured.

For proof-of-concept studies, the housekeeping gene glyceraldehyde 3-phosphate dehydrogenase (GAPDH) was chosen as a target molecule. Due to mRNA molecules being large and able to form complex structures, finding an appropriate area to target with molecular probes can be difficult. GAPDH is involved in glycolysis and is commonly used in gene expression assays due to it being consecutively expressed in all cells. [82,83] By using a commonly used gene, this meant that reliable oligonucleotide sequences to target were readily available in published literature, meaning that less time was wasted with optimisation of the probes. [84]

Three main avenues were explored: i) an *in situ* hybridisation approach, ii) a molecular beacon approach and iii) a nanoparticle dimerization approach. All three

methods involved the hybridisation of Raman labelled oligonucleotides to GAPDH mRNA.

The first method had no switchable signal and so was the most straight-forward. Nanoparticles were functionalised with oligonucleotides, either electrostatically or via a thiol linker. These probes were then incubated with cells and mapped using Raman microscopy to localise the probes inside the cells. Both 2D and 3D mapping were performed to determine whether the probes were entering the cells.

The second method involved a molecular beacon modified with a Raman active dye on one end and a thiol linker on the other. The beacon was attached to nanoparticles that were functionalised with a second Raman active dye. In the closed position, i.e. with no target present, SERS signal should be obtained from both dyes. However, in the presence of the target molecule the beacon should open up, resulting in a change in the SERS signal. It was hoped that by taking a ratio of the two dyes it would be possible to detect the target sequence.

Lastly, a nanoparticle dimer approach was assessed. For this method, two batches of nanoparticles were asymmetrically functionalised with oligonucleotides. Each batch was complementary to half of the target sequence. In the presence of the target, both sets of nanoparticles should come together to hybridise, resulting in formation of nanoparticles dimers and, hence, increased SERS signal due to hot spots.

There are various considerations when creating such probes. Firstly, probes must be cell permeable and biocompatible. They must be able to enter the cells and, importantly, should be free in the cytosol. If probes become trapped in endosomes or other vesicles within the cells, they will not be able to interact with the target mRNA. Furthermore, the probes should have minimal cytotoxic effects on the cells, particularly if a live cell assay is the goal.

On reaching the cytosol, the oligonucleotides on the surface of the nanoparticles must be free to interact with the cell components. This means that they must not become surrounded by other components of the cell or cell media, such as proteins,

which have the potential to block access to the target. The formation of a protein corona is thought to be minimised by surface functionalisation of the nanoparticles, however may still occur to an extent. [85]

Another issue is aggregation. In the high salt environment of the cell cytosol, aggregation is likely. This can have two effects; firstly, aggregation will result in enhanced Raman signals improving sensitivity. However, it may also prevent nanoparticle from being free to move within the cell – thus preventing target hybridisation. Further, aggregated probes are unlikely to be removed from the cells, which may cause problems in probes with no switchable signal.

Another issue with these nanoprobes is the relatively large size difference between the nanoparticles and the oligonucleotides used for target detection. A nanoparticle which is 40 nm in diameter has a surface area of approximately 5000 nm^2. In comparison an oligonucleotide is approximately 2 nm wide and several nm long, depending on the number of bases. Assuming the oligonucleotides are bound on the nanoparticle surface, the binding to the target molecule must be extremely strong to hold the relatively huge nanoparticle in place. This becomes an even larger issue when nanoparticle dimers are the goal, requiring the target duplex to bring two nanoparticles into close proximity, and overcome steric hinderance.

2. Experimental

2.1 Materials

Malachite green isothiocyanate (MGITC) was purchased from Thermo Fisher Scientific (MA, USA). All other chemicals were purchased from Sigma Aldrich (Dorset, UK).

Oligonucleotides were purchased from ATDBio (Southhampton, UK), unless otherwise stated. 1 mL millipore water was added to each oligonucleotide which was then aliquoted and frozen (-20 °C) until further use.

Oligonucleotides for the Y-shaped dimers chapter (chapter 5) were purchased from Exiqon (Vedbaek, Denmark) and prepared in the same way as above.

Roslyn Park Memorial Institute 1640 (RPMI) cell media was purchased from Thermo Fisher Scientific (MA, USA) and supplemented with 10 % fetal bovine serum (FBS), 1 % penicillin-streptomycin and 1 % fungizone prior to use.

2.1.1 Buffer Preparation

0.172 g phosphate buffer (PB) powder was dissolved in 10 mL of dH_2O to give a 100 mM solution. This was then diluted 1 in 10 to give a working solution of 10 mM (pH 7.2).

1.75 g sodium chloride was dissolved in 10 mL dH_2O to give a 3 M working solution.

6.45 g sodium citrate was dissolved in 10 mL dH_2O to give a 250 mM solution.

A PBS tablet was dissolved in 200 mL dH2O to give a 10 mM solution (0.01 M phosphate buffer, 0.0027 M potassium chloride and 0.137 M sodium chloride, pH 7.4).

2.2 Instrumentation

Nanoparticles were characterised using extinction spectroscopy, dynamic light scattering (DLS) and Zeta potential.

Extinction spectroscopy was carried out using a Cary 60 UV-Vis spectrophotometer (Agilent Technologies, USA) or, for measurements requiring temperature control, a Cary 300 UV-Vis spectrophotometer fitted with a 6 x 6 cell changer and a Peltier temperature controller (Agilent Technologies, USA). Both spectrophotometers have a 1 cm path length.

Dynamic light scattering (DLS) was used to measure the size and Zeta potential using a Zetasizer Nano ZS (Malvern Instruments, UK).

Solution Raman spectra were taken using a SnRI Sierra 638 Benchtop spectrometer (Snowy Range Instruments, USA) with a 40 mW, 638 nm laser and a 1 second acquisition time, unless otherwise stated. Matlab 2016 software was used to background correct the spectra.

Mapping spectra were taken using a Renishaw InVIA Raman microscope system (Renishaw, UK) with a 500 mW, 633 nm laser at 10 % power with a 0.2 second acquisition time (unless otherwise stated).

A POLARstar Omega plate reader (BMG Labtech, Germany) was used for absorbance measurements following MTT assays.

Scanning electron microscopy (SEM) images were acquired using a Sirion 200 Shottky field emission microscope (Hillsboro, USA).

2.3 Methods

2.3.1 Nanoparticle Synthesis

All glassware was soaked in aqua regia (3:1 HCl:HNO$_3$) for a minimum of 2 hours and rinsed with distilled water prior to synthesis. Nanoparticles were synthesised according to the Frens method. [63] Briefly, 500 mL of aqueous sodium tetrachloraurate (see Table 2.1 for concentration) was heated until boiling. 10mL of aqueous trisodium citrate was added to the solution which was then left to boil for 15 minutes with continuous stirring. The reaction mixture began as a pale yellow colour, before changing to dark blue and finally ruby red.

Altering the concentrations of sodium tetrachloraurate and sodium citrate allows for manipulation of the size of the nanoparticles. Larger particles were synthesised using a lower concentration of citrate, which acts as a capping agent, allowing the size of the particles to be tuned.

Table 2.1 - Concentrations required for differing sizes of AuNP

Desired Nanoparticle Size	Sodium Tetrachloraurate	Sodium Citrate
20 nm	0.25 mM	25 mM
40 nm	0.3 mM	17.25 mM

2.3.2 Nanoparticle Characterisation

Extinction spectroscopy was used for nanoparticle characterisation. Extinction spectra can give information on the size, dispersity and concentration of the nanoparticle solution. The Beer-Lambert law can be used to estimate the concentration of the colloid solution, because the concentration is proportional to the absorbance.

For spherical gold nanoparticles, the λ_{max} should be ~ 520 nm for 20 nm particles and it red shifts as the nanoparticle size increases. The width of the peak indicates the

dispersity in the size of the particles, with a wider peak indicating a more polydisperse suspension.

Samples were diluted 1:1 with dH$_2$O prior to analysis and a baseline measurement of the solvent only was carried out prior to all measurements. Extinction was measured between 200 – 800 nm.

Dynamic light scattering was also used for nanoparticle characterisation – both size and zeta potential were determined for neat nanoparticle suspensions.

SEM was used to image nanoparticles. 10 µL of nanoparticle solution was spotted onto the silicon wafer and left to dry before imaging.

2.3.3 Nanoparticle Functionalisation

2.3.3.1 Raman Dye Measurements

Malachite green isothiocyanate (MGITC) was added to gold nanoparticles at various MGITC:AuNP ratios (500:1, 1000:1 and 2000:1) and sonicated for three minutes. Samples were then centrifuged at 4000 rpm for 20 minutes to pellet the nanoparticles and the supernatant was removed. Functionalised particles were then resuspended in water and analysed using a 638 nm laser.

2.3.3.2 Electrostatic Attraction via Spermine

MGITC-oligonucleotides (various concentrations) were pre-mixed with spermine (final concentration 16 nM) before being added to AuNP (0.4 nM, 20nm). Samples were shaken for 15 minutes prior to use.

For comparison of single-stranded and double-stranded DNA, MGITC-oligonucleotides were pre-mixed with spermine before being added to AuNP. The mixture was shaken 15 minutes before the target was added. Samples were heated

to 85 °C for 10 minutes and allowed to cool before being analysed using a 638 nm laser.

2.3.3.3 Thiol-Oligonucleotide Functionalisation

Thiol-oligonucleotide was added to AuNP (1 mL, 40 nm) at a ratio of 4000:1 and the sample was shaken for 15 minutes. Sodium citrate (80 µL of 250 mM, pH 2.9) was added and samples were shaken for a further 15 minutes. Samples were then centrifuged for 20 minutes at 5000 rpm to pellet the nanoparticles. The supernatant was removed and the nanoparticles were resuspended in 500 µL water.

Extinction spectroscopy was used to determine the approximate concentration of the oligonucleotide functionalised particles before addition of the dye.

MGITC was added at a ratio of 3000:1 and sonicated for 3 minutes before particles were centrifuged for 20 minutes at 5000 rpm. The pellet was then resuspended in water.

2.3.3.4 AuNP for pH Determination

4-Mercaptobenzoic acid (MBA) was added to 1 mL particles to give a final concentration of 100 µM and shaken for 15 minutes. Particles were then centrifuged at 4000 rpm for 20 minutes and the nanoparticle pellet was resuspended in 0.1 M PBS. PBS was buffered to the appropriate pH (1-12) by adding HCl or NaOH.

2.3.3.5 Beacon Functionalisation

MBA was added to AuNP at a ratio of 1500:1 and shaken for 5 minutes before being centrifuged at 4000 rpm for 20 minutes. The MBA-AuNP pellet was then resuspended in water. Beacon was then added at a ratio of 1200:1 and particles were shaken for a further 30 minutes. PEG was added and particles were shaken for 15 minutes. Sodium citrate was added and samples were shaken for 15 minutes. Samples were then centrifuged – multiple centrifuge steps were performed at low rpm (2000-3000 rpm,

10 minutes) in order to maintain stability of the particles. The nanoparticle pellet was then resuspended in 500 µL of a 0.1 M PBS solution. Samples were then heated to 50 °C for 10 minutes and left to cool to ensure the beacon was pre-formed.

For hybridisation experiments, the target was added to the particles which were incubated at 60 °C for 30 minutes. Samples were then left to cool prior to analysis.

2.3.3.6 Asymmetric Nanoparticle Functionalisation

Glass coverslips were immersed in piranha solution (1:3 30 % H_2O_2:conc. H_2SO_4) for 30 minutes.

Asymmetric nanoparticles were produced according to the methods published previously. [86,87] Glass slides were incubated with piranha solution (1:3 H_2O_2:H_2SO_4) for 30 minutes. They were then washed three times in water, then in ethanol. Slides were then immersed in 10% aminopropyltriethoxysilane (APTES) solution for 30 minutes before being washed again – firstly in ethanol, then in water.

The activated slides were then immersed in 0.1 M AuNP before being rinsed with water to remove any unbound particles. The AuNP-coated slide was then immersed in 100 µM PEG (MT-800) for 2 hours. After 2 hours, the slide was washed with water and sonicated for 2 minutes in 0.01 M PB + 0.01 % Tween20. Sonication was used to remove the PEG-coated particles from the glass, resulting in a suspension of particles asymmetric PEG-AuNP. The PEG-coated particles were then concentrated by centrifugation before the addition of oligonucleotides.

Oligonucleotide (probe A or probe B) was added to PEG-coated AuNP and left to shake for 15 minutes. 40 µL citrate was added before being shaken for another 15 minutes. Dye was then added and the mixture was shaken for another 15 minutes before centrifugation. Samples were centrifuged at 3000 rpm for 20 minutes and the supernatant was removed. Samples were then resuspended in the buffer of choice.

2.3.3.7 Fully Coated Nanoparticle Functionalisation (Y-Shaped Probes)

Thiol-modified oligonucleotide was added to AuNP and left to shake for 30 minutes. 25 µL sodium citrate (250 mM) was then added and samples were left to shake for 30 minutes. Another 25 µL sodium citrate (250 mM) was added and samples were left to shake for 30 minutes. Samples were made up to 1 mL with water before being centrifuged at 4000 rpm for 20 minutes. The nanoparticle pellet was then resuspended in water and extinction spectroscopy was used to estimate the concentration of the oligonucleotide functionalised AuNP. MGITC was then added and were sonicated for 3 minutes before being centrifuged (4000 rpm, 20 minutes). The nanoparticle pellet was then resuspended in 10 mM PB.

The concentration of each component was dependent on the ratio between the component and the AuNP, for oligonucleotides, a ratio of 2000:1 was used, and for MGITC, a ratio of 2500:1 was used.

For hybridisation experiments, a final concentration of 0.02 nM of each probe was used. Probes A and B were combined in PB. 3 M NaCl was then added slowly to a final concentration of 0.3 M before addition of the target oligonucleotide.

2.3.4 DNA Melting Curve

Final concentrations of 1 µM oligonucleotide probe and target oligonucleotide (0.3 M PBS) were placed in a sealed cuvette. The temperature was cycled from 45-90 °C at 1 °C/min whilst being monitored at 260 nm.

2.3.5 Cell Culture

2.3.5.1 Cell Maintenance

PNT2 cells (normal prostate epithelium, human) were removed from liquid nitrogen and placed at 37 °C to thaw. They were then transferred to a T25 flask with 5 mL of

media (RPMI) and incubated at 37 $^\circ$C with 5 % CO_2. After 24 hours, the media was removed and replaced with fresh media.

When cells were ~ 80 % confluent they were moved up to a larger flask by first removing the media and washing them with 5mL PBS. 1 mL trypsin was added and the flask was incubated for ~3 minutes at 37 $^\circ$C. When the majority of cells had detached from the flask, 1 mL media was added to stop the trypsinisation process. The cell suspension was then added to a T75 flask and topped up to 15 mL with pre-warmed media.

2.3.5.2 Cell Counting

10 μL cell suspension was added to 40 μL Trypan blue and mixed before being applied under the cover slip of a haemocytometer. The number of cells in three sets of 16 squares were counted using a microscope and the average number of cells per set was calculated. Based on the dilution factor of 1:5 with Trypan blue and the correction factor of the haemocytometer (1×10^4), the number of cells per mL was calculated as shown in equation 3.

$$No.\ cells/mL = average\ cell\ count\ x\ 5\ x\ 10^4 \qquad \textbf{Eqn. 3}$$

2.3.5.3 Preparation of Cells for Mapping

4×10^5 cells (PNT2; normal human prostate epithelium) in 2 mL media (RPMI) were plated in wells with coverslips and incubated overnight at 37°C, 5 % CO_2. Probes were then added (various concentrations) and incubated for the desired length of time at 37 $^\circ$C, 5 % CO_2. After the desired incubation time, samples were fixed using 4 % paraformaldehyde in PBS.

Media was removed and samples were washed three times with PBS. Paraformaldehyde solution was then added and samples were incubated at room temperature for 15 minutes. The paraformaldehyde solution was then removed and

samples were washed once with PBS and twice with water before being left to air dry.

Coverslips were then mapped using a Renishaw In Via Raman microscope system with a 50x objective.

Wire 4.4 software was used to process the data by removing cosmic rays and subtracting the background from each spectrum. Direct classical least squares (DCLS) was then used to create false colour images by comparing the spectrum at each point in the map to a reference spectrum of the dye(s). 0.3 was found to be an acceptable DCLS cut-off for discriminating between dye and unrelated signals.

2.3.6 Cell Toxicity

2.3.6.1 Cell Counting

In order to assess the toxicity of the probes cell counting was employed. 4×10^5 cells were plated in 2 mL media and incubated overnight before nanoparticle probes were added. The cells and probes were then incubated overnight prior to cell counting. A cell scraper was used to ensure all cells were lifted from the bottom of the well for counting.

Each sample was carried out in triplicate and the average of three cell counts per replicate was used.

Cell viability was assessed by comparing the cells containing probes to those without probes (equation 4). Control samples were incubated without the additions of probes.

$$Cell\ viability = \frac{cell\ count\ after\ incubation\ with\ probes}{cell\ count\ of\ control}\ x\ 100\ \% \qquad \textbf{Eqn. 4}$$

2.3.6.2 MTT Assay

Cells (4×10^5 /mL in 1 mL) were incubated in a 96-well plate overnight (37 °C, 5 % CO_2). After 24 hours, nanoparticles and/or probe was added (total volume 100 µL/well, various concentrations) and incubated for a further 24 hours. 100 µL of RPMI media was added to cells as a positive control and DMSO was added as a negative control.

MTT was dissolved in PBS at 5 mg/mL and filtered. 10 µL MTT was then added to each well, resulting in a final MTT concentration of 0.45 mg/mL. Samples were then incubated for 4 hours at 37 °C.

After 4 hours, the media was removed and 100 µL of DMSO was added to each well to dissolve the formazan crystals resulting in a colour change from pale yellow to purple for wells containing live cells. The absorbance was then measured at 570 nm, with a reading taken at 690 nm used as a control.

3. Raman *In Situ* Hybridisation

3.1 Introduction

In situ hybridisation, discussed in section 1.1.4, is a method of detecting the localisation of specific oligonucleotide sequences in cells using complementary, labelled oligonucleotides. Originally, oligonucleotide probes were radioactively labelled, however it is now more common to use fluorescent labels to give fluorescence *in situ* hybridisation (FISH).

In FISH, an oligonucleotide complementary to the sequence to be detected is functionalised with a fluorescent molecule. This means that the sequence can be visualised using fluorescence microscopy when hybridisation occurs *in situ*.

Figure 3.1 shows FISH images of GAPDH mRNA detection in fixed HDF cells. The images compare the fluorescently labelled GAPDH probe (5'-Cy5-GAGTCCTTCCACGATACCA) with a fluorescently labelled negative control probe (5'-Cy5-AAAAAAAAAAAAAAAAAAAA). [84]
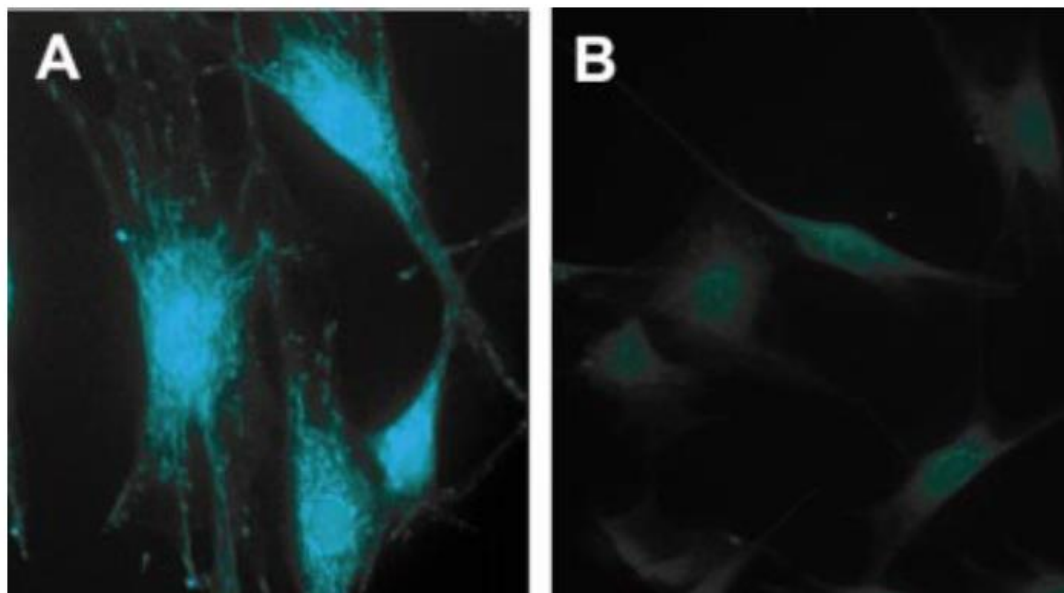
Figure 3.1 - FISH images of detection of A) GAPDH mRNA and B) negative control in fixed HDF cells. Reproduced with permission from [84]. *Copyright © 2004, Oxford University Press.*

The aim of this work was to develop a similar approach using Raman spectroscopy, termed Raman *in situ* hybridisation or 'RISH'. Due to the sensitivity limitations of spontaneous Raman spectroscopy, oligonucleotides were attached to a gold nanoparticle to provide SERS.

Unlike molecular beacon-type approaches, these probes provide no switchable signal. The probes are always 'switched on' – there is no difference in signal whether the probe is free or bound to the target – meaning that wash steps are relied on to remove unbound probes from the cells.

Two different nanoparticle probe methods were evaluated: i) oligonucleotides labelled with a Raman-active dye were attached to gold nanoparticles via spermine, and ii) an oligonucleotide and a Raman active dye were both conjugated to AuNP separately via a thiol linker. Figure 3.2 shows a schematic representation of the probes.

The assay format is the same for both probes and is relatively straightforward. Probes were incubated with cells, usually overnight. The cells were then fixed and mapped using a Raman microscope to visualise the probe location within the cells.
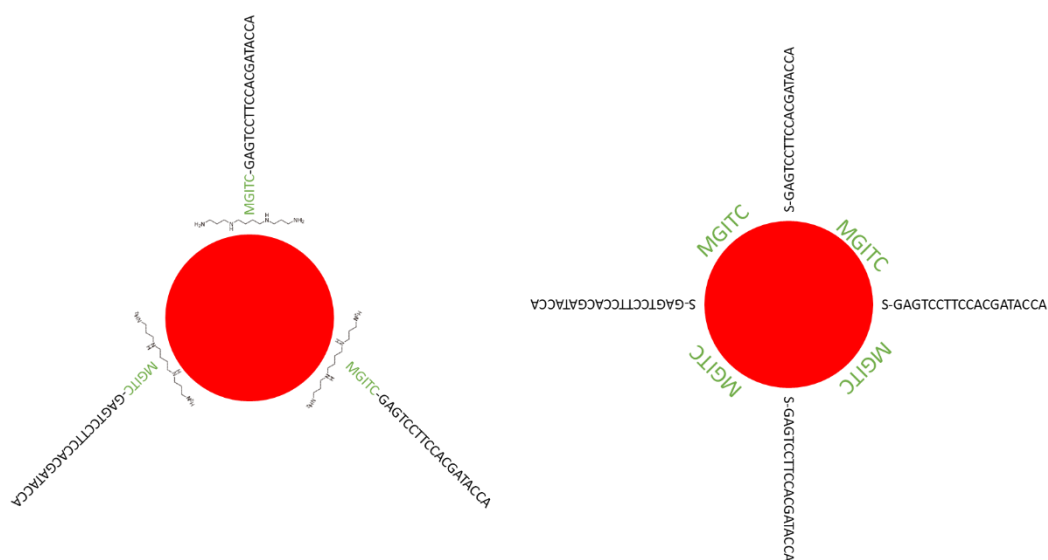
Figure 3.2 - Schematic representation of two RISH probe designs. Left – labelled oligonucleotide electrostatically attached to AuNP via spermine. Right – oligonucleotide attached to labelled-AuNP via a thiol linker.

3.2 Nanoparticle Synthesis & Characterisation

Gold citrate-capped nanoparticles were synthesised according to the Frens method. [63] Approximately 20 nm and 40 nm particles were synthesised; Figure 3.3 shows a sample of each. The larger particles have a slightly more purple colour compared with the bright-red smaller particles due to their red-shifted LSPR peak.
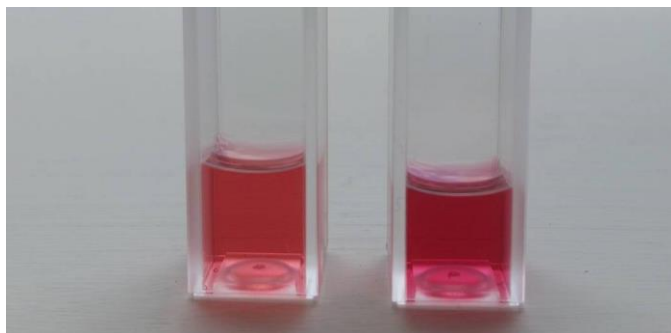

Figure 3.3 - Small and large spherical gold nanoparticles.

Extinction spectroscopy was used to characterise the nanoparticles and estimate their concentration according the Beer-Lambert law (equation 5), where *A* is absorbance, *ε* is the molar extinction coefficient, *c* is the concentration and *l* is the path length (usually 1 cm).

$$A = \varepsilon\, c\, l$$ **Eqn. 5**

Whilst the Beer Lambert law has been used to approximate concentration, it is worth noting that as nanoparticles are present as a suspension this law is not ideal due to additional scattering caused by the particles. [88] However, at low concentrations it can give an approximate value.

Figure 3.4 shows the normalised extinction spectra for the small and large nanoparticles. Due to the large extinction coefficient of gold nanoparticles, both samples had to be diluted prior to analysis (1:1 dH_2O). The smaller particles had a λ_{max} of 521 nm, characteristic of 20 nm AuNP, whilst the large particles had a λ_{max} of 530 nm.
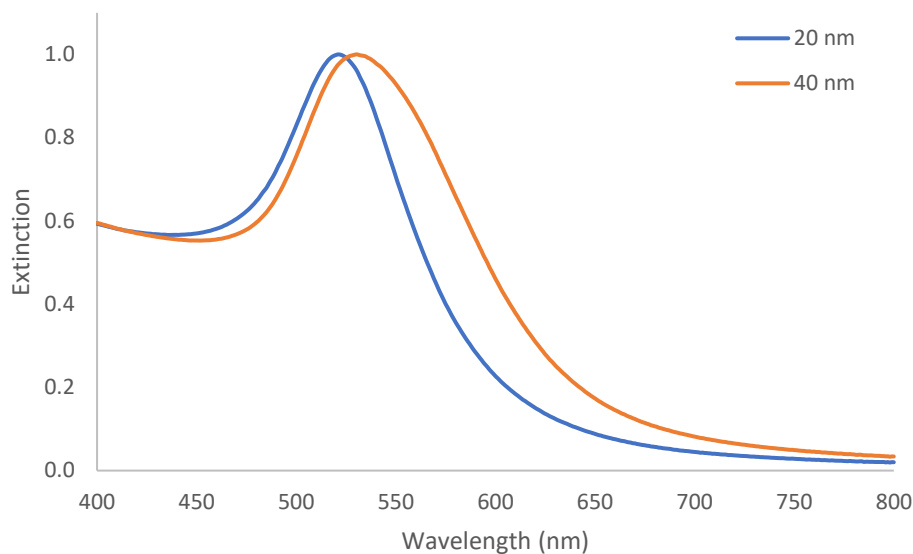
Figure 3.4 - Normalised extinction spectra of 20 nm (blue) and 40 nm (orange) gold citrate nanoparticles.

The larger nanoparticles have a slightly broader LSPR peak, indicating that they are more polydisperse than the smaller particles.

Haiss *et al.* stated that the size of spherical gold nanoparticles sized between 25 – 120 nm can be determined based on their extinction spectrum alone since the λ_{max} is correlated with the size. [89] According to this method, a λ_{max} of 530 nm corresponds to particles 46 nm in size. Since the size of the particles is determined from tabulated data correlating λ_{max} with particle diameter, it is important to note that the accuracy of this value will be linked to the accuracy of the λ_{max} reading from the extinction spectra. This will also be influenced by the polydispersity of the colloid.

The nanoparticle size was used to determine the extinction coefficient for each set of particles which, along with the absorbance (with dilution taken into account), was used to estimate their concentration.

Dynamic light scattering was also used to determine the size of the particles and the zeta potential was determined to measure the stability of the particles. For citrate-coated nanoparticles, a negative zeta potential is expected since citrate is a

negatively-charged molecule (Figure 3.5). The further the Zeta potential is from zero (no charge), the more stable the nanoparticle suspension is.
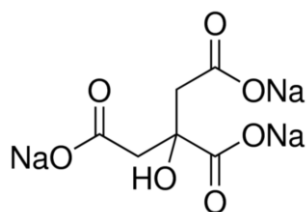

Figure 3.5 - Trisodium citrate structure.

Table 3.1 gives an example of the λ_{max}, size and zeta potential of the nanoparticles Note: multiple batches of particles were made throughout – hence why some slight shifts in λ_{max} values are seen. However, batches were kept consistent for comparable experiments.

For both sets of particles, the size determined using DLS is larger than that determined from extinction spectroscopy. DLS gives particle sizes of 48 and 57 nm, respectively for the small and large particles, however the size determined based on the SPR in the extinction spectra are in better agreement with the synthesis protocols used. SEM images also support the extinction spectroscopy determined sizes of the particles.

The 20 and 46 nm particles have a Zeta potential of -44 and -47 mV, respectively, indicating that both batches of particles are stable.

Table 3.1 - Characterisation of gold nanoparticles

Particles	λ_{max} (nm)	Size / λ_{max} (nm)	Size / DLS (nm)	Zeta potential (mV)
20 nm	520	20	48.4 ± 0.1	- 43.8 ± 0.3
40 nm	531	46	56.8 ± 0.9	- 47.1 ± 4.5

For the DLS size, peak 1 size was taken as long as this was over 80 %. For the 20 nm particles peak 1 was 93 %, indicating they are relatively monodisperse, and as expected for the 40 nm it was slightly lower at 84 %, confirming they were more

polydisperse. There is a discrepancy between the DLS data and the expected size of the particles. DLS is known to give the hydrodynamic radius of the particles, which includes any associated counterions, however this does not explain the magnitude of the size difference measured. It is possible that there are a small amount of larger particles or aggregates increasing the DLS size, particularly for the 40 nm particles which appear to be polydispersed.

Figure 3.6 shows SEM images of the 20 nm and 40 nm citrate-capped AuNP. The particles appear spherical, as expected, and relatively monodisperse. Some of the particles have formed clusters when drying on the silicon, as is commonly observed. One way to reduce this effect would be to dilute the samples further before drying. Overall, the particles were deemed acceptable for conjugation.
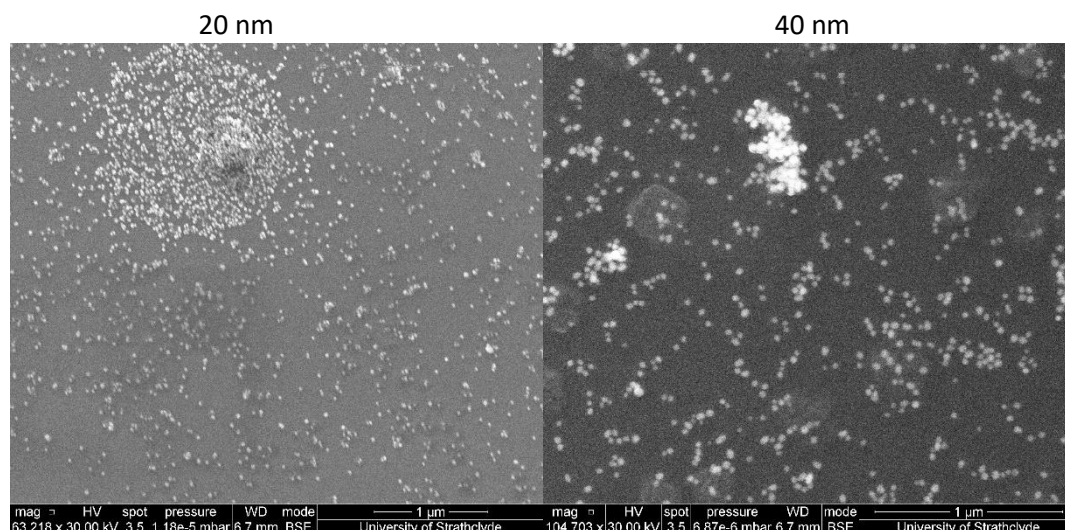
Figure 3.6 - SEM images of 20 nm (left) and 40 nm (right) AuNP.

3.3 Raman Reporter

3.3.1 Malachite Green Isothiocyanate

Malachite green isothiocyanate (MGITC) is a Raman active dye molecule with a λ_{max} ~ 630 nm making it resonant with a 633/638 nm laser line Raman setup. The isothiocyanate group facilitates conjugation to gold nanoparticles.
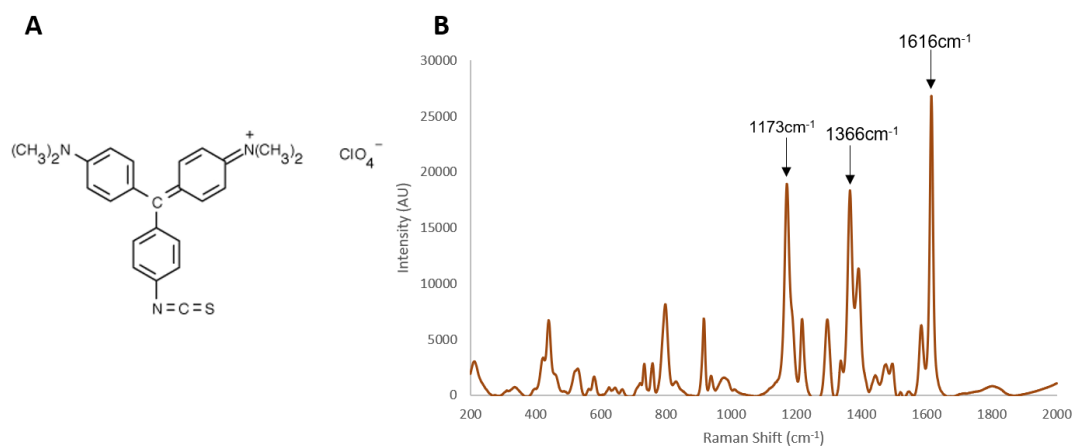

Figure 3.7 – A) MGITC Structure and B) reference SERRS spectra recorded at 638 nm (100 % power, 1 second acquisition time).

Figure 3.7 shows a standard SERRS spectra of MGITC (1 µM MGITC in 40 nm AuNP). The main signals corresponding to MGITC are at 1173 cm^{-1}, 1366 cm^{-1} and 1616 cm^{-1}. These can be attributed to in plane benzene *v9* mode, N-phenyl ring stretching and N-phenyl ring stretching and C-C stretching, respectively. Table 3.2 (adapted from Kaminska *et al.*) gives a summary of selected SERS bands. [90]

Table 3.2 - Selected bands assignments for SERS spectrum of MGITC

Signal (cm^{-1})	Assignment
421	Out-of-plane benzene ring deformation
441	E_{2u} benzene ring deformation
806	C-H bend from benzene ring
919	b_{1u} in-plane benzene ring
1177	v_9 benzene in plane
1297	In-plane C-H and C-C-H
1365	N-phenyl ring stretching
1618	N-phenyl ring & C-C stretching

3.2.2 MGITC-AuNP

Both 20 nm and 40 nm AuNP were functionalised with MGITC. Figure 3.8 shows the intensity of the main MGITC signal at 1616 cm^{-1} through a range of concentrations for both sets of particles. This peak was chosen as it gives the most intense SERRS response at the chosen wavelength.

As the concentration of MGITC is increased, initially the intensity of the 1616 cm^{-1} peak increases linearly, before reaching a plateau and subsequently decreasing. This indicates that the nanoparticles are becoming unstable as the MGITC concentration increases, causing them to precipitate out of solution. As the particles precipitate, they fall to the bottom of the solution meaning they are no longer in the laser path – hence the signal drops.
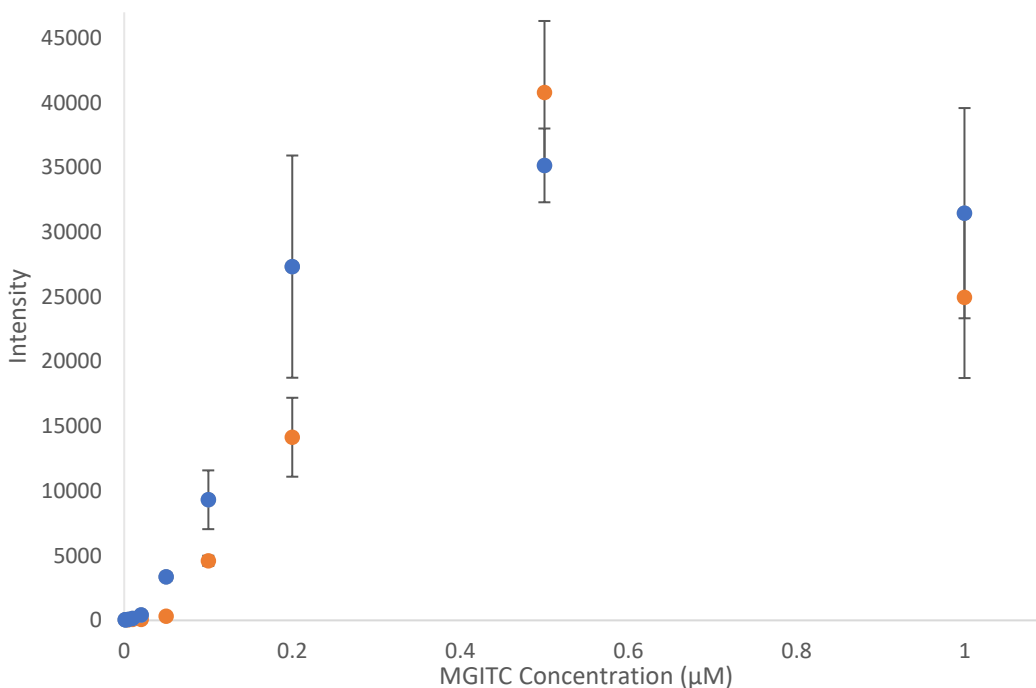
Figure 3.8 - Plot of peak intensity at 1616 cm^{-1} for MGITC-AuNP (20 nm = orange, 40 nm = blue). Values are mean ± standard deviation. Measurements made using a 638 nm laser at 100 % power and 1 second acquisition time.

The smaller, 20 nm particles have a linear range of 0.05 – 0.5 µM, whereas the larger, 40 nm particles achieved a linear range of 0.01 – 0.2 µM.

One drawback of using larger particles is that they tend to be slightly less stable than smaller particles. However, due to the greater SERS effect from larger AuNP, better sensitivity is achieved. For this reason, 40 nm particles were chosen for future experiments.

3.4 Spermine Probes

The polyamine spermine was used to electrostatically attach oligonucleotides to gold nanoparticles as shown in Figure 3.2. The aim was to create MGITC-labelled gold nanoparticles functionalised with an oligonucleotide complementary to the target sequence for hybridisation.

3.4.1 Oligonucleotide Sequences

Oligonucleotides modified with MGITC at the 5' end were purchased from ATDBio, along with the unmodified target sequence. Oligonucleotide sequences were chosen based on probes which have been published previously for GAPDH. [84] The sequences were as follows:

Probe 1: 5'-MGITC-GAGTCCTTCCACGATACCA (complementary to target)

Probe 2: 5'-MGITC-ACCATAGCACCTTCCTGAG (negative control)

Target sequence: 5'-TGGTATCGTGGAAGGACTC

3.4.2 DNA Melting Curves

The transition between single-stranded (ss) and double-stranded (ds) DNA, i.e. hybridisation, can be monitored using UV-vis spectroscopy.

Since there is no switchable signal with the RISH probes, i.e. there is no aggregation or change in SERRS expected upon target hybridisation, a DNA melting curve was carried out to ensure hybridisation did occur between the target probes and the target sequence (and not between the negative control probe and the target sequence).

As a result of stacking of the base pairs which occurs in dsDNA, dsDNA shows lower absorbance at 260 nm compared to ssDNA. This means that, when the target probe and target hybridise, a decrease in absorbance should be observed at the melting temperature (T_m) of the sequence. However, when the negative control sequence is added to the target no change in absorbance should occur.
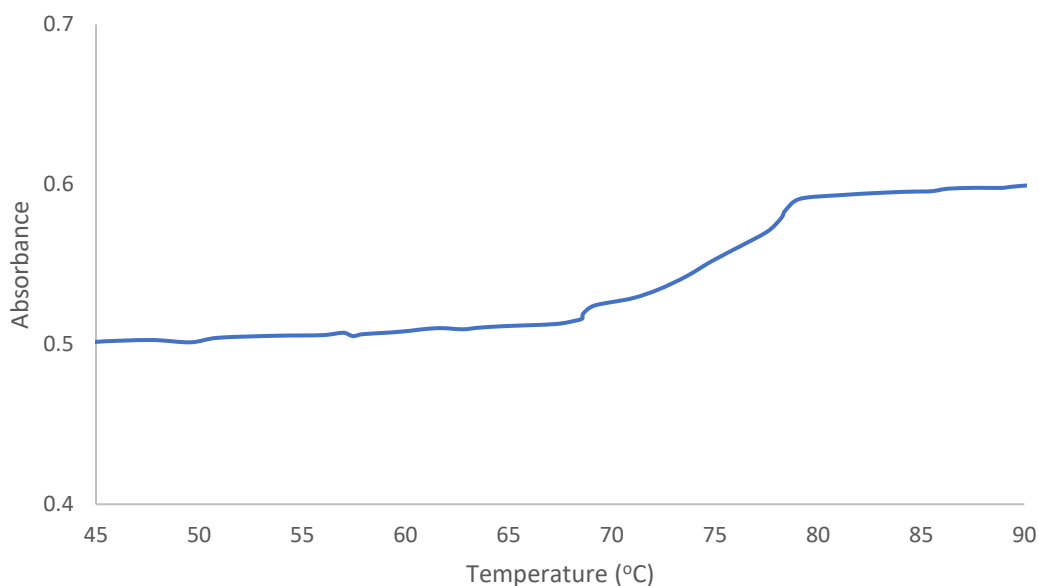
Figure 3.9 - Oligonucleotide melting curve for complementary probe and target showing a Tm of ~ 75 °C.

Figure 3.9 above shows the melting curve obtained for probe 1 with the target oligonucleotide. When the target probe was added, a characteristic sigmoidal curve was observed, indicating the hybridisation had occurred. This shape is a result of the decrease in absorbance which corresponds to hybridisation of the two strands of oligonucleotide as the temperature drops below the melting temperature.

When the non-complementary probe was added to the target no such increase was seen (Figure 3.10), indicating that the probes hybridises specifically to its target sequence. The melting curve for the non-complementary probe does show a slight increase over time, although it is linear rather than sigmoidal.

The melting temperature for the probes was found to be approximately 73 °C. This represents the temperature at which half of the DNA is in the single-stranded state and half is hybridised (i.e. double-stranded). This means that at room temperature, the probes should hybridise to the target molecule.

The melting temperature is highly dependent on both the length and the GC content of the DNA. Longer sequences and those with a high GC content, i.e. the percentage

of the sequence which is made up of guanine-cytosine hybridisations, have higher tempting temperatures. This is because guanine-cytosine bonds contain three hydrogen bonds, whilst adenine-thymine bonds contain two hydrogen bonds, making GC bonds more difficult to break.
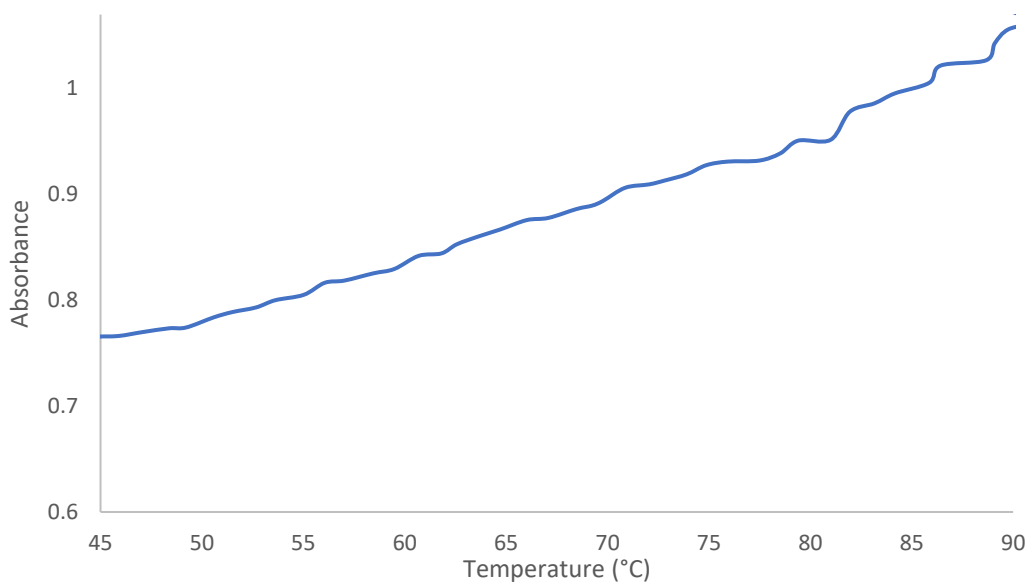

Figure 3.10 - Melting curve for non-complementary probe and target.

3.4.3 Probes Synthesis & Characterisation

In order to assess the effect of the oligonucleotide probes on the nanoparticles, an investigation was carried out with two different concentrations of probe. Figure 3.11 shows the extinction spectra of AuNP with i) no probe added, ii) a low concentration (10 nM), and iii) high concentration (500 nM) of the labelled-oligonucleotide.
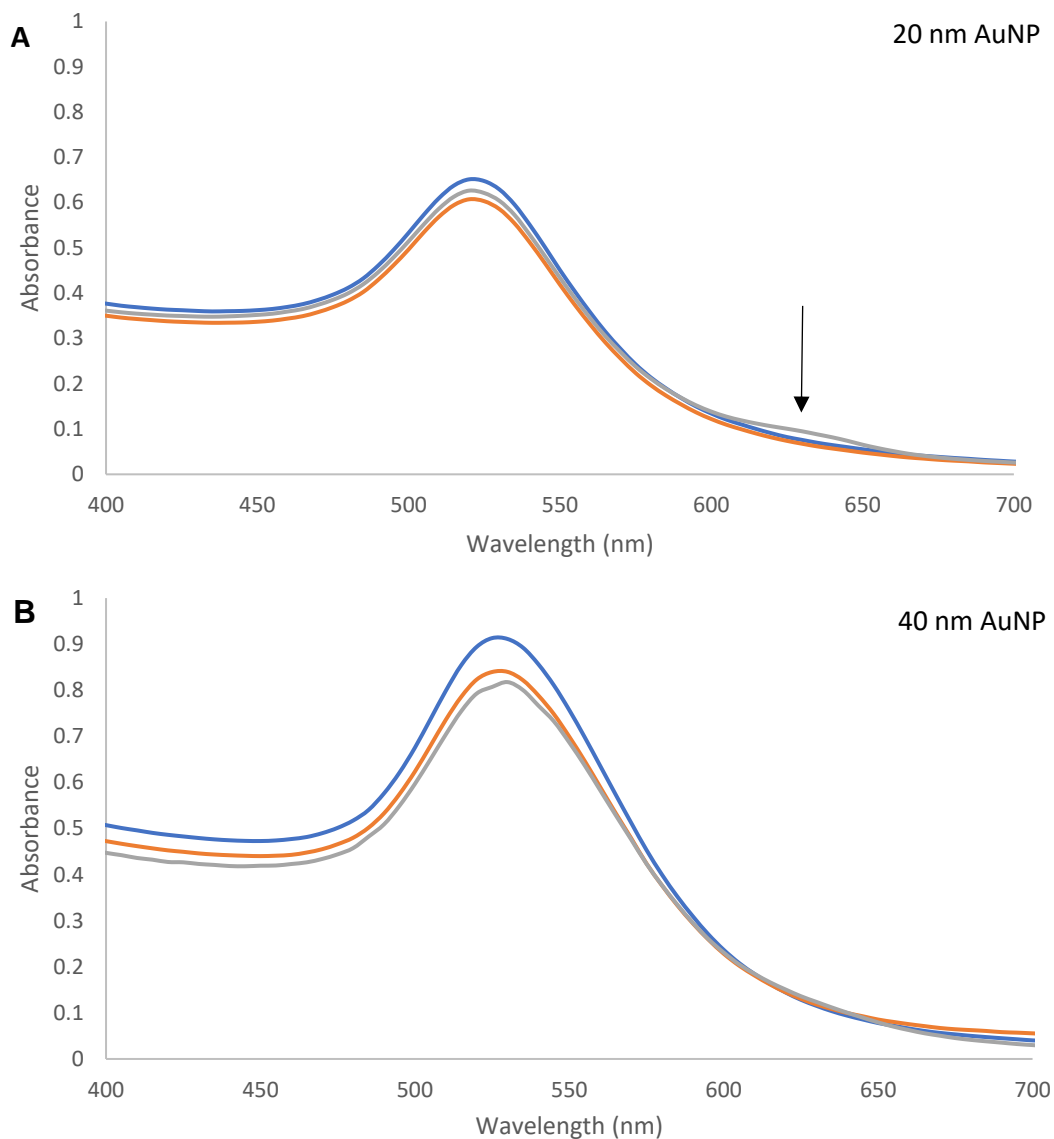
Figure 3.11 - Extinction spectra for A) 20 nm and B) 40 nm AuNP + 0 nM (blue), 10 nM (orange) or 500 nM (grey) probe 1.

A small shoulder can be seen at ~ 630 nm for the 20 nm particles containing 500 nM probe. This indicates that some aggregation has occurred. Overall, the probe doesn't appear to have a significant effect on the nanoparticles. Slight reduction in absorbance is seen, indicating that some nanoparticles have been lost – by precipitation out of solution, during the functionalisation – however, the remaining particles appear to be stable since the λ_{max} is unchanged.

Figure 3.12 shows an example Raman spectrum of the MGITC oligonucleotide probe in AuNP compared to unconjugated MGITC dye in AuNP (before any background correction). The oligonucleotide probes cause a large increase in background signal compared to the dye on its own, completely masking any MGITC signals.
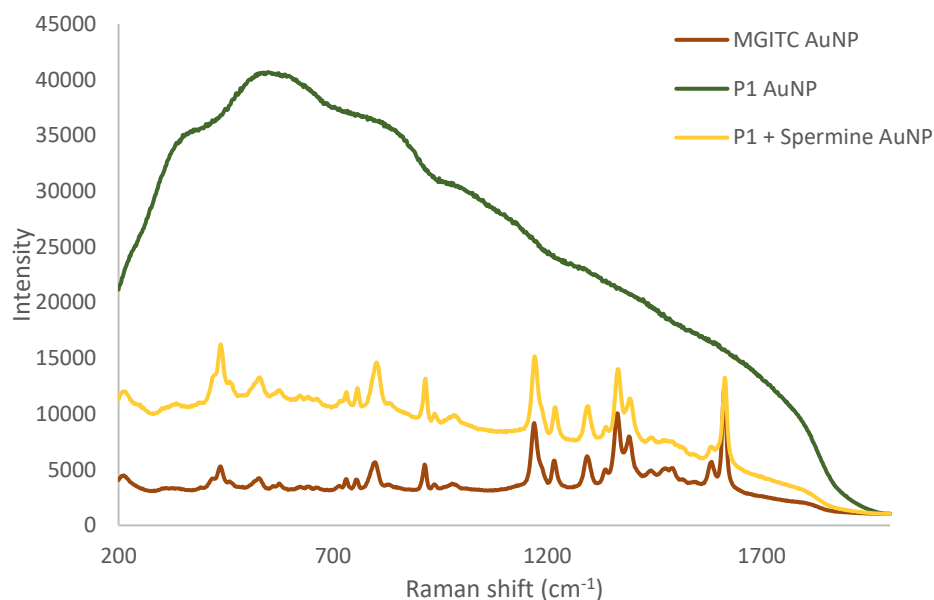
Figure 3.12 - Comparison of spectra obtained from MGITC AuNP, probe 1 AuNP (MGITC attached to oligonucleotide) and probe 1 + spermine AuNP at 633 nm.

Malachite green on its own has low fluorescence. However, Babendure *et al.* showed how its fluorescence increased when it was attached to an aptamer. [91] These experiments were performed with malachite green, not its analogue MGITC which was used in this project. However, it may be plausible to suggest that the same process is occurring here.

It is possible that the negatively charged nanoparticles are repelling the negatively charged DNA backbone, preventing the probes from coating the nanoparticles efficiently, thus the nanoparticles are not able to quench the fluorescence from MGITC.

In order to overcome this problem, spermine was introduced to the probes. Spermine (Figure 3.13) is a polyamine, i.e. it is polycationic. It is able to bring together the

negatively charged citrate surface on the AuNP and the negatively charged oligonucleotide, which would usually repel each other. [39]
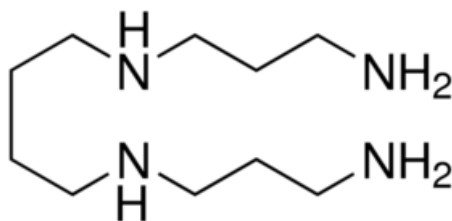

Figure 3.13 - Structure of spermine.

Adding spermine to the probe allows it to hybridise to the oligonucleotide strand, preventing repulsion between the negative charges, this can be seen in Figure 3.12. The particles containing the oligonucleotide and spermine have a much reduced background signal compared to those without spermine, indicating that they are on the nanoparticle surface. Spermine also causes aggregation of the nanoparticles, enhancing the SERRS signal.

Various spermine concentrations were assessed in order to determine which was most suitable. A final concentration of 16 nM was chosen.

Figure 3.14a shows the spectra obtained for a range of probe 1 concentrations (1 nM – 500 nM). Spermine was pre-mixed with oligonucleotide before being added to nanoparticles (0.4 nM). Figure 3.14b shows the peak intensity at 1616 cm^{-1} for each sample. Samples with higher concentrations of probe 1 show large error bars due to aggregation.

It can be seen that the background is still a problem, however it is reduced compared to the samples without spermine. As seen previously, at higher concentrations the peak intensity starts to plateau as the nanoparticles become less stable.
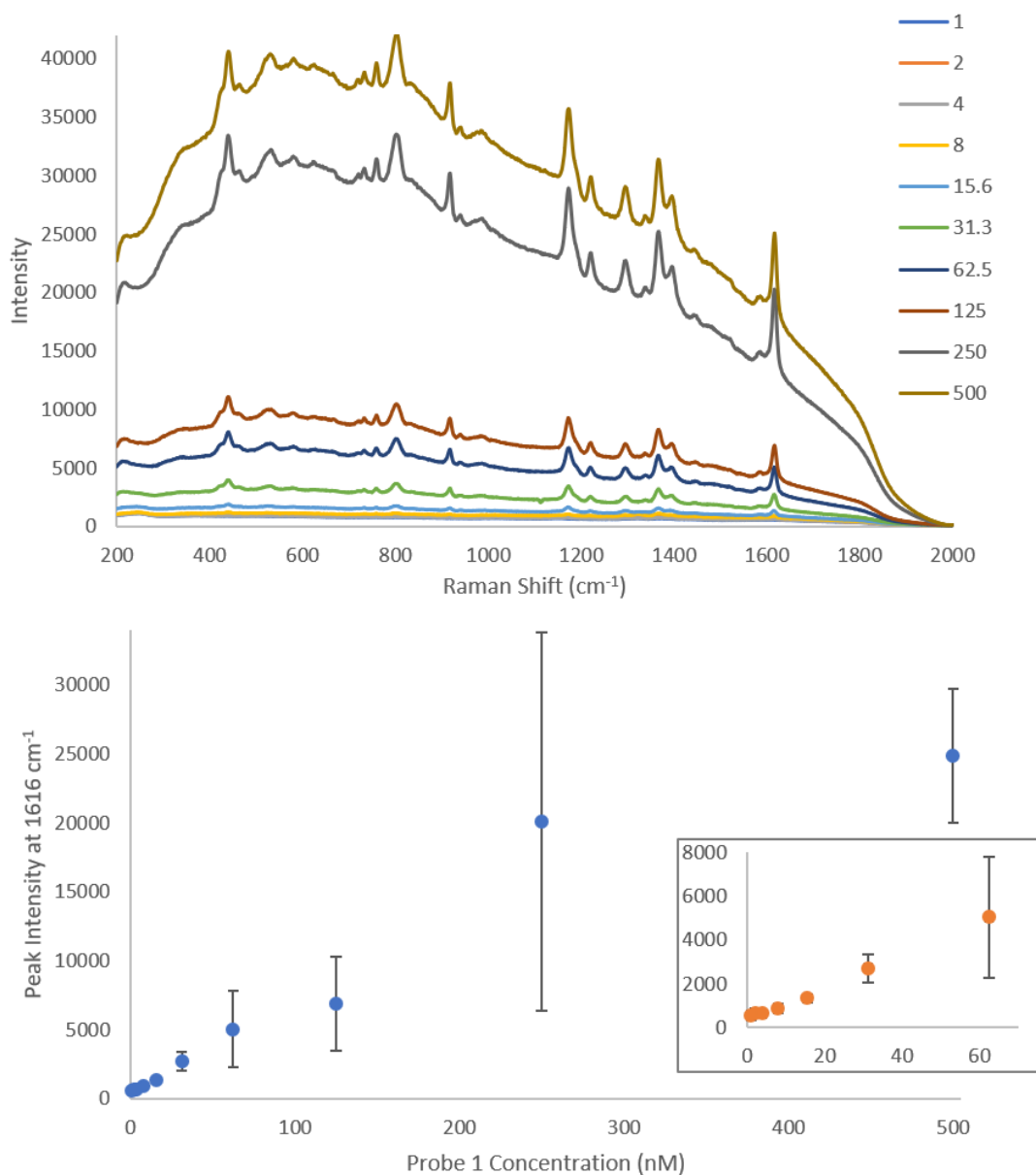
Figure 3.14 - A) Spectra obtained and B) peak intensity at 1616 cm^{-1} for various probe concentrations, inset shows lower concentrations. Spermine was pre-mixed with the probe before being added to AuNP. Samples were analysed using a 633 nm laser at 100% power and 1 second acquisition time.

3.4.4 Single-Stranded vs Double Stranded DNA

Despite there being no 'switchable' signal of the dye in the ISH assay, an investigation was carried out to determine if the Raman signals were altered by the addition of the target molecule, i.e. when the hybridisation had occurred and the oligonucleotide was in its double-stranded state.

The reason for this is that it has been shown that SERRS enhancement of silver nanoparticles may be influenced by whether DNA is in its single-stranded (ss) or double-stranded (ds) form. A SERS label was added to an oligonucleotide sequence (either ss or ds) which was combined with aggregated nanoparticles and the SERS spectra were recorded. A higher SERRS enhancement was observed with particles containing ssDNA compared to those with dsDNA. [92] Hence, a study was carried out to assess whether a similar effect is seen with gold nanoparticles.

Oligonucleotides probes were mixed with spermine before being added to AuNP. The mixture was then shaken before target was added. Each sample was heated to 85 °C (above the melting temperature) for 10 minutes and allowed to cool before being analysed by Raman spectroscopy using a 638 nm laser excitation. Table 3.3 shows the final concentration of each component of each sample.

Table 3.3 - Final concentration of each component of the mixtures

Sample	Probe 1 (nM)	Probe 2 (nM)	Target (nM)
P1	25	0	0
P2	0	25	0
T	0	0	25
P1T	25	0	25
P2T	0	25	25

Probe 1 and probe 2 are identical in terms of structure, i.e. 19 nucleotide bases conjugated to MGITC, so should give the same SERRS spectra. However, only probe 1

should hybridise to the target oligonucleotide. If the spectra is influenced by whether or not hybridisation had occurred, it would be expected that there would be a difference in the spectra of P1T and P2T.

Figure 3.15 shows the peak intensity for the main peak at 1616 cm^{-1} for each sample. The target itself has negligible intensity as it does not have a dye attached. It can be seen that there is no significant difference between ss and dsDNA indicating that the SERS spectra was not influenced by whether the DNA is in its ss or ds state.

There appears to be more variability in samples containing both probe and target, however, as this is seen for both probe 1 and probe 2, it was not thought that this effect was related to hybridisation occurring since probe 2 does not hybridise to the target. It is possible that the higher variability was a result of the target competing with the probe to occupy the nanoparticle surface. Since the target doesn't have a dye attached, if it displaces the labelled-oligonucleotide, it will affect the SERS signal.

It is also worth noting that, although the same final concentration of both probes was used, probe 2 gave a lower signal than probe 1. The probes were purchased commercially but this possibly indicates that the MGITC conjugation was less successful with probe 2 than probe 1.
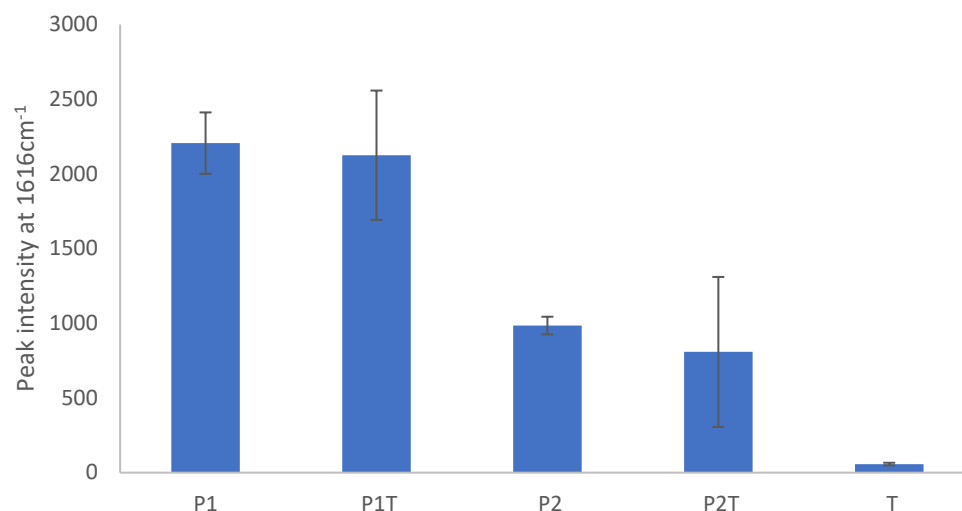
Figure 3.15 - Bar chart showing peak intensity at 1616 cm^{-1} for ss vs dsDNA SERRS. Results are mean ± standard deviation. Samples were analysed at 633 nm using 100% power and a 1 second acquisition time.

A one to one ratio of probe:target oligonucleotide was used to replicate the same conditions as for the DNA melting curve which indicated that hybridisation did occur. However, a further experiment was carried out altering the probe to target ratio. The concentration of probe 1 was kept constant whilst the target concentration was altered to assess whether any changes in SERRS intensity was seen.

Four samples were measured: probe 1 with no target, and 1:0.5, 1:1 and 1:2 probe:target ratios. The probe concentration was 50 nM for all samples. The result of the peak intensity at 1616 cm^{-1} for each sample is shown in Figure 3.16. Each sample was carried out in triplicate.
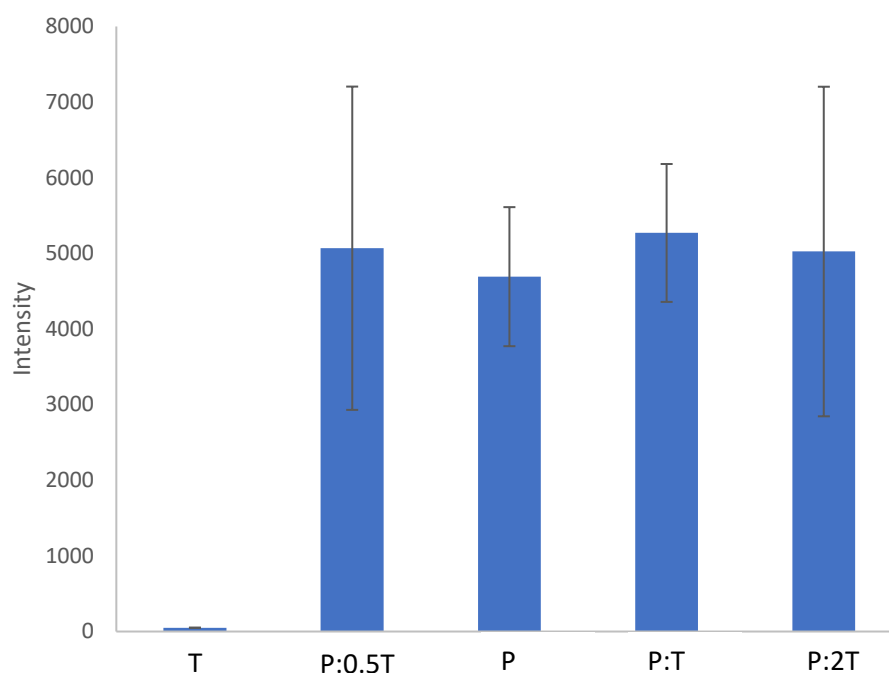
Figure 3.16 - Bar chart showing peak intensity at 1616 cm^{-1} for samples containing probe 1 with varying amounts of the target oligonucleotide. Results are mean ± standard deviation.

Again, negligible signal was seen for the target on its own. All samples containing probe 1, regardless of the concentration of target have approximately the same mean peak intensity. This indicates that the signal does not appear to be affected by the probe to target ratio, further suggesting that the SERRS effect is not influenced by DNA hybridisation.

Whilst this data does not agree with the previously reported study on silver nanoparticles, it is worth noting that in the previous study, the oligonucleotides were allowed to form a duplex before being added to the nanoparticles, whereas in these experiments the nanoparticles were functionalised with the oligonucleotides and then incubated with the target sequence. It is possible that the electrostatic binding of spermine to the oligonucleotide, whilst facilitating nanoparticle attachment, blocks the hybridisation with the target molecule.

3.4.5 Cell Mapping

In order to determine whether the probes could be used to detect GAPDH mRNA in cells, they were incubated with PNT2 cells. GAPDH is a housekeeping gene, therefore it should be expressed in all cell types. Moreover, it has previously been measured in PNT2 cells using gene expression analysis. [93,94]

Cells were mapped using a 638 nm laser excitation with 10 % power with a 0.2 second acquisition time to reduce burning. WiRE[TM] 4.4 software was used to remove cosmic rays and subtract the background from each spectrum. DCLS was then used to create false colour images by comparing the spectrum at each point in the map to a reference spectrum of the dye. The DCLS cut-off was determined by examining the signal for each score. A score of 0.3 was found to be an acceptable DCLS cut-off for discriminating between MGITC and unrelated signals/background.

Using DCLS is advantageous over other methods of focussing on one area of the spectrum, such as the intensity at one point, as it looks at the whole spectrum at each point in the map and compares it to a reference spectrum of the dye. This makes false positive signals less likely. For example, for MGITC the main Raman signal at 633 nm is ~ 1600 cm^{-1}, however when cells are burnt by the laser a large peak appears from ~ 1500 – 1700 cm^{-1} due to aromatic carbon which can completely mask this signal (Figure 3.17). [52] By only looking at the signal intensity at 1600 cm^{-1}, any areas of burning in the cell would give false positive signals.

As well as potentially giving false positives, cell burning can mask dye signals resulting in false negatives. For this reason, it is important to choose parameters which minimise any cell burning, i.e. shorter integration times and lower laser power. It is not always possible to completely avoid burning the cells, however a compromise has to be sought between conditions which give the best sensitivity (i.e. longer integration times and higher laser power) whilst causing minimal burning to the sample. The optimal conditions depend on the individual sample with factors such as the cell type and the presence of nanoparticles or other substances added having an

impact. Due to nanoparticles heating in the presence of the laser, they can make cells more likely to burn.
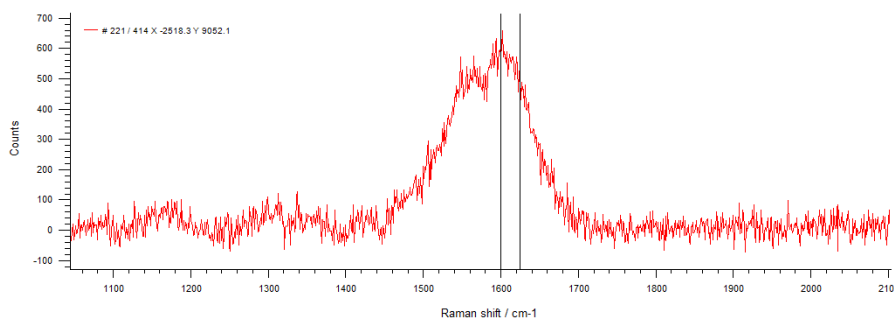

Figure 3.17 - Example spectrum showing the broads peaks characteristic of cell burning during Raman mapping.

Initially, starting with the simplest concept, the MGITC-labelled oligonucleotides only were incubated with PNT2 cells. This method would be comparable to FISH since no nanoparticles were used.

No signal could be measured from PNT2 cells after overnight incubation with the MGITC-oligonucleotide probe at 200 nM with the acquisition settings used. This was to be expected due to the inherent lack of sensitivity with Raman spectroscopy. Due to the quantity available/cost of the MGITC-oligonucleotide it was not feasible to use higher concentrations and some cell burning was already observed meaning higher acquisition times were not possible. For this reason, the next step was to incorporate gold nanoparticles into the assay to make use of their enhancement effect.

Figure 3.18 shows bright field images of cells after incubation with A) media only, B) AuNP (0.1 nM, 40nm), and C) 100 nM probe 1 + spermine + 0.1 nM. The cells incubated with bare nanoparticles appear to show dark spots both within and surrounding the cells. These are most likely aggregated nanoparticles which have precipitated in the cell media, then been fixed to the glass slide. It is impossible to tell from bright field images alone whether these particles have entered the cell or are on the surface. The cells incubated with nanoprobes (oligonucleotide + spermine + AuNP) show less of these dark spots, indicating that these probes are more stable than bare AuNP in the cell media.
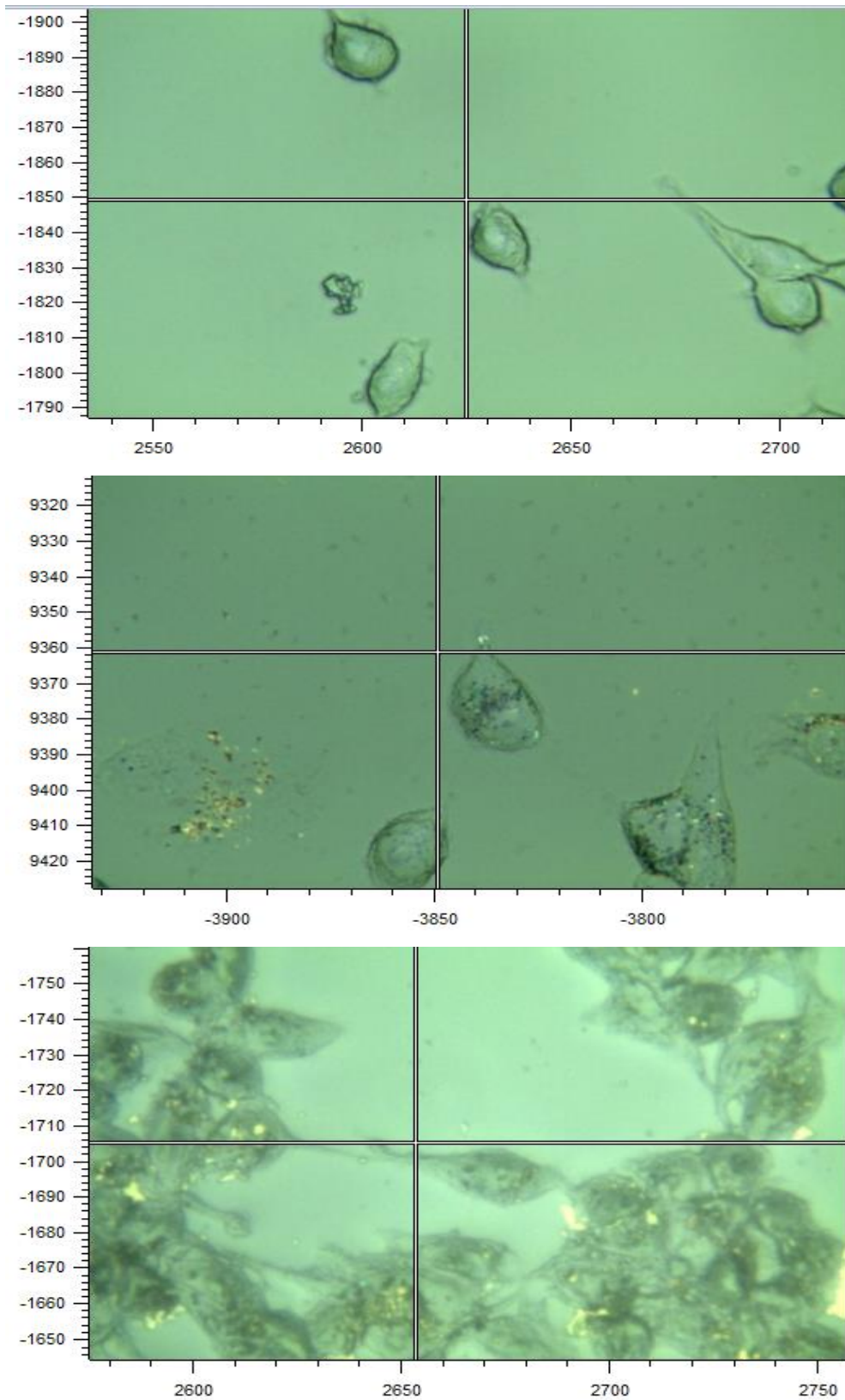
Figure 3.18 - Bright field images of cells incubated with A) media only, B) bare AuNP and C) nanoprobes.

Figure 3.19 shows false colour cell mapping images for the complementary nanoprobes in PNT2 cells (100 nM probe 1 + spermine + 0.1 nM AuNP). It was expected that probe 1 would bind to the target mRNA inside the cell, resulting in signal, whilst probe 2 would not bind and so would be removed from the cell. Figure 3.20 shows the cells incubated with the probe 2 nanoprobes (random control).
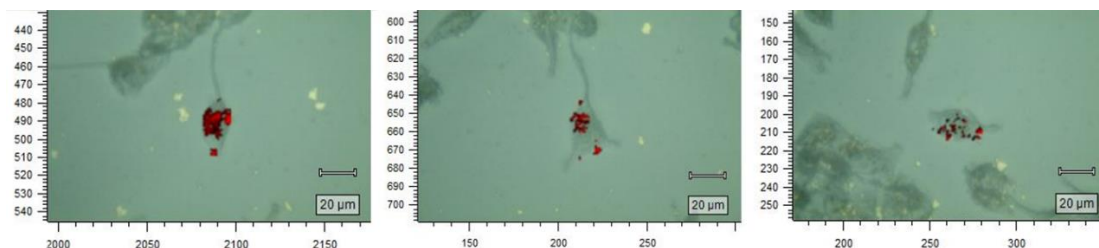

Figure 3.19 - False colour images for PNT2 cells incubated with 100nM probe 1 (complementary to GAPDH mRNA) + spermine + 0.1nM AuNP (40 nm). Cells were mapped using a 633 nm laser at 10 % power and 0.2 second acquisition time. Spectra were taken at 1 μm steps.

Both sets of samples indicated probe signal in/around the cells. From the bright field images, it was not possible to confirm if the probes were inside the cells.

No significant difference was observed between the signal observed for probe 1 and probe 2. Both samples show significant signal from the probes, indicating a lack of specificity for the target probe.
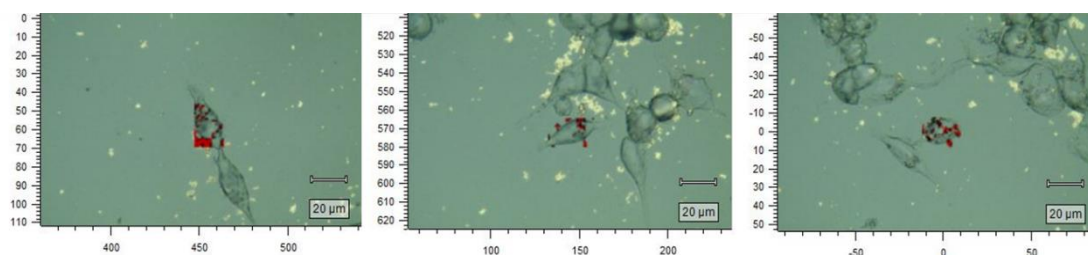
Figure 3.20 - False colour images for PNT2 cells incubated with 100 nM probe 2 (random control) + spermine + 0.1 nM AuNP (40 nm). Cells were mapped using a 633 nm laser at 10 % power and 0.2 second acquisition time. Spectra were taken at 1 μm steps.

The bright spots in and surrounding the cells were thought to be scattered light from salt crystals from PBS. In order to reduce this, an additional water wash step was included at the end of the fixing process.

Although MGITC signal can be observed in the samples, it was difficult to determine whether it is coming from within the cell or the cell surface. In order to determine whether the probes were actually inside the cells 3D mapping was carried out. To take a 3D Raman map of a cell, 2D maps are taken at various points along the z-axis to build a 3D picture of the cell (Figure 3.21).
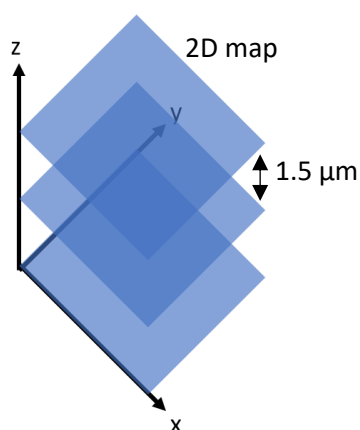
Figure 3.21 - Schematic representing how 3D cells maps are built.

Figure 3.22 shows a representative 3D map. The signal is distributed throughout the z plane, indicating that the probes are within the cell.

For this experiment a lower concentration of gold nanoparticles was used in an attempt to improve specificity (100 nM probe + 0.02 nM AuNP). Figure 3.23 shows a comparison between probe 1 and 2 at these concentrations (top-down facing images shown only to demonstrate measured signal). When the probe concentration was also lowered proportionally to the particles very little signal was observed (Figure 3.24).
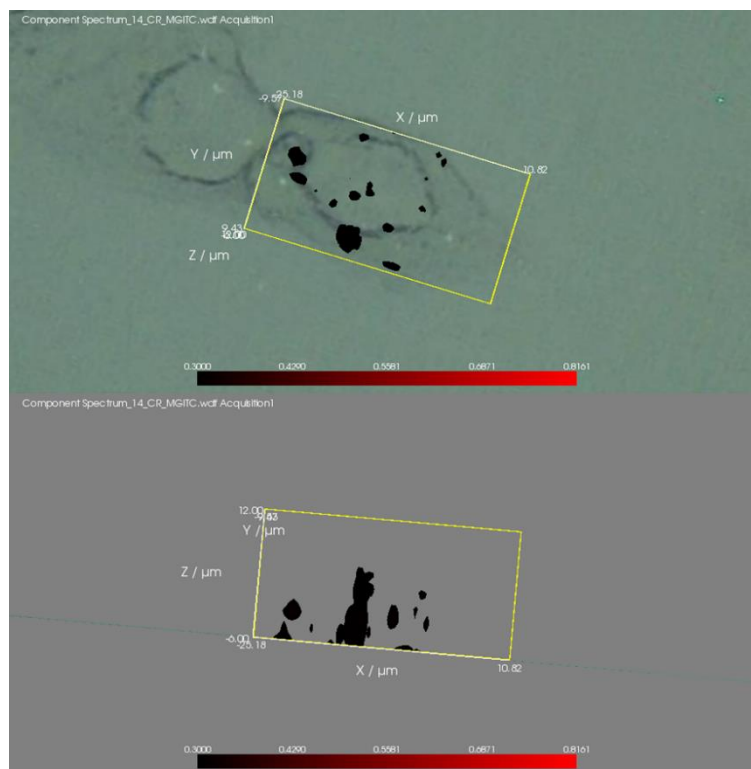
Figure 3.22 - Representative 3D map showing distribution of MGITC signal within a cell (top – face down view, bottom – side on view). Cell was mapped using a 633 nm laser with 10 % power and 0.2 second acquisition time, steps were taken at 1 μm in the x and y directions and 1.5 μm in the z plane.

The distribution of signal throughout the different cell depths mapped indicates that the probes entered the cells. Published literature also shows that functionalised nanoparticles tend to enter cells through endocytosis. [48,80] However, despite the probes getting into the cells there does not appear to be any difference between probes 1 and 2.
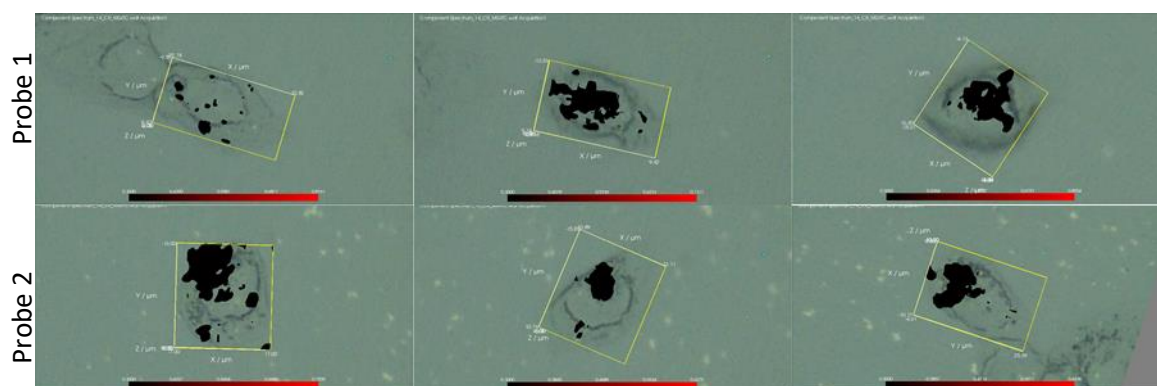
Figure 3.23 - False colour images for PNT2 cells incubated overnight with 100 nM probe 1 (top) or probe 2 (bottom) + 0.05 nM AuNP. Cells were mapped using a 633 nm laser at 10 % power and 0.2 second acquisition time. Spectra were taken at 1 μm steps in the x and plane and 1.5 μm in the z plane.

The lack of discrimination may be due to aggregation of the particles. If aggregation occurs it is possible that the aggregated particles are too large to be removed from the cell. Therefore the probes would stay within the cells whether they are bound to the target or not, resulting in non-specific signal. Similarly, it is possible that the particles are trapped inside a vesicle so are not able to find the target within the cell.

Figure 3.24 - False colour images for PNT2 cells incubated overnight with 50 nM probe 1 + 0.05 nM AuNP. Cells were mapped using a 633 nm laser at 10 % power and 0.2 second acquisition time. Spectra were taken at 1 μm steps in the x and plane and 1.5 μm in the z plane.

3.4.6 Lower Ratio

Initially, oligonucleotide:AuNP ratios were considered based on standard oligonucleotide-nanoparticle assays where approximately 2000:1 is usually a good starting point to achieve a single-layer coating. However, after further consideration of this assay format (using spermine instead of thiol for attachment), it was hypothesised that the oligos may be flat, i.e. lying horizontally on the nanoparticle

surface, rather than standing upright. Figure 3.25 shows a schematic representation of this. Based on this theory, lower ratios of oligonucleotide were assessed since, if they are lying flat on the surface, they will take up more surface area meaning less will be able to attach.
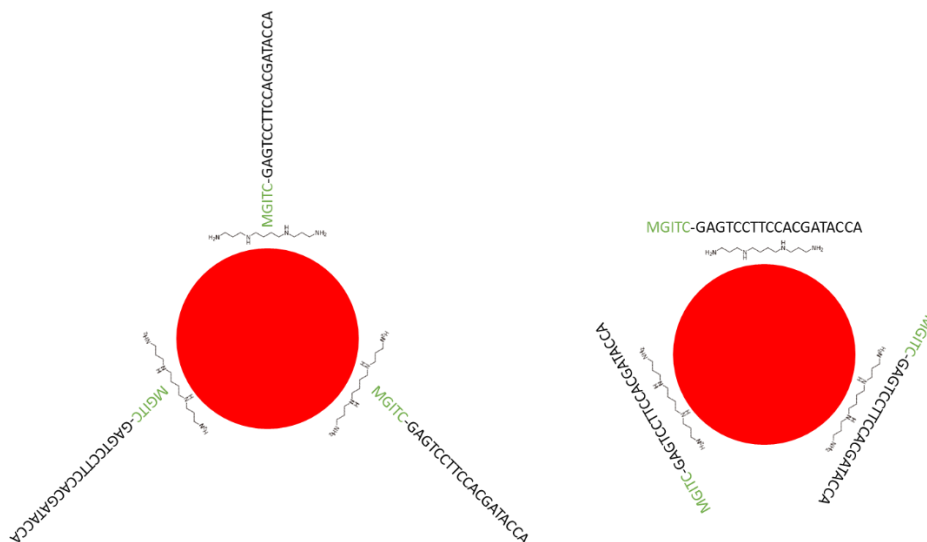

Figure 3.25 - Schematic comparison different orientations of oligonucleotide on nanoparticle surface. Left – oligonucleotides standing upright, i.e. at 90° to the surface, right – oligonucleotides attached via spermine lying flat on the surface.

Figure 3.26 shows the SERS spectra obtained for various probe:AuNP ratios. The concentrations of probe 1 and spermine were kept constant for each sample and the nanoparticle concentration was varied. Probes without spermine are shown for reference. It can be seen that as the probe:nanoparticle ratio decreases so does the background signal. One possible reason for this is that at higher probe ratios there are multiple layers of oligonucleotide on the nanoparticle surface. Although nanoparticles are known to quench fluorescence from molecules on the surface, surface enhanced fluorescence can be observed for molecules slightly further from the surface which may be the reason for the large background at high ratios. [95]
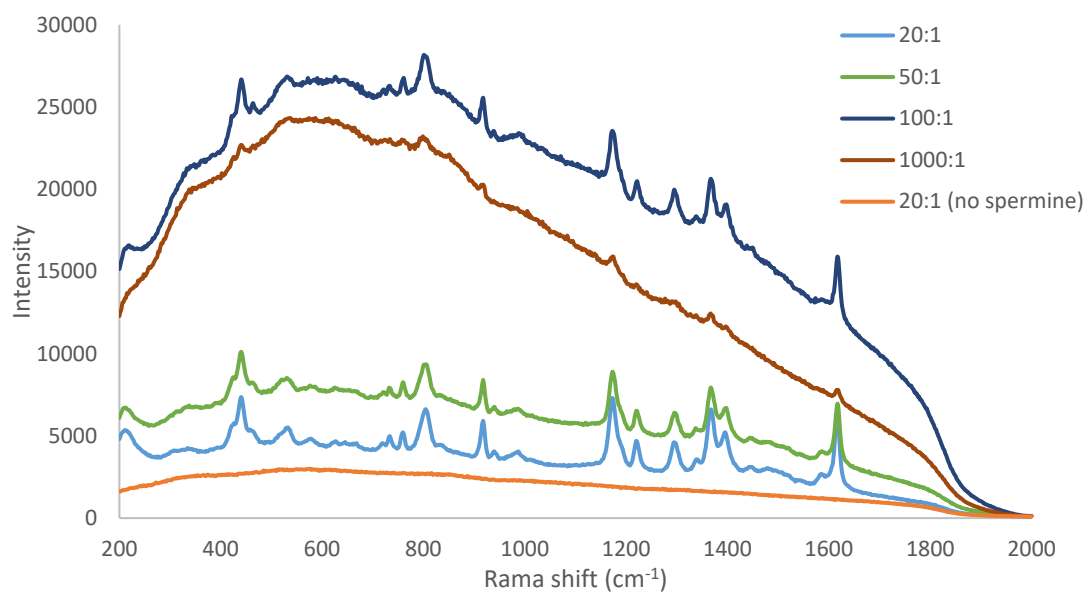
Figure 3.26 - SERS spectra obtained for various probe:AuNP ratios. Probe and spermine concentrations were kept constant at 10 nM. Spectra were taken with a 633 nm laser at 67 % power and a 0.5 second acquisition time.

Figure 3.27 shows the false colour images for cells incubated with these lower ratio probes. As opposed to the original experiment, where a probe:AuNP ratio of 1000:1 was used, probes were functionalised with a ratio of 50:1. Figure 3.28 shows the 3D images for reference – the probes appear to be distributed throughout the cell.
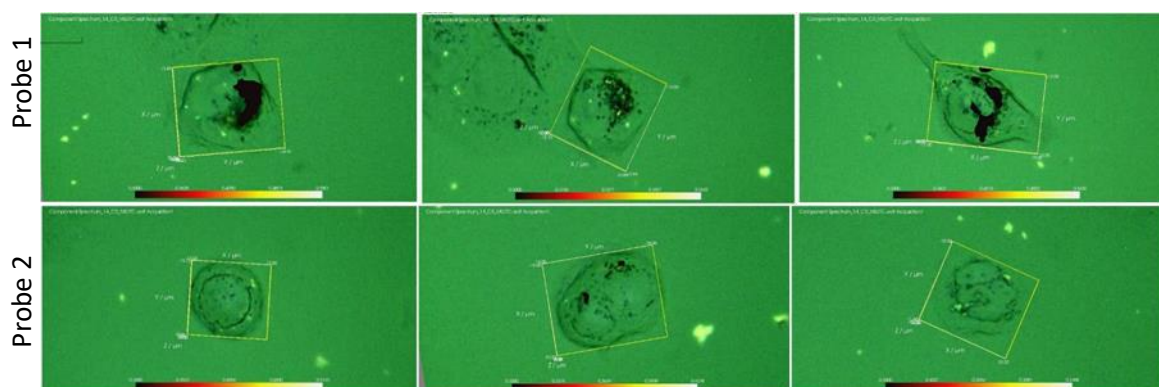
Figure 3.27 - False colour images for PNT2 cells incubated overnight with 50 nM probe (top – probe 1, bottom – probe 2) + 1 nM AuNP. Cells were mapped using a 633 nm laser at 10 % power and 0.2 second acquisition time. Spectra were taken at 1 μm steps in the x and plane and 1.5 μm in the z plane.
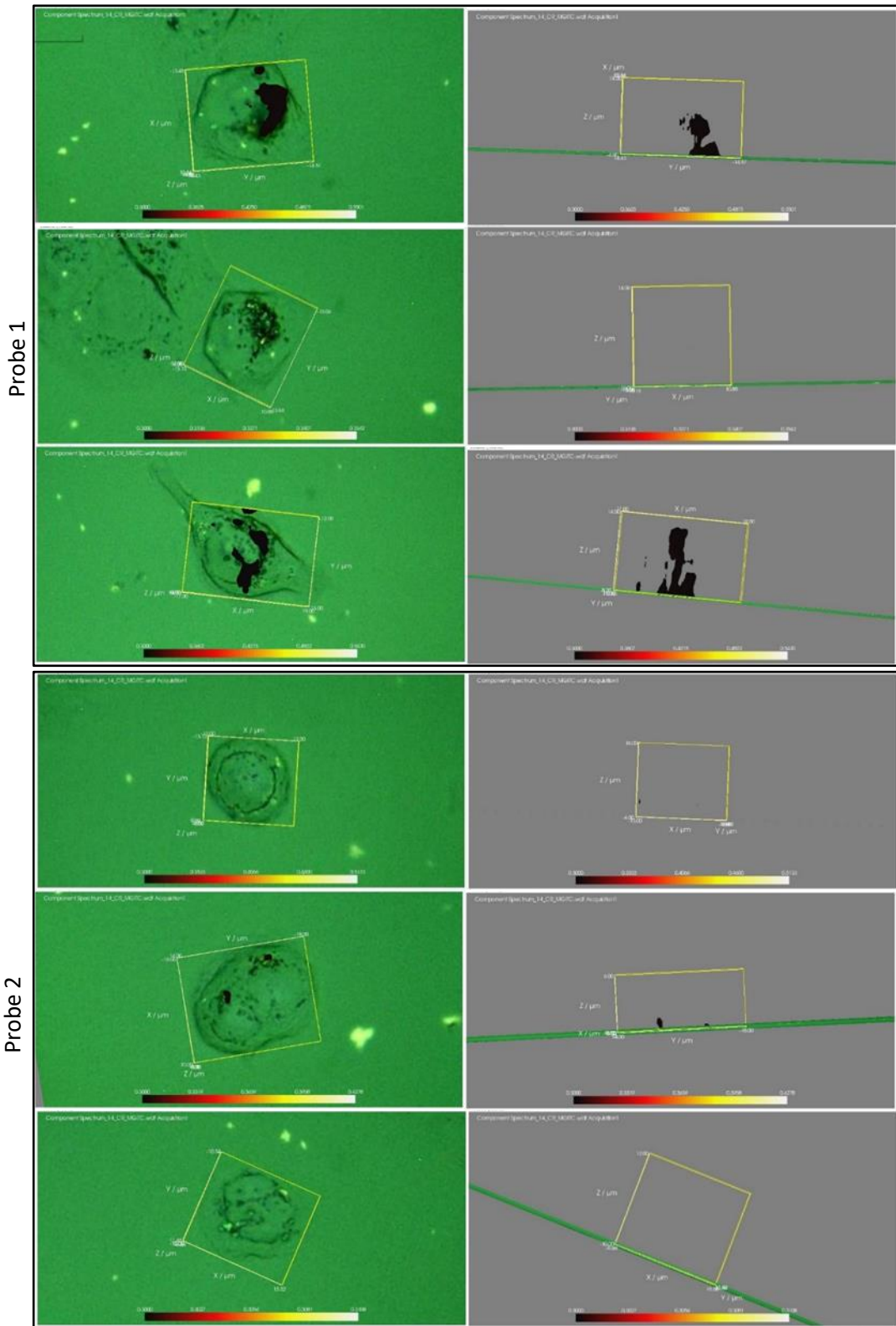
Probe 1

Probe 2

Figure 3.28 - 3D false colour images for cells incubated with lower ratio probes overnight.

Although there appears to be a slight difference in the cell signal for probe 1 and probe 2, the levels of intra-sample variability were high. Furthermore, when this experiment was repeated there was no difference between the two probes, meaning that this method is unreliable for measuring mRNA. For these reasons, it was decided not to progress with this method.

3.4.7 Separate additions

An alternative format was assessed by adding each component of the probe to cells separately. It was hoped that without the nanoparticles attached to the oligonucleotide probes, they would hybridise more readily to the target mRNA. As the probe on its own has already been shown not to give a strong enough Raman signal, nanoparticles were also added to the cells separately in the hope that their presence would increase the signal from the oligonucleotide. Figure 3.29 shows the false colour images obtained.
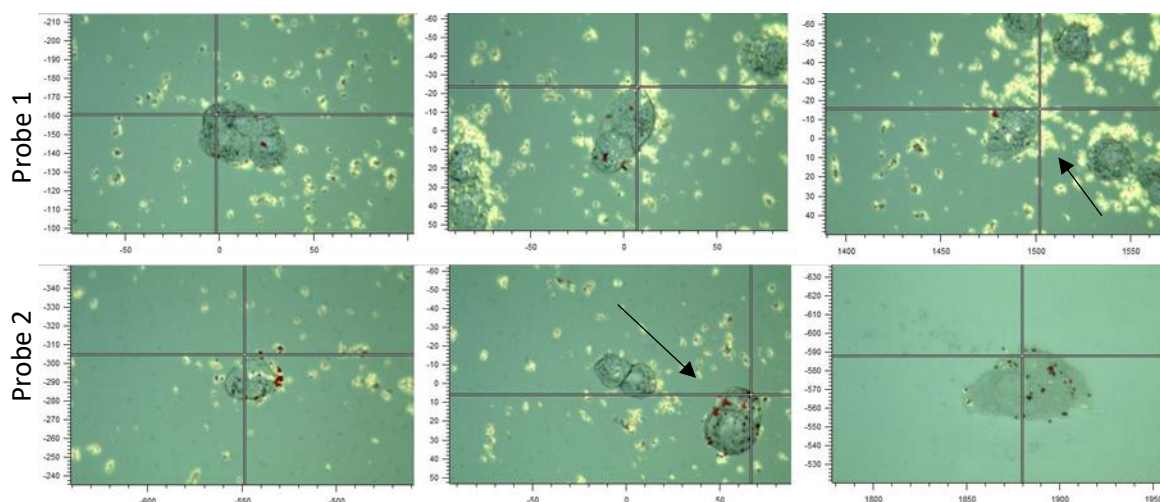

Figure 3.29 - False colour images for PNT2 cells incubated with probe (top = probe 1, bottom = probe 2), spermine and AuNP, each added separately (arrow points to mapped cell(s)). Cells were mapped using a 633 nm laser at 100 % and 0.2 second acquisition time.

Signal was observed following separate additions, demonstrating that SERS can be obtained from nanoparticles 'free' in the cell, even when not attached to the Raman

active dye. However, the signal was considerably weaker than for previous experiments where the oligonucleotide was on the nanoparticle surface.

As with previous experiments, no significant difference was observed for the two oligonucleotides, demonstrating a lack of specificity.

3.4.8 Cell Toxicity – MTT Assay

An MTT assay was used to assess the cytotoxicity of the probes. The MTT assay is a cell toxicity assay which uses a tetrazolium salt (MTT; 3-(4,5-dimethylthiazol-2-yl)-2,5-diphenyl tetrazolium bromide) to colourimetrically assess cell viability by measuring the activity of dehydrogenase enzymes within the cells. In live mitochondria, the tetrazolium ring is reduced to formazan (Figure 3.30) resulting in a colour change from pale yellow to purple in live cells. Dead cells, on the other hand, should not show any change in colour due to the absence of an active mitochondria.[96]
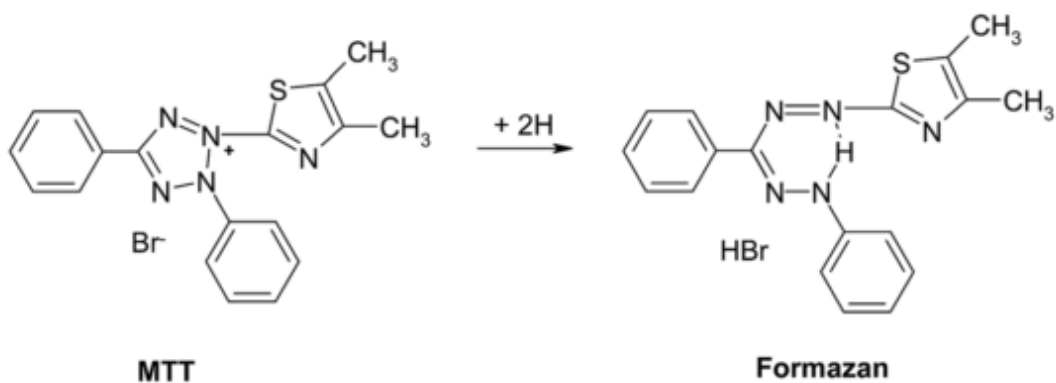

Figure 3.30 - Conversion of tetrazolium ring to formazan by reduction. [97]

MTT is dissolved in PBS and added to cells and incubated for 4 hours at 37 °C. The purple formazan product is insoluble in cell media therefore a solubilizing agent is required before the optical density can be measured using a plate reader at 570 nm.

The absorbance is directly proportional to the number of live cells and it is possible to detect as little as 200 living cells.

The assay is commonly used for nanoparticle toxicity studies as nanoparticles quench fluorescence, making them incompatible with many other toxicity assays that depend on measurement of fluorescence. Furthermore, the MTT assay doesn't involve any wash steps making it relatively rapid.

The results of the MTT assay are shown below, colour coded to represent the viability of the cells. Each sample was carried out in triplicate and the results are the average. Each sample was compared to the control sample, which had nothing added, to give the percentage viability.

Table 3.4 - Viability of cells incubated with components of probes overnight

Sample	% Viability
Positive Control	100
Negative Control	1
Spermine	89
50 nM P1	104
200 nM P1	104
400 nM P1	97
0.2 nM 20 nm AuNP	61
0.02 nM 20 nm AuNP	97
0.2 nM 40 nm AuNP	97
0.02 nM 40 nm AuNP	97

Each component of the probes – i.e. oligonucleotide, spermine and AuNP – was assessed individually (Table 3.4), as well as combined (Table 3.5). 20 nm and 40 nm AuNP were assessed at 0.2 nM and 0.02 nM. The oligonucleotide was assessed at 50 nM, 200 nM and 400 nM. Oligo and AuNP (with and without spermine) were assessed at 50 nM, 200 nM and 400 nM.

Table 3.5 - Viability for cells incubated with AuNP probes overnight

20 nm (no spermine)	% Viability	40 nm (no spermine)	% Viability	20 nm (with spermine)	% Viability	40 nm (with spermine)	% Viability
50 nM P1	83	50 nM P1	93	50 nM P1	53	50 nM P1	28
200 nM P1	78	200 nM P1	84	200 nM P1	59	200 nM P1	48
400 nM P1	73	400 nM P1	70	400 nM P1	71	400 nM P1	94

All samples, with the exception of those containing a combination of nanoparticles, oligonucleotide and spermine, had a viability greater than 70 %, indicating that the negative effect of the probes on the cells is minimal. The negative control, as expected, had a viability of 1 % indicating that almost all cells had been killed.

The oligonucleotide sequence on its own had no significant effect on the cells at any of the concentrations assessed. The viability was ~100 % at 50 nM, 200 nM and 400 nM. Viability greater than 100 % can be attributed to experimental variability.

Nanoparticles on their own also had no significant effect, with the exception of the higher concentration of 20 nm AuNP. This may be a result of the smaller particles being more able to penetrate organelles within the cells and cause disruption to cellular processes.

For cells containing AuNP with oligonucleotide, viability was slightly lower than either nanoparticles or oligonucleotide individually. However, for all of these samples viability was greater than 70 %.

Cells that contained AuNP with oligonucleotides and spermine viability dropped considerably. Spermine on its own, however, had only a small effect on vability (89 %). One possible explanation for this is that spermine causes the nanoparticles to aggregate and the larger aggregates resulted in a higher disruption to cellular processes.

The importance of the effect on viability of the probes will depend on whether the assay will be used on live cells and the timescales required. As it currently stands, the assay is aimed to be a tool for biologists and will most likely be used on fixed cells. In

this case the cells are no longer living so the toxicity of the probes is of less importance. If the assay were to be used in living cells this would need further investigation.

3.5 Thiol Probes

3.5.1 Oligonucleotide Sequences

In order to overcome the issues associated with spermine in the probes, thiol-modified oligonucleotides were assessed. Sulfur groups have a strong affinity for gold, therefore spermine was no longer needed to attach the oligonucleotide. [98] By using oligonucleotides with a terminal thiol group a gold-sulfur bond is formed, attaching the oligonucleotide to the nanoparticle surface, and omitting the need for electrostatic attachment.

The oligonucleotide sequences are shown below:

Probe 1: HS-C6-GAGTCCTTCCACGATACCA (complementary to target)

Probe 2: HS-C6-ACCATAGCACCTTCCTGAG (random control)

Target: 5'-TGGTATCGTGGAAGGACTC

A DNA melting curve was carried out again to ensure the probes hybridised as expected. The result is shown in Figure 3.31. As expected, target oligonucleotide plus probe 1 gave a sigmoidal curve on heating, indicating that it hybridises to the target and separates at high temperature. Probe 2 plus target gave a linear spectra, as did probes 1 and 2 combined, indicating that only probe 1 is specific to the target.
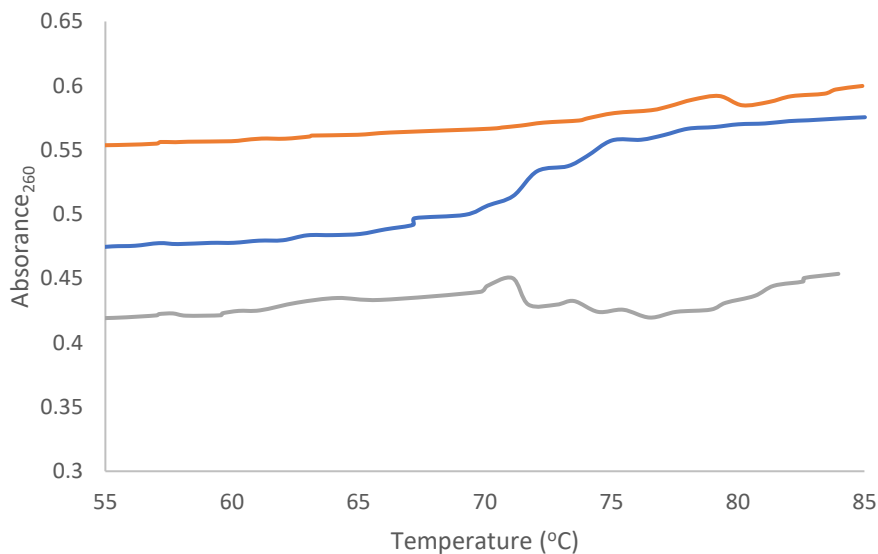
Figure 3.31 - DNA melting curves for thiol-oligonucleotides. Blue - probe 1 (complementary probe) + target, orange - probe 2 (random control) + target, grey - probe 1 + probe 2. It can be seen that only the blue trace shows a sigmoidal curve associated DNA denaturation, indicating that the target oligonucleotide hybridises to the complementary probe only.

3.5.2 Probe Synthesis & Characterisation

To build these nanoprobes, AuNP were functionalised with MGITC and oligonucleotide, both via a sulfur group. Figure 3.32 shows the extinction spectrum for the functionalised AuNP. As expected, a slight red shift was seen in extinction maximum upon functionalisation with the oligonucleotides, indicating the functionalisation has been successful. As is commonly seen with oligonucleotide-AuNP, one probe (probe 1) appears to be more stable than the other, indicated by the broadening of the LSPR for probe 2. This may indicate that probe 2 is self-hybridising, forming small duplexes between adjacent probes.
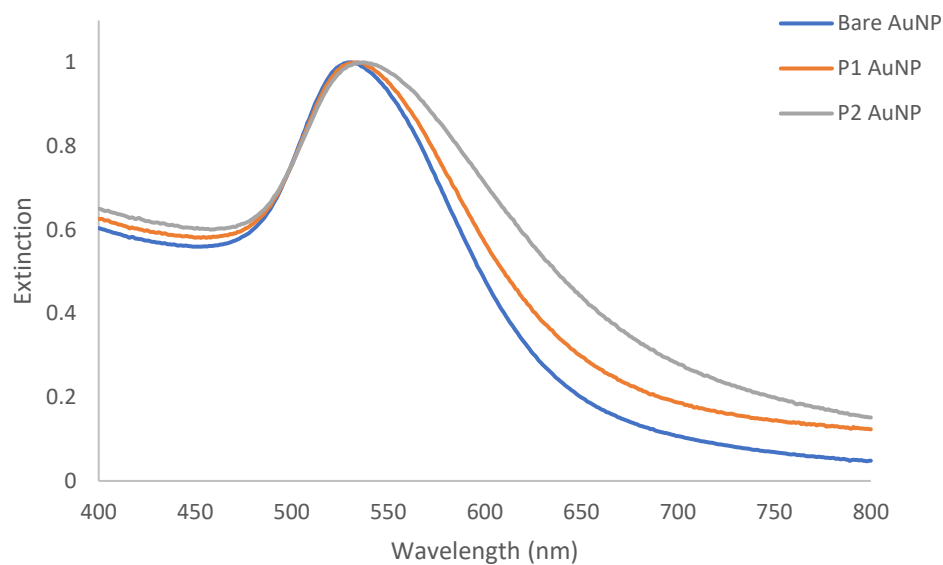
Figure 3.32 - Normalised extinction spectra for AuNP functionalised with thiol probes 1 and 2.

Figure 3.33 shows the normalised spectrum for addition of MGITC to P1-AuNP. The corresponding spectra for probe 2 are shown in Figure 3.34. On addition of MGITC a slight broadening of the LSPR is seen, however the particles still appear to be stable with a λ_{max} of 531 nm.
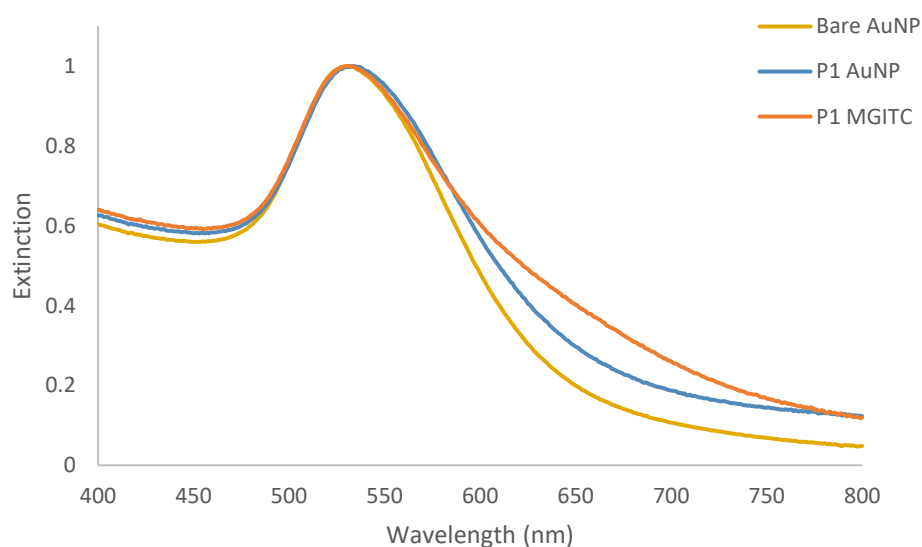

Figure 3.33 - Normalised extinction spectra for bare AuNP, P1 functionalised AuNP and P1 + MGITC functionalised AuNP.
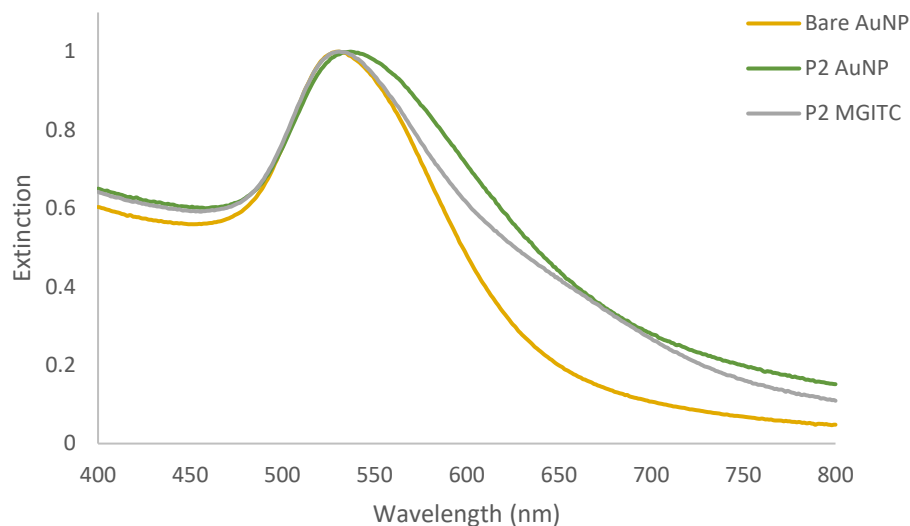
Figure 3.34 - Normalised extinction spectra for bare AuNP, P2 functionalised AuNP and P2 + MGITC functionalised AuNP.

3.5.3 Cell Mapping

Figure 3.35 shows cell mapping images following incubation with the nanoprobes. PNT2 cells were incubated with either probe 1 or probe 2 overnight (probe = oligonucleotide + MGITC-AuNP).
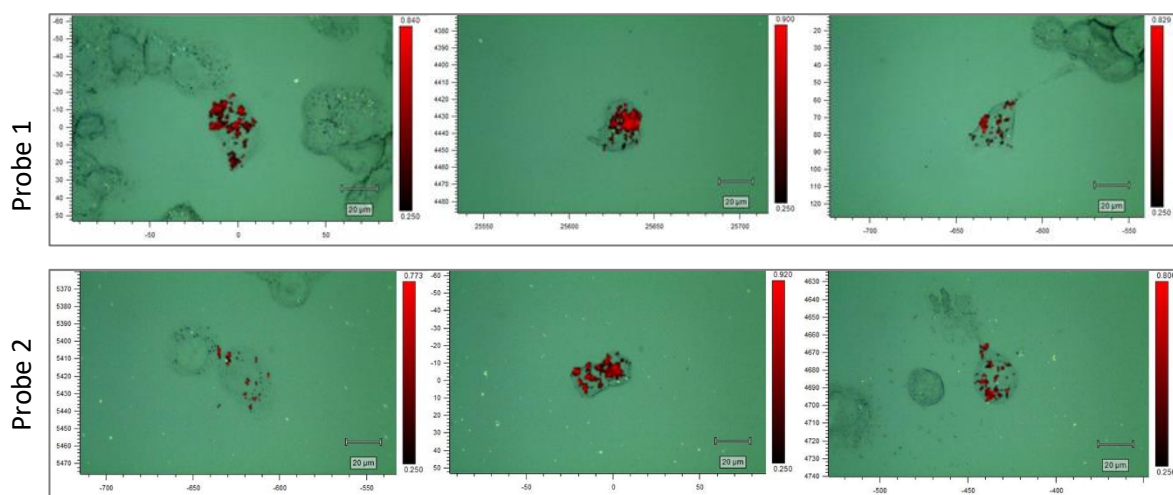

Figure 3.35 - False colour images for PNT2 cells incubated overnight with probe 1 (top) or probe 2 (bottom) at 4000:3000:1 ratio. Cells were mapped using a 633 nm laser at 100 % power and 0.2 second acquisition time.

Signal could be detected in cells incubated with both probes – Figure 3.36 shows a representative spectrum. The measured spectra shows a clear match with the MGITC reference spectra. However, there does not appear to be any significant differences in signal between probe 1 (complementary to target) and probe 2 (random control), again indicating a lack of specificity of the probe. Both cells appear to show high amounts of signal.
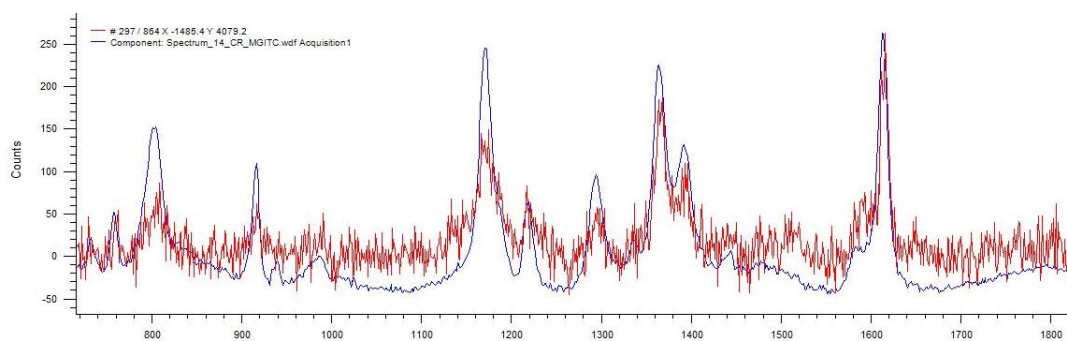

Figure 3.36 - Representative spectrum from false colour images. Blue trace = reference MGITC spectrum, red trace = measured spectrum, DCLS software compares the two and gives each spectra a score depending on the match.

Cells were also incubated with probes with a higher ratio of oligonucleotide to nanoparticle. The probe concentration was kept the same. Figure 3.37 shows the false colour images.
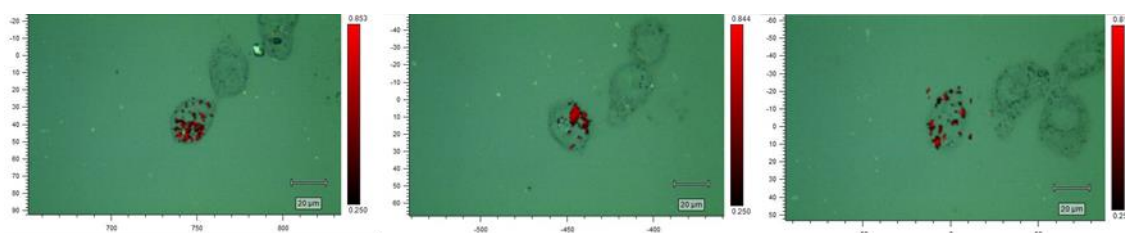

Figure 3.37 - False colour images for PNT cells incubated overnight with probe 1 (complementary to target) at 5000:3000:1. Cells were mapped using a 633 nm laser at 100 % power and 0.2 second acquisition time.

As with the spermine probes, 3D mapping was used in order to determine if the probes were inside the cells. Figure 3.38 shows a representative images for probes 1 and 2. Despite the cell mapped for probe 1 having a low signal, it still appears to be

distributed throughout the z-plane, indicating it is within the cell and not on the surface. The probes also appear to be distributed throughout the cell for probe 2.
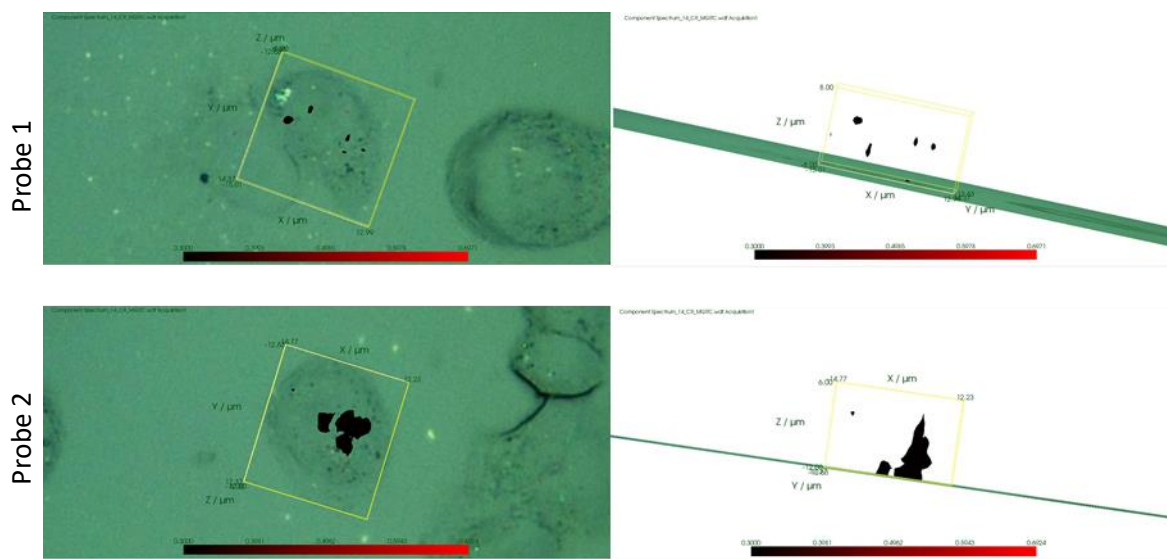

Figure 3.38 - Representative 3D images for probe 1 (top) and probe 2 (bottom). Left-hand images show top down view, right-hand images show side on view.

In order to determine whether the lack of specificity was due to the length of the incubation time, a shorter incubation time was assessed. Cells were incubated with probes for 2 hours before being fixed and mapped. Figure 3.39 shows the false colour images.
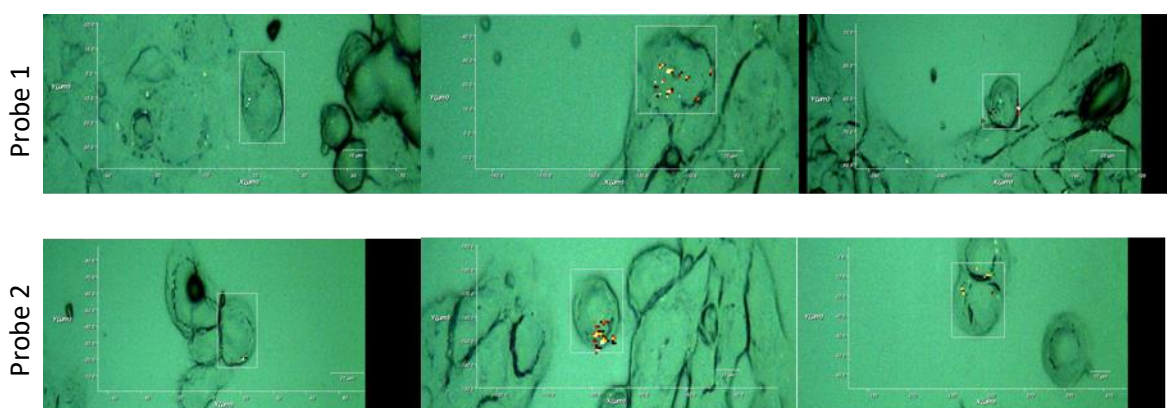

Figure 3.39 - False colour images for PNT2 cells incubated with thiol probes (top - probe 1, bottom - probe 2) for 2 hours before fixation. Cells were mapped using a 633 nm laser at 100 % power and 0.2 second acquisition time.

Similarly to the 24 hour timepoint, no significant difference was seen between the two probes and both sets of probes showed significant intra-sample variability. Compared to the overnight timepoint significantly less signal was present for both sets of samples. This indicates that 2 hours is not long enough for the probes to enter the cells.

If this method were to be progressed further, it may be of interest to look into longer timepoints, e.g. 48 hours. It is possible that unbound probe (probe 2) would leave the cells if given more time, whilst probe 1 would remain bound.

Pre-fixation was assessed to determine whether this impacted the specificity of the probes. Cells were incubated with cover slips overnight to give them time to bed down before being fixed using the same method used previously. Once fixed, the cells were incubated with probes for 2 hours before being washed and mapped.

Figure 3.40 shows the false colour images for the pre-fixed cells. Whilst significantly more signal was detected in these cells (Figure 3.39 shows cells with the same probe concentration and incubation time fixed after probe incubation), this was the case for probes 1 and 2. As seen previously significant variability in the amount of signal was also observed.

Despite the pre-fixed cells giving strong probe signal, some of it appears to originate outside of the cells. It is not possible to determine from the bright field images alone if the signal is coming from inside the cell; 3D mapping would be required to confirm this.
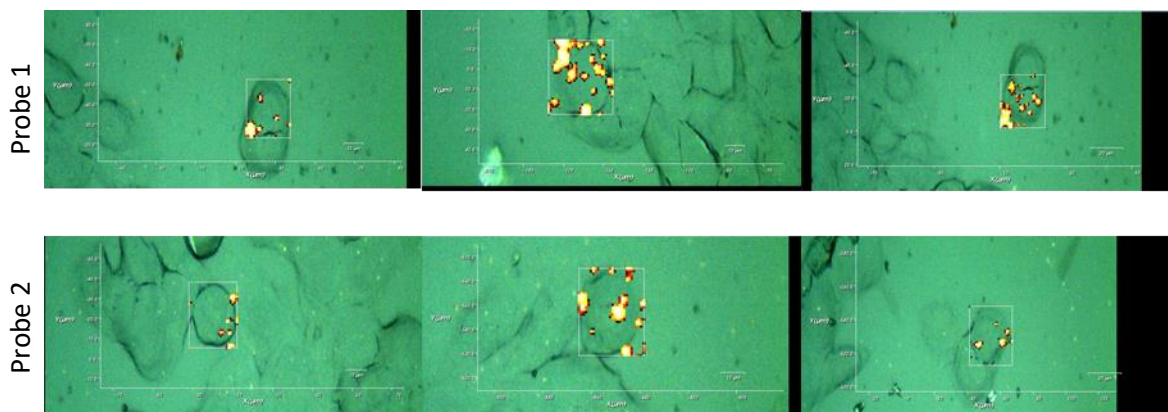
Figure 3.40 - False colour images for pre-fixed cells incubated with probes (top - probe 1, bottom - probe 2) for 2 hours.

3.5.4 Cell Toxicity

Cell counting is an alternative method of assessing cell viability. It can be advantageous over other methods, such as fluorescent staining which requires additional wash steps which can wash away dead cells – affecting the reliability of the data. Fluorescent staining uses a fluorescent molecule to visualise living cells. An issue with including wash steps in a cell viability assay is that wash steps can remove dead cells, resulting in viability appearing higher than it actually is since only live cells are labelled.

By counting the cells and comparing the count to a control, it is possible to determine whether any exogeneous substances have had a negative effect on the cells, seen by a decreased cell count. Cell counting also requires no additional reagents or equipment, other than that already used in cell culture. One minor drawback is that manual cell counting can be time consuming.

Gold nanoparticles (bare, MGITC-coated, MGITC + oligonucleotide 1 coated, MGITC + oligonucleotide 2 coated) were added to PNT2 cells and incubated overnight before cell counting was performed. Each sample was carried out in triplicate to obtain a mean result. Figure 3.41 shows the results. Viability was determined by comparing the count for each sample to the count for the samples which had no probes added (i.e. blank). As the blank samples had nothing added, they should continue to grow

and proliferate as normal. On the other hand, cell samples with nanoparticles and/or other substances added may experience a decline in proliferation due to toxicity effects.
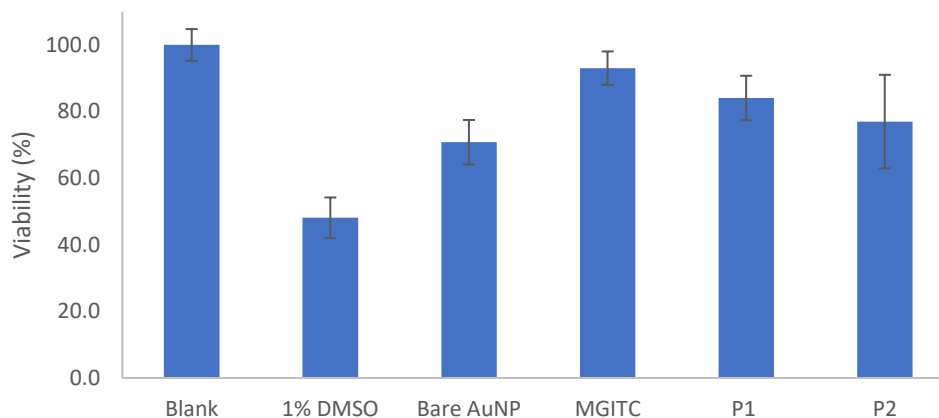

Figure 3.41 - Cell viability (mean ± standard deviation) following incubation with AuNP probes (bare, MGITC only, MGITC + probe 1/2).

As expected, when DMSO was added to the cells (1% solution) the viability dropped drastically. This is because DMSO is cytotoxic. Bare AuNP had a mean viability of 71±7 %. This indicates that the bare nanoparticles have a slight cytotoxic effect on the cells. AuNP functionalised with MGITC had only a minor effect with a mean viability of 93±5%. This may be a result of the MGITC layer on the outside of the particles providing a 'shield' from the particle surface, thus protecting the cells. AuNP functionalised with both MGITC and a thiol-modified oligonucleotide showed a slight drop in viability compared to those coated with only the dye but still higher than that of bare AuNP. There was a slight difference in viability between the target oligonucleotide probes (84±7 %) and the negative control probes (77±14 %), however this is not significant.

3.6 Alkyne-Tagged Oligo

In an attempt to overcome the issue of the non-specificity, which was believed to be caused by the nanoparticles, a third method was assessed that omitted nanoparticles altogether. In this method, an oligonucleotide was modified to incorporate 5'-ethynyl-2'-deoxyuridine (EdU) in place of two of the thymine bases. EdU (Figure 3.42) is an analogue of thymidine in which the 5' methyl group has been replaced with a terminal alkyne, giving it a large Raman cross section.

Figure 3.42 - Structure of EdU. [99]

Alkynes make ideal Raman reporters for this purpose since they have a distinct signal in the cell silent region (1800-2800 cm^{-1}) of the spectrum. Also, due to their small size, they are less likely to have a significant effect on the intrinsic properties of the systems being studied. [99]

Yamakoshi *et al.* were able to monitor EdU, as a cell proliferation probe, in live cells using Raman microscopy. [100] As EdU can be incorporated into DNA during cell replication, replacing un-modified thymine bases, it can be used to label cell nuclei. [101]

To further increase the sensitivity, SRS could be used. As previously mentioned, SRS can be used to enhance specific signals, such as the alkyne signal of EdU. As a result of this improved sensitivity, it may be possible to detect labelled oligonucleotides without the presence of nanoparticles to invoke SERS.

3.6.1 EdU Cell Mapping

To ensure EdU signal could be measured, cells were incubated with EdU on its own (100 µM, 24 hours), fixed and then mapped using Raman spectroscopy (2 s acquisition, 100 % power, 532 nm laser). Figure 3.43 shows the result. An alkyne signal can be seen at 2114 cm^{-1} in the cells incubated with EdU in a pattern consistent with that expected of the nucleus. The control cells show no signals in this region. For the false colour images, the lower cut off was determined at three times the baseline.

It should be noted that most cell spectra show a peak at ~ 2300 cm^{-1}. This is apparent in both blank and sample cells alike. This signal has been attributed to atmospheric nitrogen.
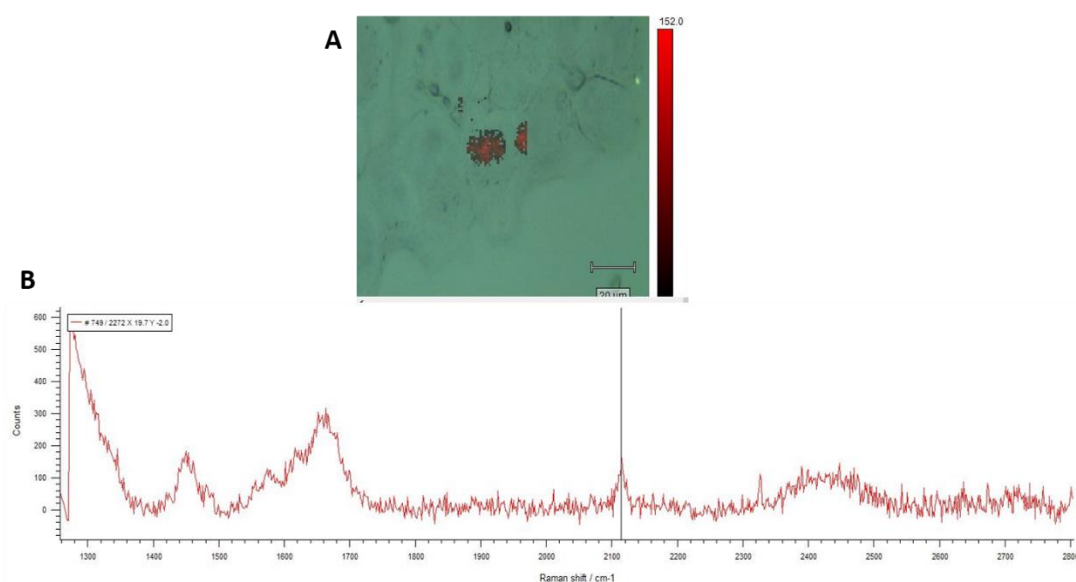

Figure 3.43 – A) False colour cell overlay of peak intensity at 2114 cm^{-1} representing to localisation of the cell nucleus, B) Raman spectra showing signal at 2114 cm^{-1} for EdU. Cells were mapped using a 532 nm laser at 100 % power and 2 second acquisition time.

3.6.2 EdU Modified Oligo

Similarly, cells were incubated with the EdU-modified oligonucleotide probe. Although the mechanism of the probe is different to that of free EdU in cells, it was hoped that since the signal was apparent for the free EdU, it would also be apparent

for the probe. Two thymine nucleotides within the oligonucleotide sequence were replaced with EdU, the probe sequence is shown below:

Probe 1: 5'-GAGXCCXTCCACGATACCA   Where X = EdU

Figure 3.44 shows the results. Despite increasing the integration time to 20 seconds, no EdU signal was observed. This was most likely due to the fact that the signal is too low to be measured using Raman spectroscopy. Unlike free EdU, which can essentially replace every thymine in the nucleus giving a strong signal, the EdU oligonucleotide probe should only bind to specific RNA sequences which means that it is much less abundant in the cell and, hence, the signal is unfortunately too weak to detect with conventional Raman spectroscopy.
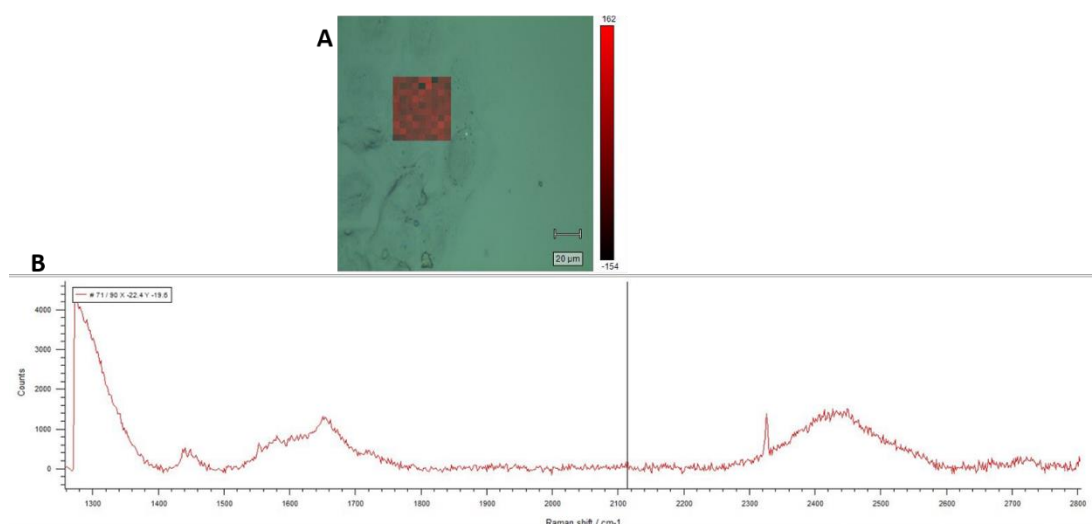

Figure 3.44 - A) False colour cell overlay of peak intensity at 2114 cm^{-1}, heat map guide on left shows that no signal is observed above the noise, B) Raman spectra showing no signal at 2114 cm^{-1} where EdU is expected. Cells were mapped using a 532 nm laser at 100 % power and 20 second acquisition time.

Due to the cost of the probe it was not feasible to increase the concentration of the probe any higher. A possible solution could be to add nanoparticles separately to the EdU oligonucleotide probe in order to measure SERS. Despite not being attached, it is possible that the nanoparticles would come into proximity with the probes, improving the sensitivity.

Another possible solution could be to use SRS. SRS is useful for measuring the signal at a specific frequency and since alkynes are present in the cell silent region there are no competing signals.

3.7 Conclusions

Despite having no on/off signal, it was hoped that RISH would provide a simple means of measuring mRNA in cells using Raman spectroscopy and oligonucleotide-labelled gold nanoparticles. The simple concept relies on labelled oligonucleotides binding to specific sequences inside cells and being visualised using Raman spectroscopy. Due to the inherent weakness of Raman scattering, gold nanoparticles were incorporated into the assay to enhance the spectra. Electrostatic and thiol-attachments were utilised to attach specific oligonucleotides to AuNP with a Raman active dye to provide a measurable SERS signal.

After incubation with cells overnight, no observable difference in signal was observed between the target probe and the random control sequence. 3D mapping indicated that the probes were entering the cells since the signal was dispersed through the depth of the cells.

One possible explanation for the lack of specificity is that the nanoparticles are becoming stuck inside the cells. Since these probes are always 'switched on' any probe which is inside the cell will give rise to signal. This means that whether the probes have hybridised to the target or not, they are staying within the cell and, hence, no difference in signal is seen.

Assuming that the reason for the probes remaining in the cells is due to the attachment to the nanoparticles, further work could be carried out on an alkyne-labelled oligonucleotide probe. Despite EdU labelled oligos proving too weak to be detected using Raman spectroscopy, SRS, which can improve the sensitivity of

conventional Raman, could be used instead. Furthermore, oligonucleotides with more EdU modifications could be assessed.

Similarly, instead of using EdU which contains a single alkyne, oligonucleotides could be labelled with a molecule containing multiple alkynes to increase the Raman cross section.

Although there are further avenues which could be explored in order to progress this assay format further, it may be better to focus on probes with an 'on/off' signal. This would overcome any problems associated with signal arising from unbound probes remaining inside the cells.

4. SERS Beacon

4.1 Introduction

Currently, one of the most common methods of detecting mRNA is fluorescence *in situ* hybridisation (FISH), which is capable of single molecule detection. [30] However, one of the issues with the FISH method is that the signal produced is always 'on'. Other methods, such as molecular beacons, provide the advantage of having a switchable signal, i.e. one which is 'turned on' in the presence of the target.

Molecular beacons are commonly used with fluorescence spectroscopy. Figure 4.1 shows a schematic of a typical fluorescent molecular. The oligonucleotide sequence has ends which are self-complementary, this causes it to take a hairpin loop structure. One end of the oligonucleotide is functionalised with a fluorophore, whilst the other has a quencher molecule preventing fluorescence emission in the closed hairpin loop structure. In the presence of the target DNA, which is complementary to the loop sequence, the beacon opens up, separating the fluorophore from the quencher, resulting in the emission of fluorescence.
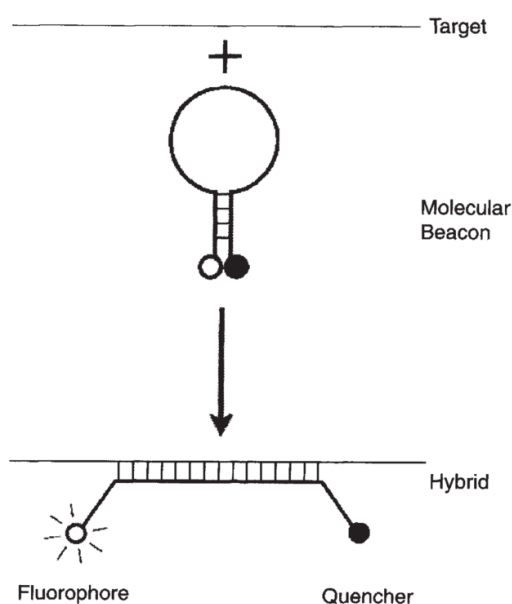
Figure 4.1 - Schematic of a molecular beacon. Reproduced with permission from [102].
Copyright © 1996, Springer Nature.

An alternative method uses gold nanoparticles to replace the quencher in these beacons, resulting in an improved quenching efficiency. [37] For example, Pan *et al.* were able to detect four different mRNAs in cells using molecular beacons hybridised to nanoparticles. [73]

Faulds *et al.* reported SERS beacons, similar to fluorescent molecular beacons with a Raman reporter on one end, attached to a silver nanoparticle, and a fluorescent molecule (FAM) on the other end. When closed, the beacon gave SERRS signals from the Raman reporter and FAM. However, in the open position the signal changed as FAM moved away from the nanoparticle surface and fluorescence was observed. [46] Although effective, the main method of detection was still based on fluorescence.

The aim of this piece of work is to create a molecular beacon which utilises Raman spectroscopy for detection. The beacon consists of an oligonucleotide sequence in the classic hairpin loop structure. One end of the sequence is functionalised with a Raman active molecule, whilst the other has a thiol modification for attachment to a gold nanoparticle. The gold nanoparticle is also functionalised with another Raman active dye. In the closed position, the Raman dye attached to the oligonucleotide is in close proximity to the nanoparticle surface, resulting in SERS signals from both the oligo-dye and the dye attached to the nanoparticle. When the hairpin loop opens up, the oligo-dye moves further away from the nanoparticle surface (Figure 4.2). This results in a decrease in the SERS signal from the oligonucleotide dye, however the signal from the nanoparticle dye should remain constant as it is unaffected by the target oligonucleotide, thus an increase in the ratio between the two dyes should be observed. This ratio can be related to the presence of the target oligonucleotide.
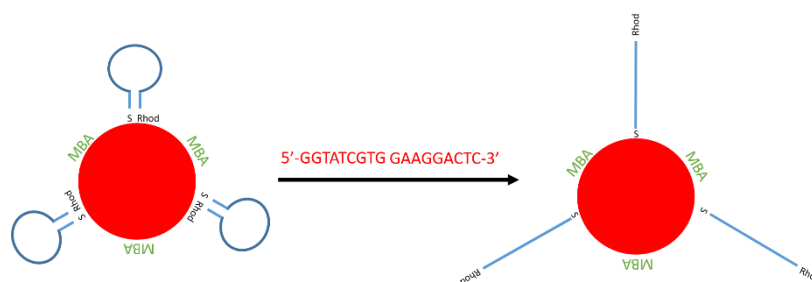
Figure 4.2 - Schematic representation of SERRS beacon.

4.2 4-Mercaptobenzoic Acid

4-Mercaptobenzoic acid (MBA) – a pH sensitive molecule – was selected to be the dye functionalised to the nanoparticle surface, therefore MBA should always be present to give a SERRS signal. [103,104] It was hoped that, as well as being able to detect the presence of the mRNA, the pH of the probe environment would also be determined.

The pH sensitivity is shown in Figure 4.3 which shows the SERRS spectra obtained from MBA coated AuNP covering a pH range from 1 to 12.

AuNP were functionalised with MBA by adding 100 µL of stock solution to 1mL of AuNP, resulting in a final concentration of 100 µM, and shaken for 5 minutes. The MBA-AuNP were then centrifuged at 4000 rpm for 20 minutes and the pellet was resuspended in water. 100 µL of MBA-AuNP was added to 400 µL of pH adjusted PBS (pH 1-12). Samples were analysed at 633 nm with a 1s acquisition time and 100 % power.

The two main peaks in the MBA spectrum ($\sim$1080 cm^{-1} and 1590 cm^{-1}) are a result of aromatic ring vibrations and are not pH dependent, therefore their intensity is maintained throughout the experiment.

The peaks at $\sim$1400 cm^{-1} and 1700 cm^{-1} are assigned to symmetric stretching of the COO^{-} group and the symmetric stretching of the C=O bond, respectively. [103,105] At low pH, the intensity of the peak at $\sim$1700 cm^{-1} (C=O) increases whilst the peak at 1400

cm^{-1} (COO$^-$) decreases. As the pH increases, the intensity of the peak at 1400 cm^{-1} increases and the peaks at 1700 cm^{-1} decreases. The peak at 1400 cm^{-1} also shifts slightly from 1397 cm^{-1} to 1420 cm^{-1} with increasing pH.
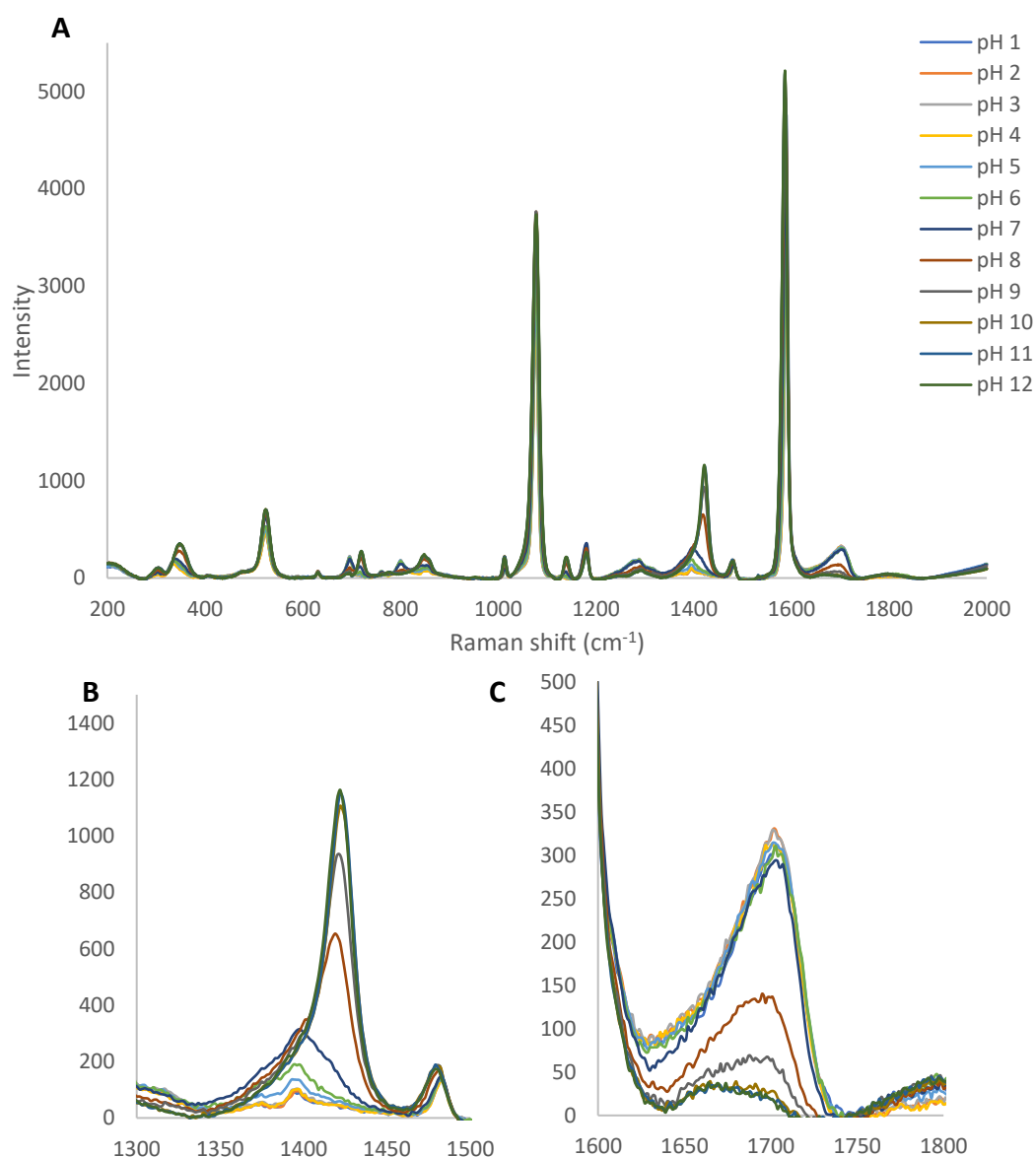

Figure 4.3 – (A) SERRS spectra for MBA-AuNP in pH adjusted PBS (pH 1-12), (B and C) zoomed spectra of signal at ~ 1400 cm^{-1} and 1700 cm^{-1}, respectively. Samples were taken using a 638 nm laser at 100% power with a 1 second acquisition time.

Figure 4.4 shows the calibration curve obtained from the ratio of the intensity of the peaks at 1400 cm^{-1} (pH sensitive) and 1078 cm^{-1} (constant) is taken. As expected, the curve shows a sigmoidal curve with a linear range from approximately pH 6-9, making

MBA an ideal pH sensor for cellular environments. Intracellular pH is tightly regulated and varies slightly within different organelles, with cytosol pH maintained at 7.2. [106] Therefore, the ratio between the two peaks can be used to determine the pH of the surrounding environment.

It is worth noting that as the peak at ~ 1400 cm^{-1} shifts with pH, the exact Raman shift used in the ratio also varies with pH from 1397 cm^{-1} at pH 1 to 1422 cm^{-1} for pH 12.
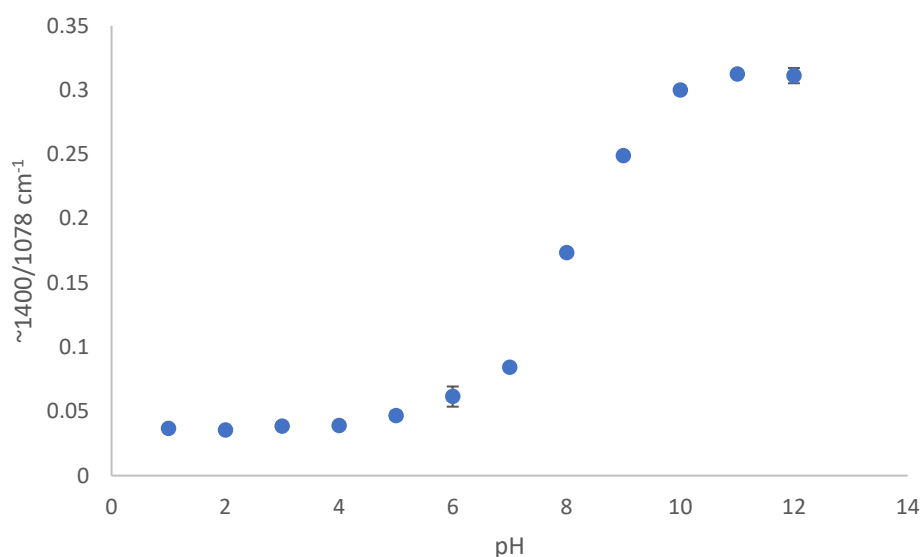

Figure 4.4 - Plot of ratio of peaks at 1400/1078cm^{-1} from pH 1-12 showing expected sigmoidal curve.

4.3 Probe Optimisation

Multiple dyes (rhodamine B, rox, eosin, dac, xrtic, fam, mgitc) were assessed to determine which combination with MBA would be optimal. These dyes were assessed by functionalising AuNP with MBA and the dye of choice. These dye-coated particles were then spun down and resuspended in pH adjusted PB. SERS spectra were then taken and the relative intensities were checked to ensure the pH sensing ability of MBA was not compromised by the dye.

Figure 4.5 shows the spectra obtained for each dye mixture (dye + MBA) over the pH range of 5 to 9.
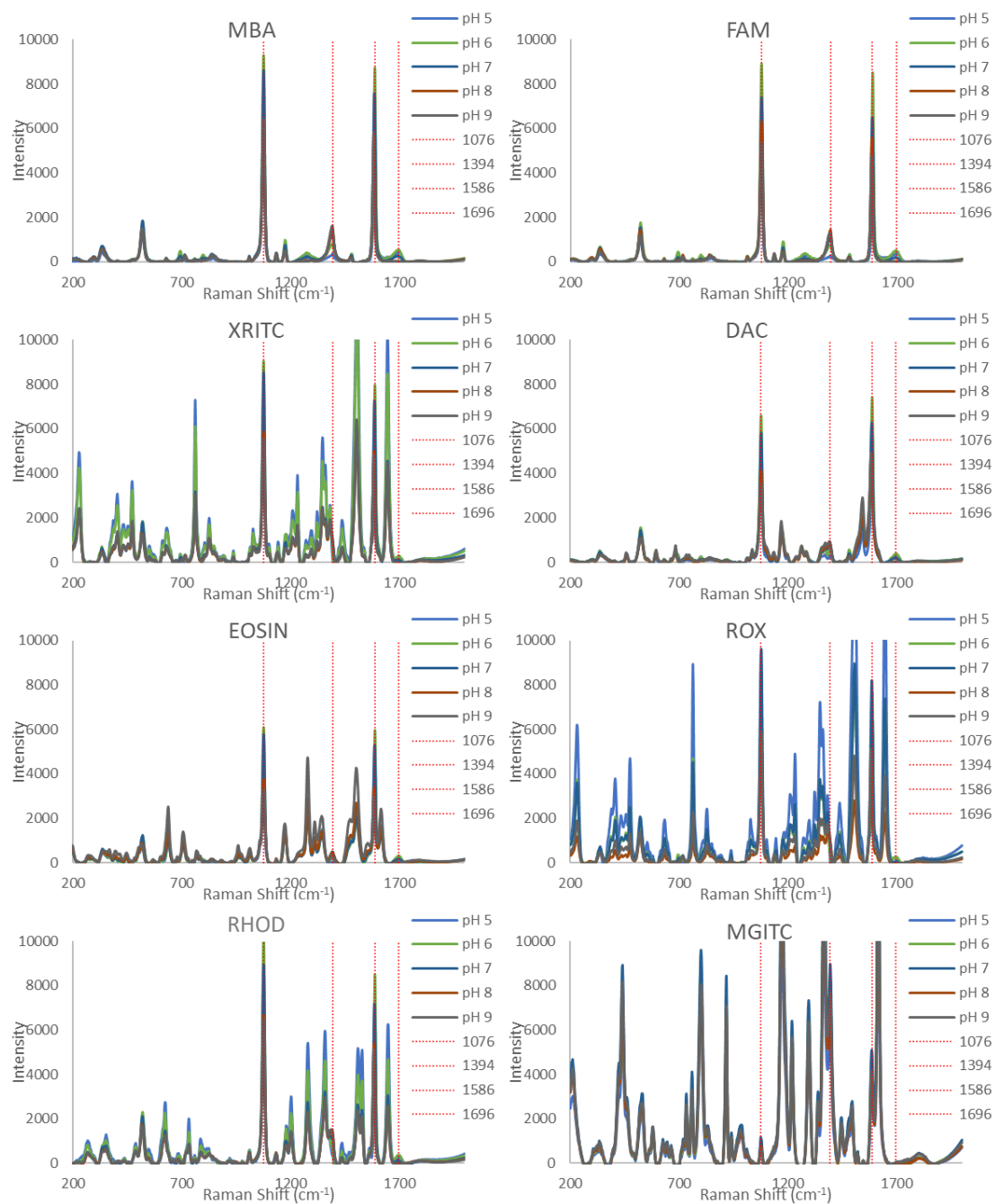
Figure 4.5 - Spectra MBA + dye mixtures. Red dotted lines indicate wavenumbers of main MBA signals for reference.

Based on signal intensity, compatibility with MBA and price, rhodamine B was chosen as the dye attached to the molecular beacon, i.e. the signal which should switch 'on' and 'off'.

Rhodamine B (rhod) did not interfere with the pH sensing ability of MBA over the pH range of 5-9 in the solution based SERRS experiments with MBA-rhod-AuNP. Figure 4.6 shows the calibration curve obtained for MBA alone and MBA + rhodamine.
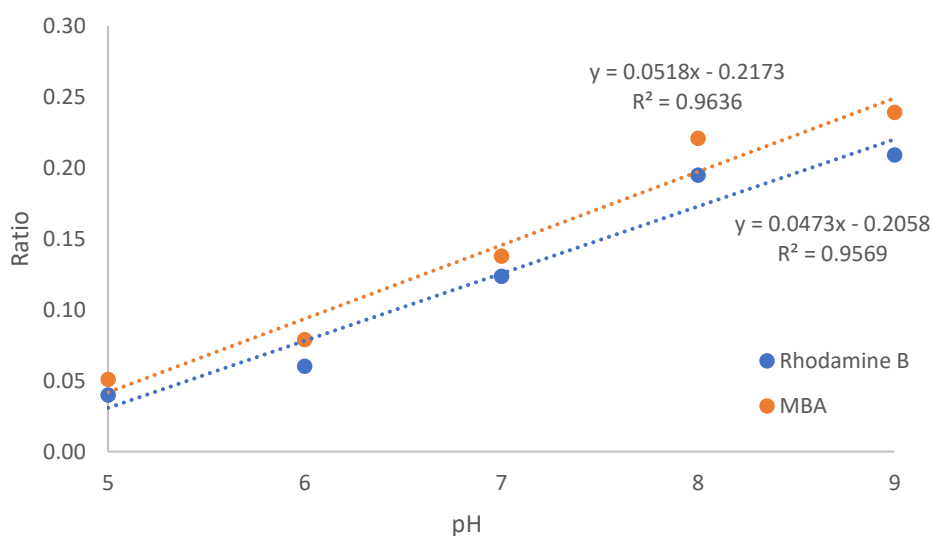

Figure 4.6 - Plot of ratio versus pH for MBA-AuNP and MBA+Rhodamine-AuNP showing that the addition of rhodamine does not appear to interfere with the pH sensing ability of MBA.

MBA alone has an R^2 value of 0.924. The only dye which gave an R^2 value greater than 0.9 when combined with MBA was rhodamine B, indicating that the presence of the rhodamine peaks did not interfere with the ability to determine pH. Rhodamine also had signal strength comparable to MBA, and the SERS signals were not obscured, therefore allowing a ratio between the two dyes to be straight forward to determine. Figure 4.7 shows the spectra of MBA-rhod-AuNP at pH 7.
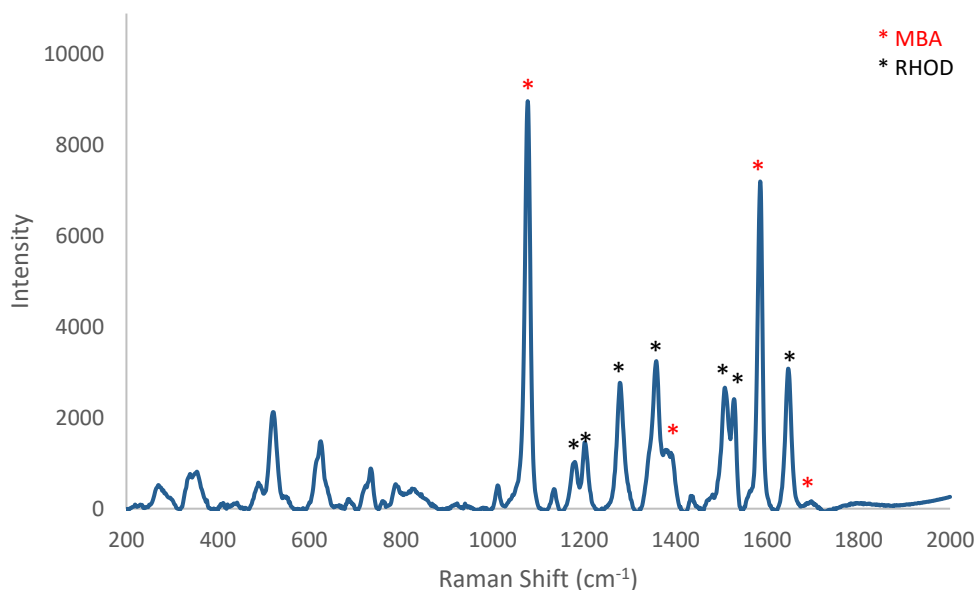
Figure 4.7 - MBA-Rhodamine B-AuNP spectra at pH 7.

4.4 Synthesis & Characterisation of Probes

As this is a proof of concept study, the same GAPDH mRNA sequence was targeted as for the RISH probes. The beacon sequence is shown below:

Beacon sequence: 5' HS-CGACGGAGTCCTTCCACGATACCACGTCG-rhodamine B

Target sequence: 5' TGGTATCGTGGAAGGACTC

Various ratios of labelled beacon and MBA dye were assessed to create a stable probe where signals from both dyes were obtained. Ultimately, MBA was added to 1 mL of 40nm AuNP to give a final concentration of 375 nM. The sample was shaken before being centrifuged. The nanoparticle pellet was resuspended in water and the beacon solution was added at a final concentration of 300 nM. The solution was then shaken and thiol-PEG-200 was added to create stability. 80 µL sodium citrate (250 mM, pH 2.9) was added and the solution was shaken for 15 minutes. Sodium citrate reduces the repulsion between the DNA backbone and the AuNP surface, facilitating

functionalisation. Samples were then centrifuged and re-suspended in 500 µL 0.1 M PBS (pH 7.4).

The samples were heated to 60 °C for 5 minutes and cooled to room temperature to ensure beacon formation (hairpin loop structure) before the target oligonucleotide was added (ratio 2:1).

Figure 4.8 shows the extinction spectra for MBA-beacon-AuNP. Upon functionalisation the λ_{max} shifts by approximately 3 nm and the peak broadens indicating that the molecules are on the surface of the particles due to a change in refractive index. There is also a drop in signal as some particles are being lost to precipitation during the functionalisation.
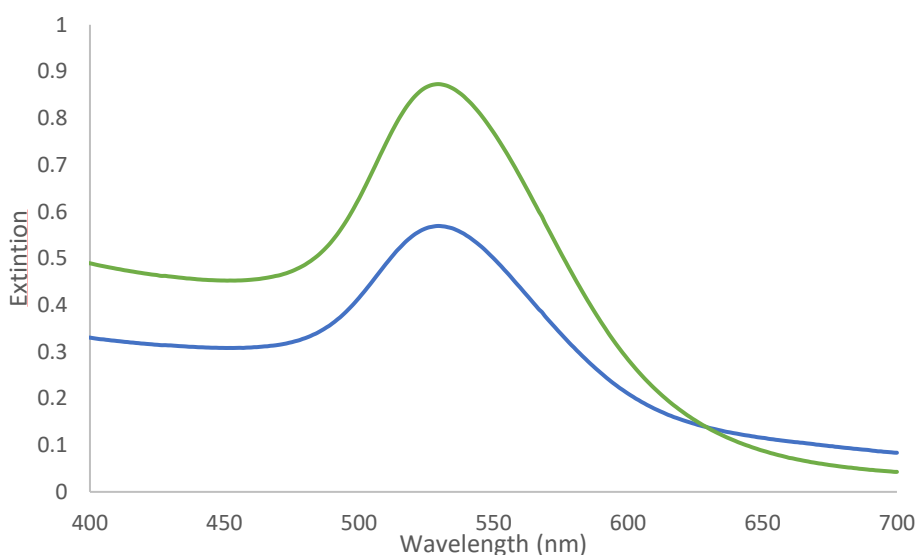

Figure 4.8 - Extinction spectra for bare AuNP (green) and MBA-beacon-AuNP (blue).

4.5 Solution Based Hybiridisation

Samples were incubated with the target (ratio 2:1) at 60 °C for 15 minutes and left to cool prior to analysis by SERS at 638 nm laser excitation.

Originally, probes were synthesised without PEG (only MBA and beacon were functionalised to the AuNP surface). However, upon incubation with the target, the SERS spectra showed a drop in all signals. This effect doesn't seem to be related to

target hybridisation. Instead, it indicated that rather than the beacon opening up, which should only result in a drop in specific signals, the nanoparticles were becoming unstable and aggregating, causing them to precipitate. This was confirmed by extinction spectroscopy which showed a drop in the λ_{max}. Figure 4.9 shows the SERS and extinction spectra for the probes both before (MBA Beacon) and after (MBA Beacon T) incubation with the target.

To increase the stability of the MBA-beacon AuNP, methoxy polyethylene glycol 200 (PEG200) was used. The optimal MBA/beacon/PEG:AuNP ratio was found to be 1500/1200/2000:1, respectively. This combination resulted in similar signal strengths from MBA and rhodamine, with stability from PEG.
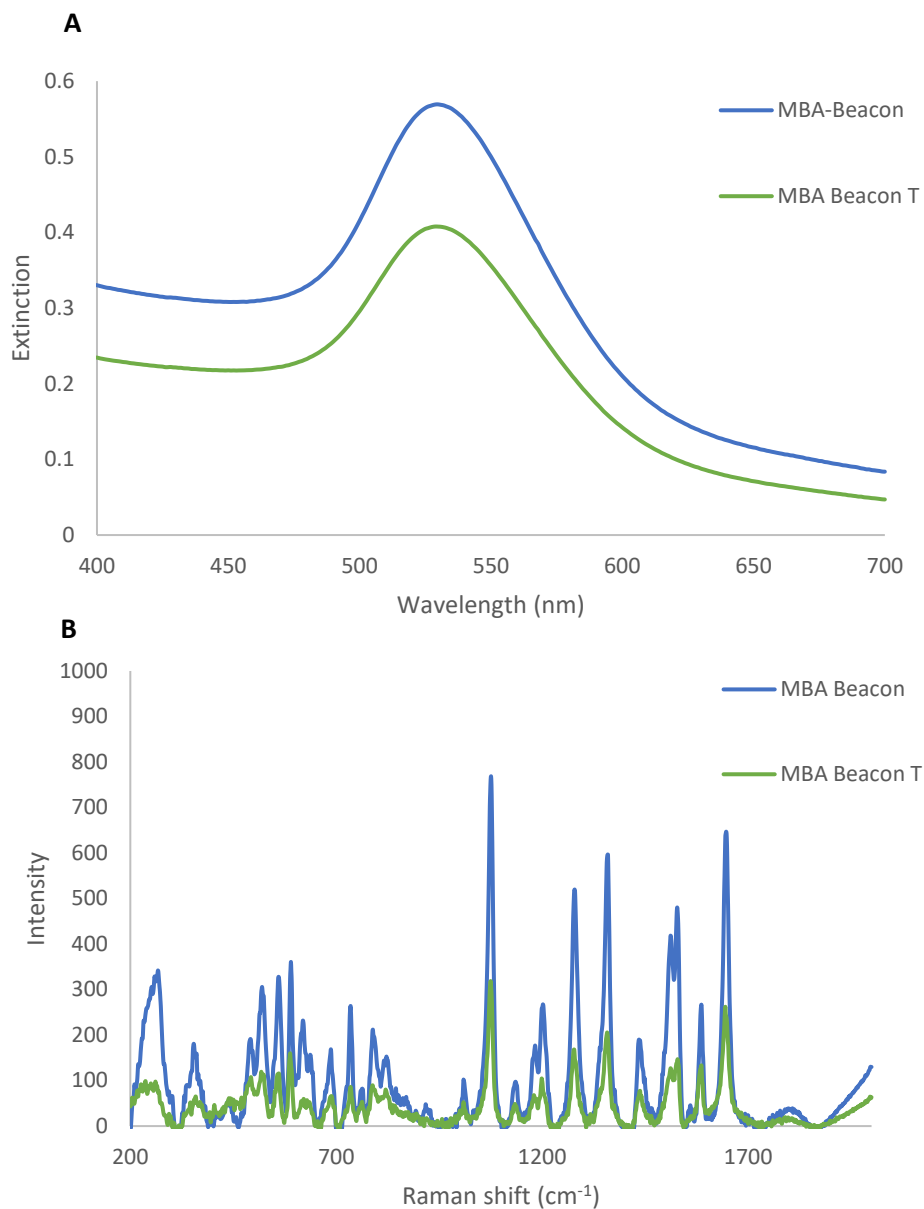
A

B

Figure 4.9 – A) Extinction and B) SERRS spectra for MBA-beacon-AuNP (minus PEG) before (MBA Beacon) and after (MBA Beacon T) addition of the target sequence. SERRS spectra measured using a 638 nm laser with a 1 second acquisition time.

Figure 4.10 shows the extinction spectra for the MBA-beacon-PEG-AuNP before and after incubation with the target oligonucleotide. In the presence of the target molecule the peak broadens very slightly, accompanied by a slight drop in intensity – indicating that some aggregation may have occurred – however, the λ_{max} remains unchanged.
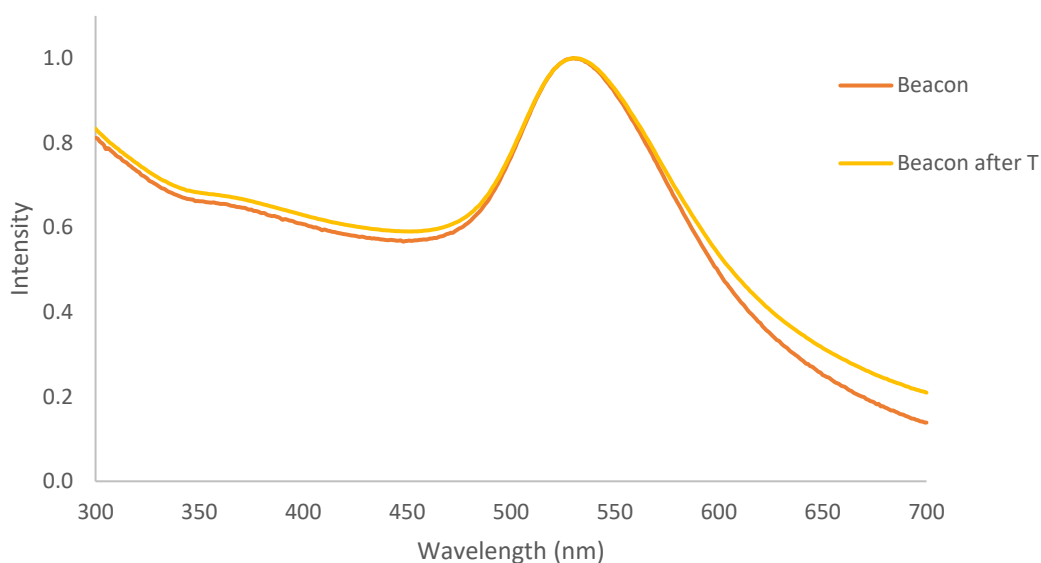
Figure 4.10 - Extinction spectra of beacon AuNP probes before and after incubation with target oligonucleotide.

As the SERS analysis relies on a ratio between two Raman reporters instead of an absolute measurement of the reporter intensity, slight aggregation of the particles should not affect the result.

Figure 4.11 shows the SERS spectra obtained for the nanoprobe both before and after the incubation with the target oligonucleotide. Signals corresponding to MBA remain mostly unchanged whilst the rhodamine B signals drop by approximately half in the presence of the target. This is to be expected based on the assumption that in the presence of the target the beacon opens up, moving the rhodamine further away from the nanoparticle surface and hence decreasing the SERS.
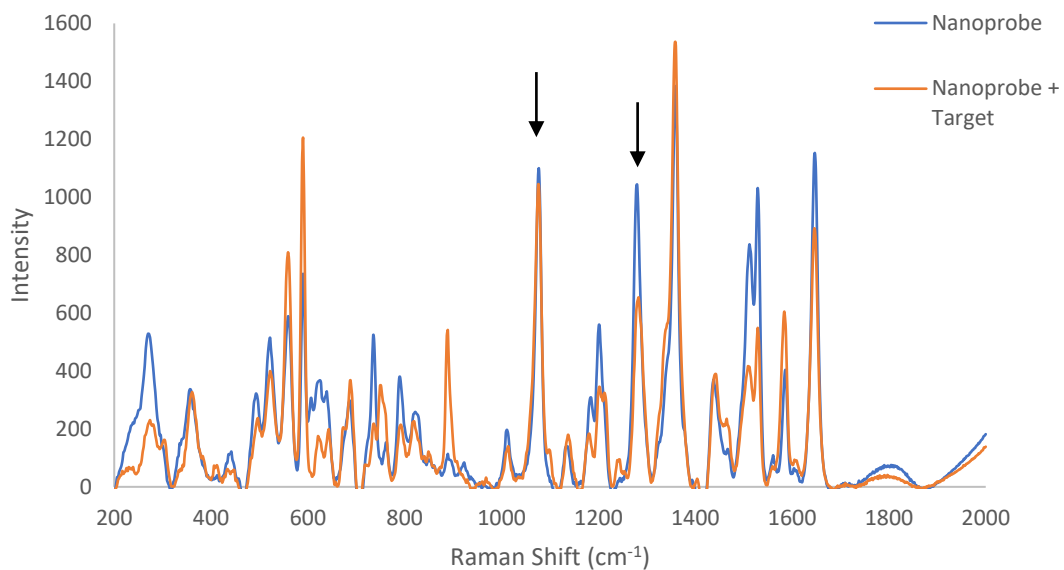
Figure 4.11 - SERRS spectra for beacon-AuNP before and after incubation with target oligonucleotide. Arrows indicate the signals used to determine ratio (1078 and 1280 cm^{-1}). Spectra measured using a 638 nm laser with a 1 second acquisition time.

Figure 4.12 shows the ratio of the peaks at 1078 cm^{-1} (MBA) and 1280 cm^{-1} (rhodamine b), i.e. the relative intensity of the MBA and rhodamine signals. Upon incubation with the target molecule the ratio increases as expected due to the drop in the rhodamine signal.
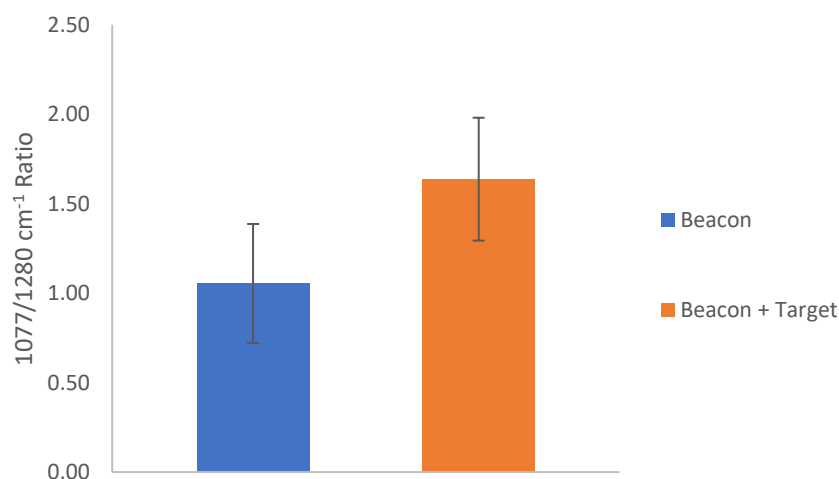

Figure 4.12 - Ratio of MBA:Rhodamine B SERRS signals (1077/1280 cm^{-1}) before and after incubation with the target oligonuceotide. Values are mean ± standard deviation.

For this experiment, a ratio of 1:2 beacon:target was used. In order to determine whether the ratio change is quantitative, various ratios would need to be assessed.

In Figure 4.11, it can be seen that whilst most signals in the spectrum change follow the expected trend, i.e. staying the same (MBA) or dropping in intensity (rhodamine), there are some signals which increase after incubation with the target.

One possible explanation for this is that when the beacon opens up, and rhodamine moves further from the nanoparticles surface, it creates more space on the surface of the particle causing MBA to change orientation.

4.6 Cell Mapping

The overall goal of this project is to develop a probe which can be used to detect mRNA in cells. To achieve this the probes must be detectable in cells. In order to assess this probes were incubated with PNT2 cells. Probes were added to cells and incubated overnight, similarly to in chapter 3. After incubation cells were fixed and mapped using a 633 nm laser excitation.

Figure 4.13 displays the false colour images for PNT2 cells incubated with the beacon-AuNP which show that signal was present in all of the cells mapped. To confirm that the probes had entered the cells and signal was not from AuNP stuck of the glass, 3D mapping was used. Figure 4.14 shows the result, as well as the reference spectra used to create the false colour images, along with an example spectrum from the maps.
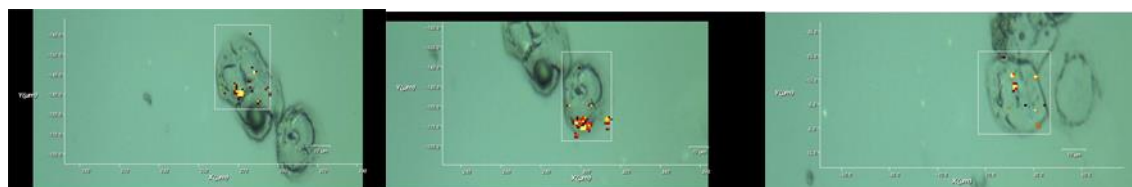

Figure 4.13 - False colour images for PNT2 cells incubated with beacon-AuNP overnight.

Despite low signal intensity, it appears that the probes are within the cell. However, it was not possible to determine ratios of the peaks at 1077/1280 cm^{-1} at the intensities measured.
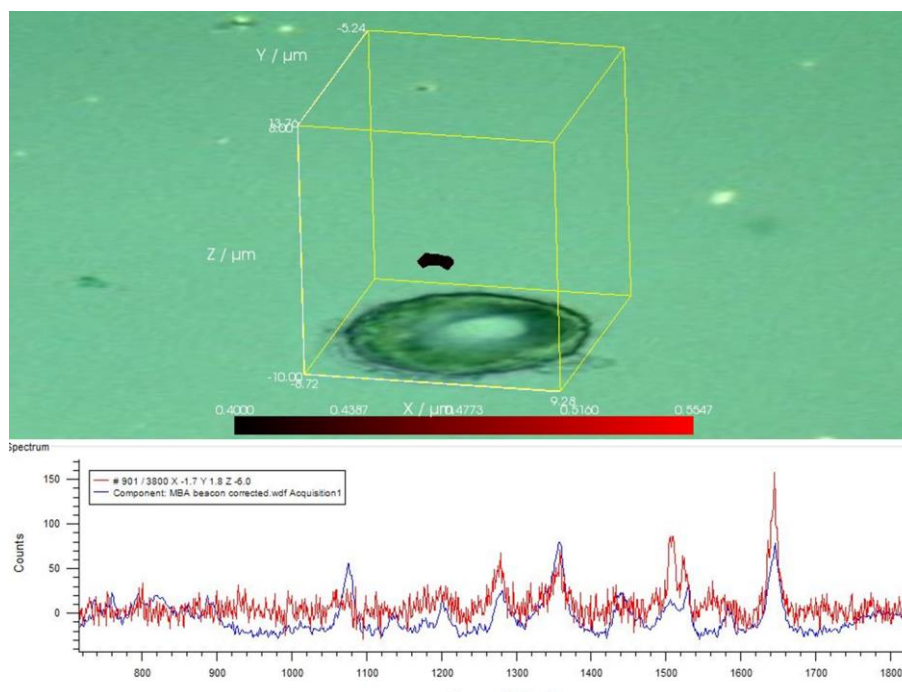
Figure 4.14 - 3D false colour image showing signal from beacon probe which appears to be within cell. 3D box represents predicted cell area which was mapped. Bottom shows example spectra for beacon-AuNP. Blue trace - reference spectra, red trace - measured spectra.

There are many possible ways to increase the intensity in future. A higher probe concentration could be used as well as a higher laser power or longer accumulation time. However, when increasing the laser power or accumulation time sample burning must also be taken into consideration.

4.7 Conclusions

The aim of this work was to create a molecular beacon type probe for detection of mRNA which could be used with Raman spectroscopy. To do this, gold nanoparticles

were functionalised with a constant dye (MBA), a labelled molecular beacon (Rhod) and PEG (for stability).

On incubation with the target oligonucleotide the beacon opened up, increasing the distance between the label and the nanoparticle. This resulted in a change in the SERRS spectrum which could be measured by taking the ratio between the most intense signal for each dye. The changing ratio determined whether the target had bound.

Overall, the Raman beacon probe successfully detected the target, however further work would be required to determine the limits of the assay and whether the beacon functions inside cells. Due to issues with supply this was not possible in this project.

Further work would be needed to determine whether this measurement can be used quantitatively. This can be achieved by incubating the probe with varying concentration of target to determine whether or not the response is concentration dependent. Furthermore, at the concentration assessed the probe could be detected in cells, however due to low signal it was not possible to determine signal ratios. In order to determine whether the probe is hybridising in cells a higher concentration would have to be assessed. Further work would then be required comparing the probe to a random beacon sequence to ensure that any change in signal is specific.

5. Y-Shaped Dimers

5.1 Introduction

Following on from the discovery by Mirkin *et al.* that self-assembly of AuNP could be achieved by functionalisation with DNA [69], there have been many examples of using such functionalised AuNP for DNA detection.

Most of these methods involve nanoparticles which have a uniform coating covering their entire surface resulting in uncontrolled aggregation.

Guo *et al.* showed a novel way of controlling this aggregation to preferentially form dimers by asymmetrically functionalising the nanoparticles. In this method, nanoparticles are bound to a glass slide and functionalised with PEG such that the entire surface of the particle will be coated with the exception of the area in contact with the glass. The particles are then removed from the glass and functionalised with an oligonucleotide. Since the majority of the surface of the particle is coated with a layer of PEG the oligonucleotide should bind to the free area resulting in an asymmetrically functionalised particle. Figure 5.1 shows a schematic of their formation.
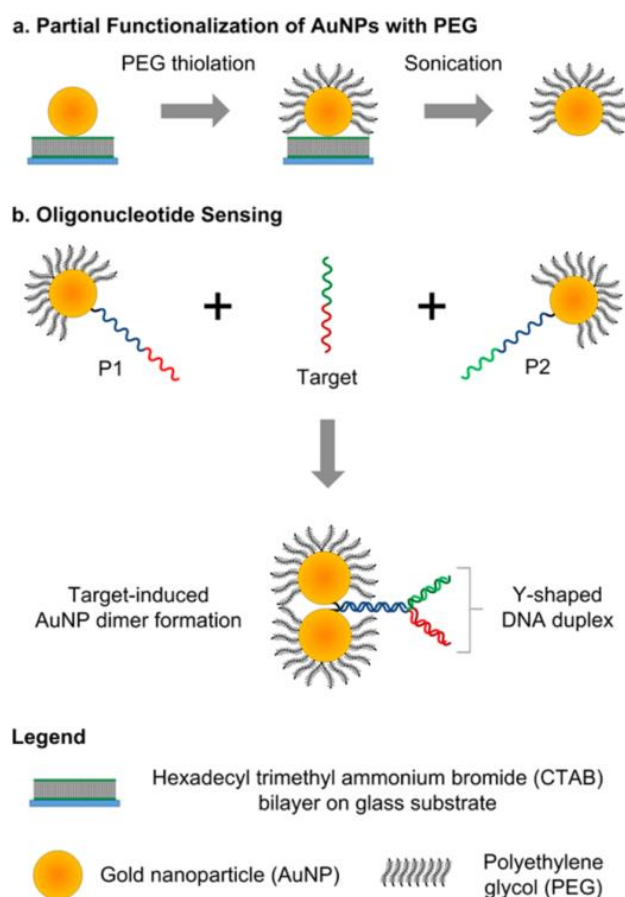
Figure 5.1 - Schematic of asymmetric functionalisation of nanoparticles. Reproduced with permission from [87]**. *Copyright © 2013, American Chemical Society.***

When two batches of these asymmetrically functionalised particles are combined with their target for detection, due to the limited amount of DNA on the surface which is localised in a small area, dimers are preferentially formed – Figure 5.1. This was confirmed through SEM imaging. Since the formation of these dimers results in a colour change – from red to blue – due to coupling of plasmons, it is possible to use colourimetric detection. A peak at 600 nm appears when the dimers form, in addition to the original peak ~ 500 nm. Figure 5.2 shows a normalised extinction spectrum before and after binding of the target. This method was found to be quantitative.

It has also been noted that the shift in plasmon is related to the inter-particle gap within the dimer, with smaller gaps giving larger shifts, this is another reason why the y-shaped dimer orientation is optimal compared with conventional (linear) methods.

Comparing linear and y-shaped asymmetric dimers showed that the conventional aggregates only resulted in a slight shift, due to sub-optimal particle gaps, compared to the y-shaped duplexes. [87]
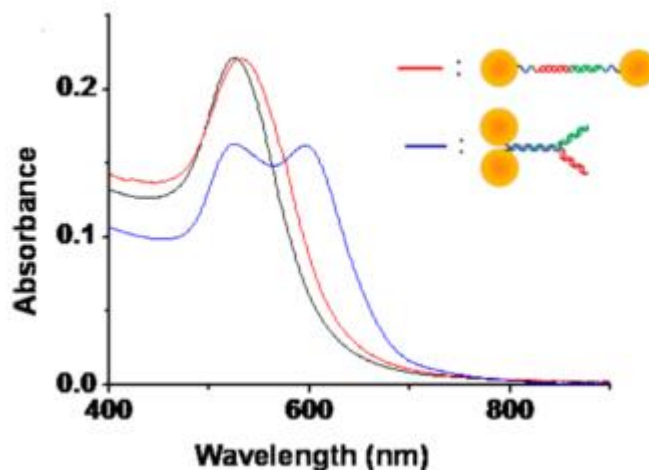
Figure 5.2 - Normalised absorption spectra for dimer formation (black = prior to target addition, red = linear dimers, blue = y-shaped dimers). Reproduced with permission from [87]. *Copyright © 2013, American Chemical Society.*

Zhou *et al*. extended the Y-shaped dimer approach by incorporating SERS analysis for the detection of microRNA (miRNA). The formation of dimers results in hot spots which increases the SERS enhancement. The signal is essentially 'turned on' in the presence of the DNA target. This can be used in cells by using alkynes and nitriles as Raman reporters on the nanoparticle surface as their peaks fall in the cell silent region allowing for easy analysis Figure 5.3. [86]

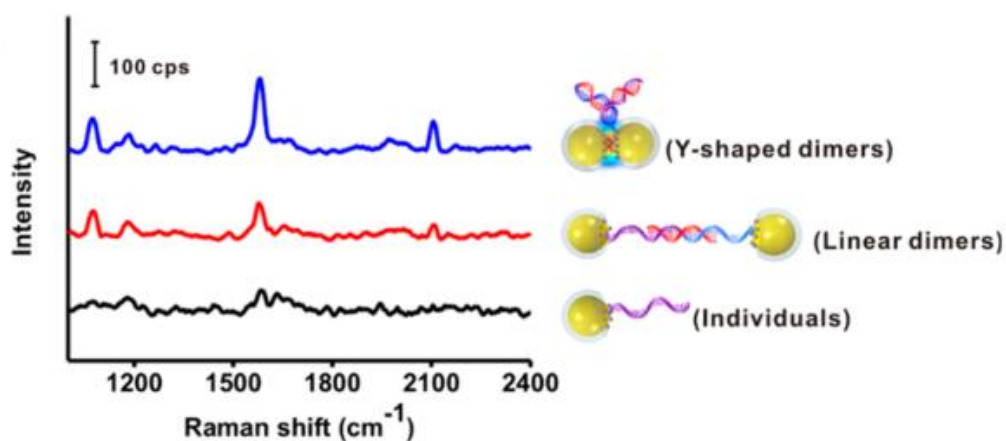A further example of asymmetrically functionalised nanoparticles for dimer formation has been shown using antibodies as the recognition moiety instead of nucleic acids. [107]

By controlling the aggregation, the stability of the conjugates is increased. It is difficult to control the aggregation of fully coated nanoparticles as there is an abundance of DNA available for hybridisation to another nanoparticle covering the whole surface, resulting in large aggregates of unknown size which will eventually precipitate out of solution. By coating the majority of the surface with a layer of PEG and controlling the DNA localisation to one side, it is now difficult for the nanoparticles to form larger aggregates and so dimers are preferentially formed, improving reproducibility. This also increases the sensitivity and dynamic range compared with fully coated particles.

5.2 Probe Sequences

The oligonucleotide sequences used are shown below, Figure 5.4 shows a schematic of the probes hybridising. The region of the probes involved in hybridisation with the target is a sequence which has been used previously as a GAPDH probe. The first nine bases of each probe are complementary to each other, allowing the probes to configure in their Y-shape as shown in Figure 5.4.

Probe A: 5' HS-CTGTTACTGCACGATACC

Probe B: 5' GAGTCCTTCCAGTAACAG-SH

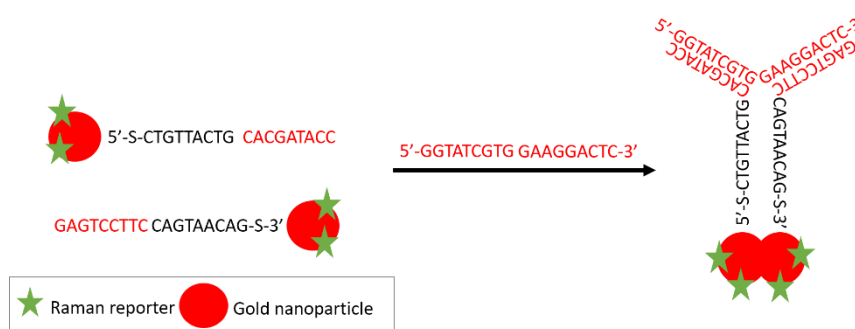Target sequence: 5' TGGTATCGTGGAAGGACTC

Figure 5.4 - Schematic of Y-shaped dimer probe hybridisation.

Figure 5.5 shows the melting curve to confirm that when the probes are incubated alone no hybridisation occurs, however when they are incubated with the target oligonucleotide a characteristic increase in absorbance is seen showing hybridisation is occurred. Therefore, non-specific binding isn't an issue.
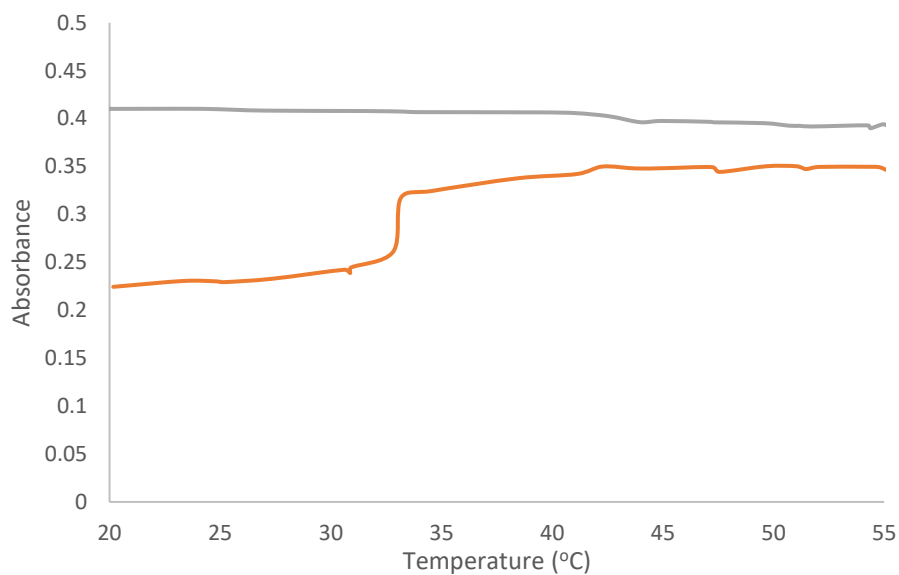
Figure 5.5 - Melting curve for y-shaped probes showing that for the probes alone (grey) no change in absorbance is seen on heating, indicating no hybridisation has occurred. However, when the probes are incubated with the target oligonucleotide (orange) an increase is seen indicating hybridisation has occurred.

5.3 Asymmetric Probes

5.3.1 Probe Synthesis & Characterisation

Asymmetric nanoparticles were produced according to the methods previously reported. [86,87] Briefly, glass slides were cleaned with piranha solution prior to being washed – firstly in Millipore water, then in ethanol. Slides were then activated with 10 % APTES for 30 minutes before being washed again – firstly in ethanol, then with water. APTES converts the silanol groups present on the glass surface to amine groups, to which gold nanoparticles readily attach (Figure 5.6).

Figure 5.6 - Schematic representation of activation of glass slide for AuNP attachment. Reproduced with permission from [107]. *Copyright © 2017, American Chemical Society.*

The activated slides were then immersed in AuNP for 5 minutes before being rinsed with water to remove any unbound particles. Figure 5.7 shows a glass slip coated in gold nanoparticles. Pink tint indicates that particles are bound to the glass. The AuNP-coated slide was then immersed in 100 µM PEG (MT-800) for 2 hours. After 2 hours, the slide was washed with water and sonicated for 2 minutes in 0.01M PB + 0.01% Tween20. Sonication was used to remove the PEG-coated particles from the glass, resulting in a suspension of particles asymmetric PEG-AuNP.

The PEG-coated particles were then concentrated by centrifugation before the addition of oligonucleotides.
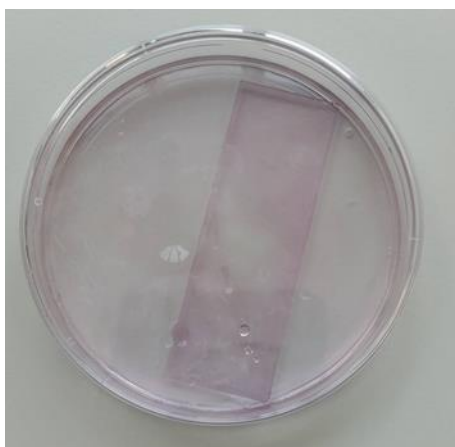
Figure 5.7 - Glass slide coated with gold nanoparticles.

Oligonucleotides (probe A or probe B) were added to PEG-coated AuNP and left to shake for 15 minutes. 40 µL of citrate was added before being shaken for another 15 minutes. Dye was then added and the mixture shaken for another 15 minutes before centrifugation. Samples were centrifuged at 3000 rpm for 20 minutes and the supernatant removed. Samples were then resuspended in the buffer of choice (either PB or PBS). A limitation of this method is that there are a limited number of sites on the glass for nanoparticle attachment, for this reason the resultant nanoparticle suspension is very weak and multiple batches must be combined for further use.

Figure 5.8 shows the normalised extinction spectra for the 'asymmetric' nanoparticles (bare/PEG only/PEG+DNA). Upon coating the particles with PEG a slight red shift is seen (~2 nm), indicating that the surface on the AuNP has changed and the coating has been successful. When the oligonucleotide was added the plasmon doesn't show any significant shift. This is to be expected due to the asymmetric nature of the functionalisation meaning only a small amount is functionalised to the surface.
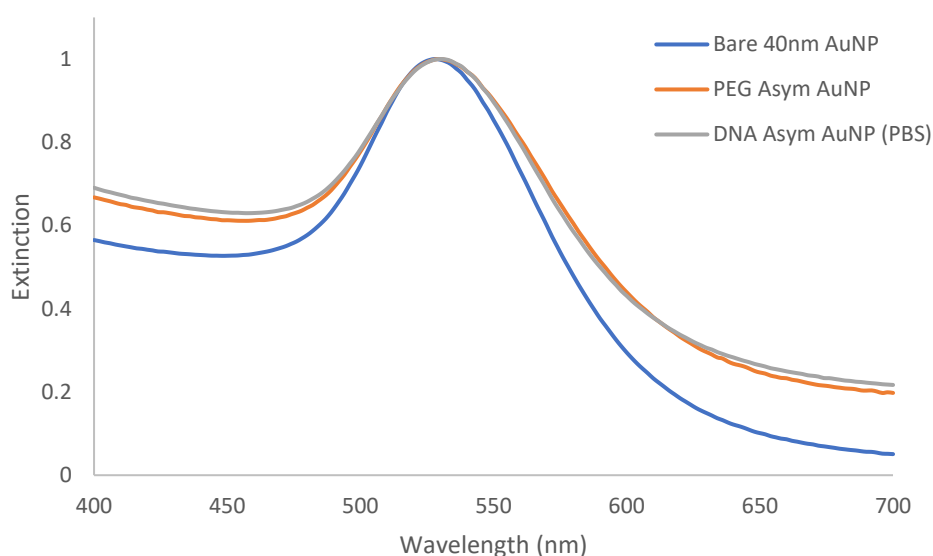
Figure 5.8 - Normalised extinction spectra for bare AuNP (blue), asymmetric PEG-coated AuNP (orange), and asymmetric probes (grey).

5.3.2 Solution Based Hybridisation

The probes were assessed with and without the addition of the target oligonucleotide to determine whether the hybridisation was occurring. Figure 5.9 shows the extinction profile for the asymmetric probes with and without addition of the target molecule. As seen in Figure 5.2, it was expected that in the presence of the target oligonucleotide that the nanoparticles would dimerise resulting in a change in the extinction spectra. However, there was no change in the profile, indicating that no hybridisation occurred.
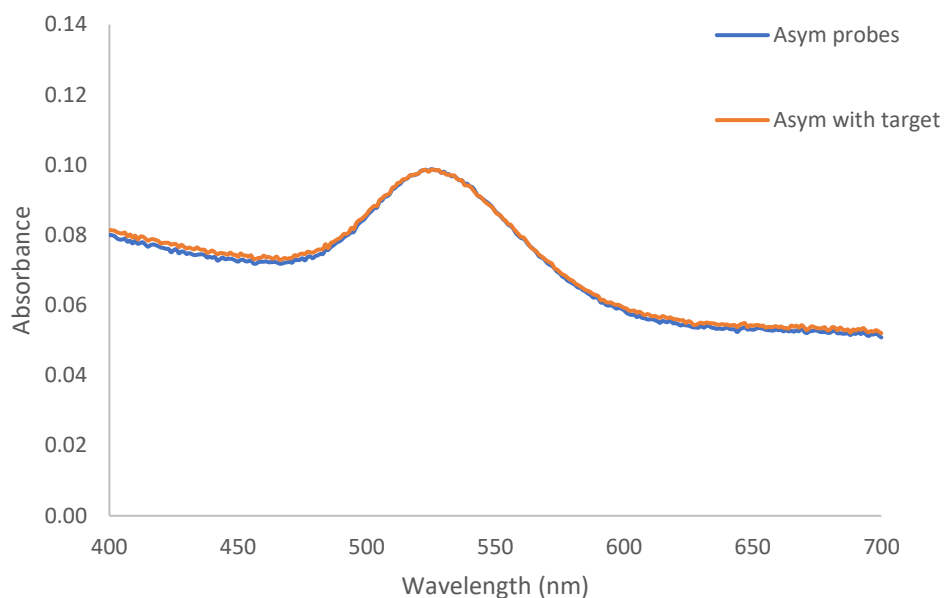
Figure 5.9 - Extinction spectra for asymmetric probes before and after incubation with target oligonucleotide.

There are two possible explanations as to why the hybridisation did not occur; i) steric hinderance, and ii) the probes aren't functionalised with DNA.

A slight change in the extinction spectra was seen after the functionalisation with DNA suggesting that there is a change in the surface chemistry, i.e. DNA has attached to the AuNP surface. As only a small amount of DNA was expected to attach to the surface, only a small change in the extinction spectra can be expected.

Another explanation is that steric hinderance from the PEG molecules is preventing the DNA from hybridising to the target. A solution to this may be using a smaller PEG molecule to reduce the steric hinderance and allow hybridisation to occur.

Another possible explanation is that DNA is not attaching to the particles. It could be possible that the PEG layer is coating too much of the surface resulting in not enough surface space for the DNA to attach. A solution to this may be to try using less PEG.

5.4 Fully Coated Probes

5.4.1 Probe Synthesis & Characterisation

Due to issues with the asymmetric probes, nanoparticles were fully coated with the Y-shapes oligonucleotides to determine whether hybridisation could be achieved.

Figure 5.10 shows the extinction spectra for the fully oligonucleotide coated nanoparticles. Slight dampening is seen for the functionalised particles, however they are still stable in solution. A shift of ~ 2 nm was observed on functionalisation of the particles, indicating that the surface has been successfully coated. When the two separate probes were combined, no change was seen in the extinction spectrum demonstrating that no self-hybridisation occurred between the two sets of oligonucleotides.
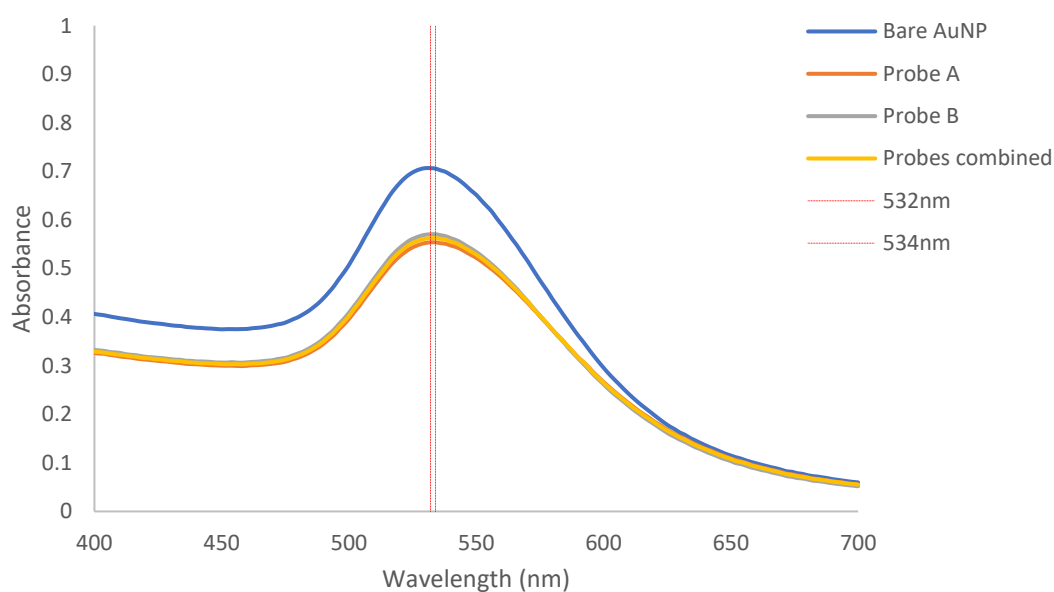
Figure 5.10 - Extinction spectra for AuNP fully coated with Y-shaped oligonucleotides.

The fully coated probes were also stable in PBS buffer, confirming that the DNA has attached to the surface (Figure 5.11). In comparison, bare nanoparticles aggregated when resuspended in PBS.

119
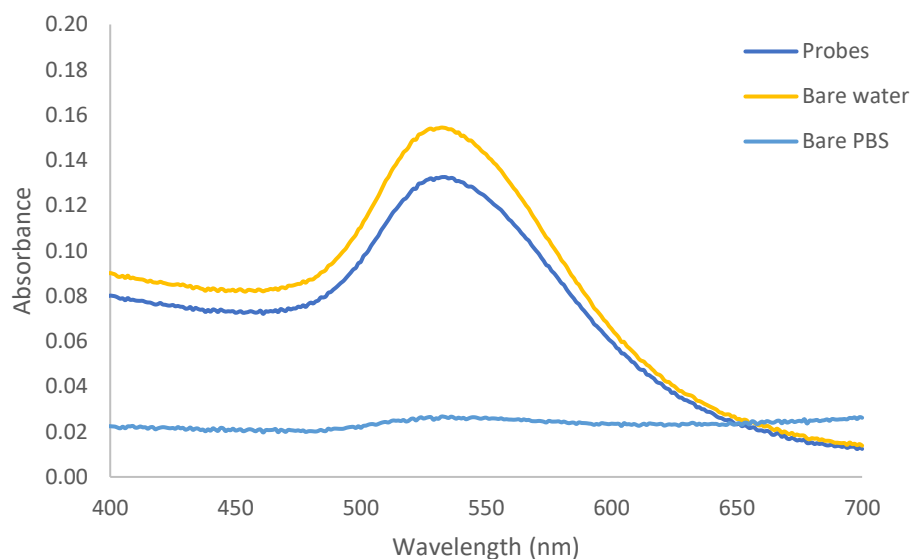
Figure 5.11 - Extinction spectra for fully coated oligonucleotide AuNP suspended in PBS buffer, compared to bare nanoparticles in water and buffer. Bare particles aggregate when suspended in PBS, however the probes are stable indicating that the surface is protected a DNA coating.

5.4.2 Solution Based Hybridisation

The fully coated probes were assessed with and without the target oligonucleotide to determine whether hybridisation occurred. Figure 5.12 shows the extinction spectra for the fully coated probes incubated with the target oligonucleotide at two concentrations. After incubation with the target oligonucleotide a change in colour was seen from pink to colourless. This is confirmed in the extinction spectra by dampening and broadening of the plasmon peak, indicating that aggregation occurred.
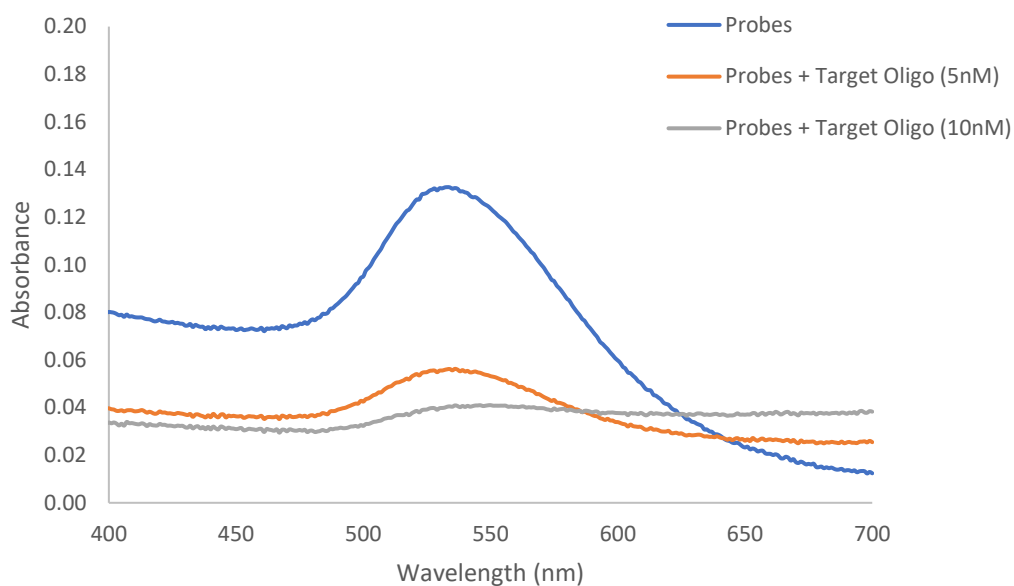
Figure 5.12 - Extinction spectra for fully coated nanoparticles incubated with target oligonucleotide.

To confirm that the aggregation was a result of hybridisation of the oligonucleotides the samples were re-heated to denature the DNA. Denaturing the DNA should cause the nanoparticles to re-disperse. Figure 5.13 shows the extinction spectra obtained. The plasmon peak at ~ 530 nm reappears after incubation at high temperature. This was confirmed by the reappearance of the pink colour in the samples. This confirmed that the DNA denatured and the AuNP were capable of being resuspended following hybridisation.
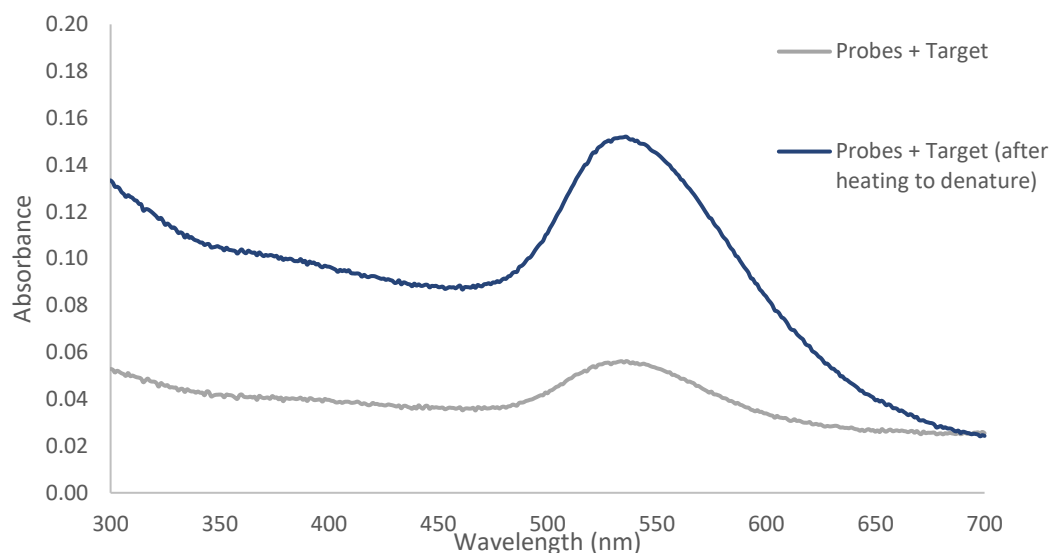
Figure 5.13 - Extinction spectra for fully coated probes after being heated to redisperse the nanoparticles.

A kinetic experiment was carried out to follow the hybridisation occurring. For this experiment, extinction spectra were taken every 5 minutes after the addition of the target oligonucleotide. Figure 5.14 shows the extinction spectra obtained for the probes alone compared to the probes with the target oligonucleotide.

For the probes incubated with target, a drop in intensity occurred after 5 minutes, indicating that hybridisation occurred almost immediately. This is demonstrated by the peak at 534 nm decreasing as a new peak at approximately 700 nm increased. The probes incubated without target do not exhibit any change in intensity as seen in the extinction spectra, as expected.
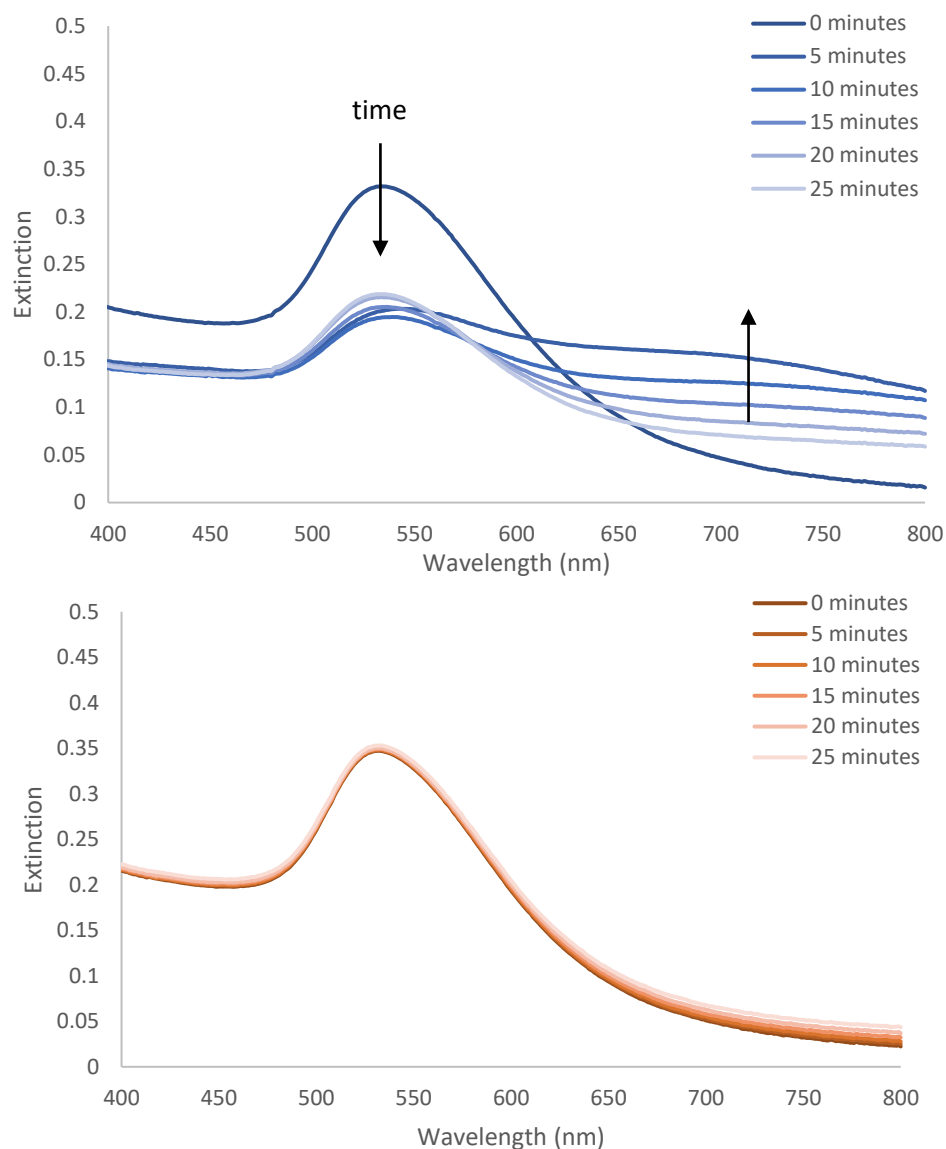
Figure 5.14 - Extinction spectra taken at 5 minutes intervals for probes + target (top) and probes alone (bottom) showing hybridisation occurring.

Figure 5.15 shows a plot of the ratio of the extinction intensity at 700 nm and 534 nm over 25 minutes for the probes with and without the target. Without the target, ratio stays constant throughout the 25 minutes since no hybridisation is occurring. As expected, in the presence of the target the ratio changes over time. On addition of the target the ratio increases due to the drop in intensity at 534 nm, it then gradually decreases as aggregation occurs.
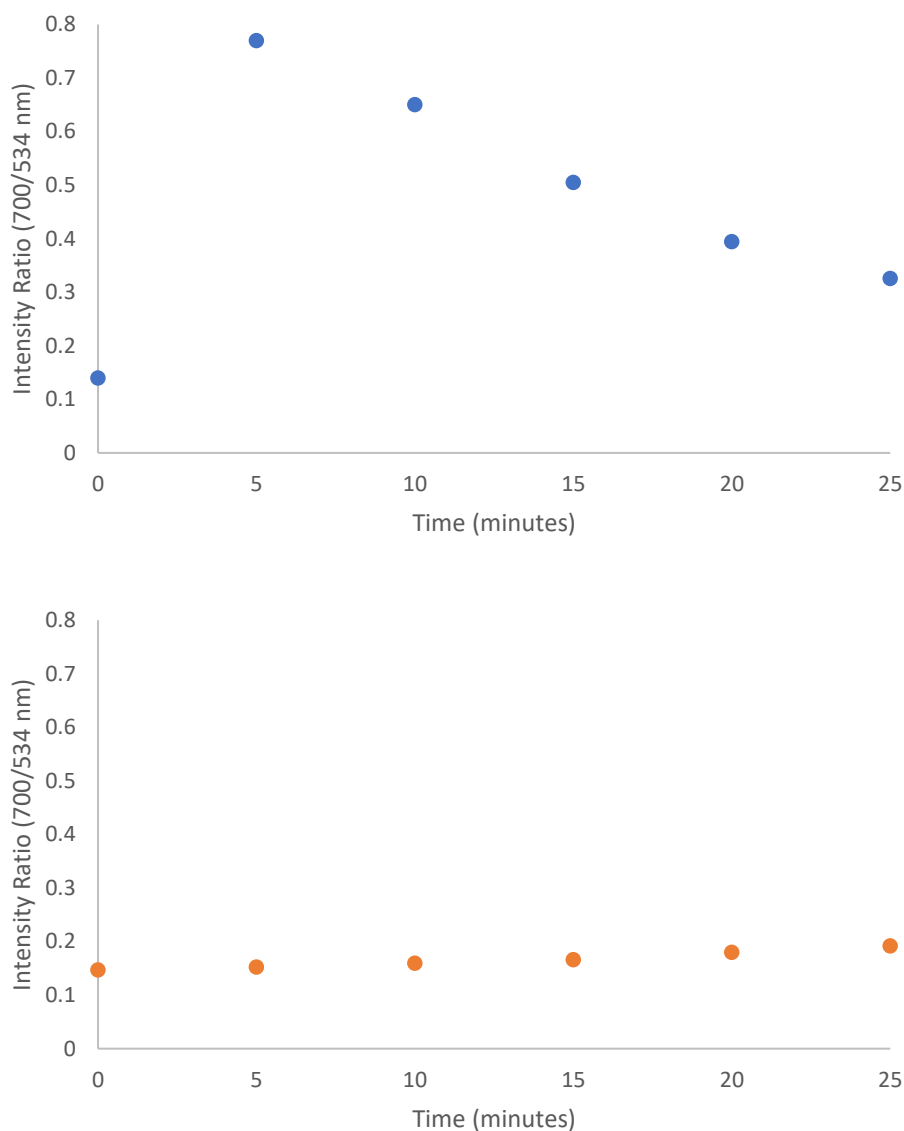
Figure 5.15 - Plot of the extinction intensity ratio at 700/534 nm over the 25 minute hybridisation for probes + target (top) and probes alone (bottom) showing the change in ratio as hybridisation occurs in the presence of the target.

In order to confirm that the hybridisation is specific, a random control target sequence could be used and compared to the target oligonucleotide.

Despite the extinction spectra indicating aggregation of the nanoparticles, a slight decrease in SERS signal was seen upon addition of the target. Figure 5.16 shows the SERS spectra following addition of the target oligonucleotide. For comparison, the

SERS response upon addition of NaCl to aggregate the nanoparticles is also shown. In the presence of NaCl the probes aggregated, resulting in an increase in SERS signal.
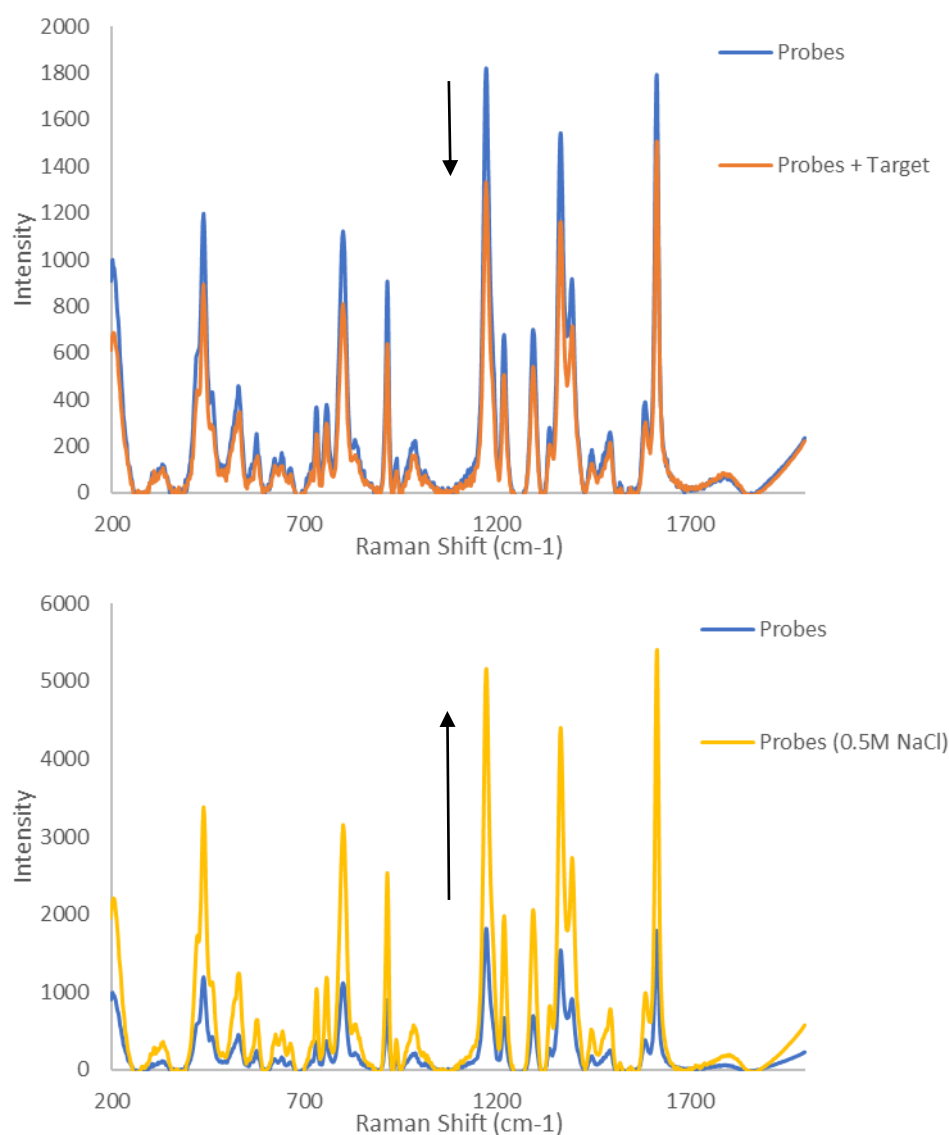
Figure 5.16 - SERS spectra for probes following incubation with target (top) or NaCl (bottom). Spectra measured using a 638 nm laser line with a 1 second acquisition time.

The previous SERS spectra were taken approximately 2 hours following target addition. In order to determine whether any SERS response was occurring, spectra were taken at 2 minute intervals following the addition of the target. Figure 5.17 shows a plot of the intensity of the main band at 1616 cm^{-1}.
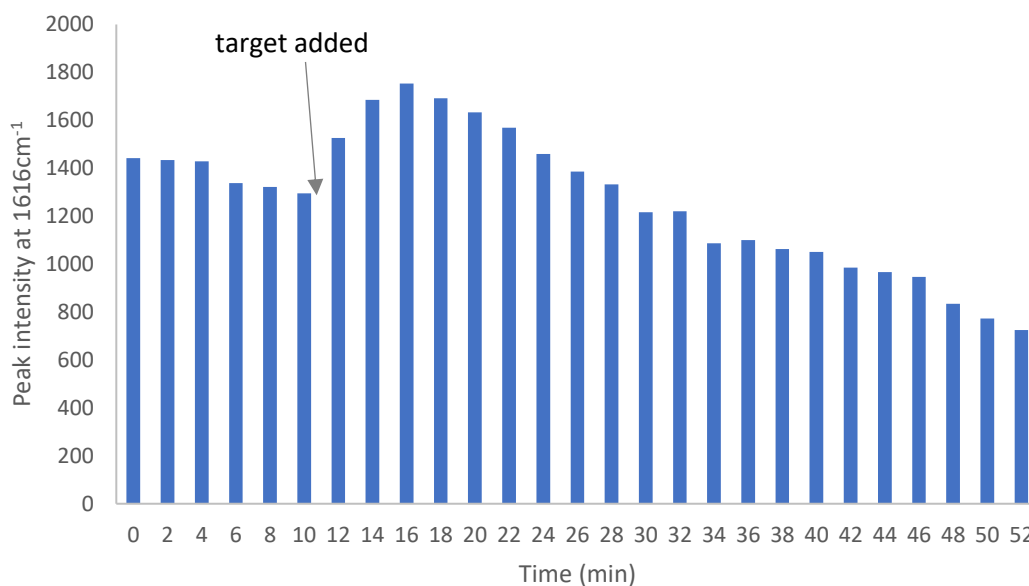
Figure 5.17 - Plot of intensity of main band at 1616 cm^{-1} following addition of target to probes.

A maximum signal was observed 6 minutes after the addition of the target, this indicated a slight change in SERS response is occurring since the extinction spectra showed that hybridisation had occurred as early as 5 minutes after target addition. However, only an approximately 1.3-fold increase is seen. Figure 5.18 shows the same experiment following the addition of 1 M NaCl. On addition on NaCl to aggregate the probes an approximate 2-fold increase in signal was observed.

It is thought that the reason for the minimal SERS response is related to the distance between the nanoparticles. When the nanoparticles aggregate as a result of DNA hybridisation it is possible that, since these probes were designed for asymmetric nanoparticles, they cannot come in close enough proximity for optimal SERS response. When NaCl is added to the particles uncontrolled aggregation occurs, hence a greater SERS response is seen.
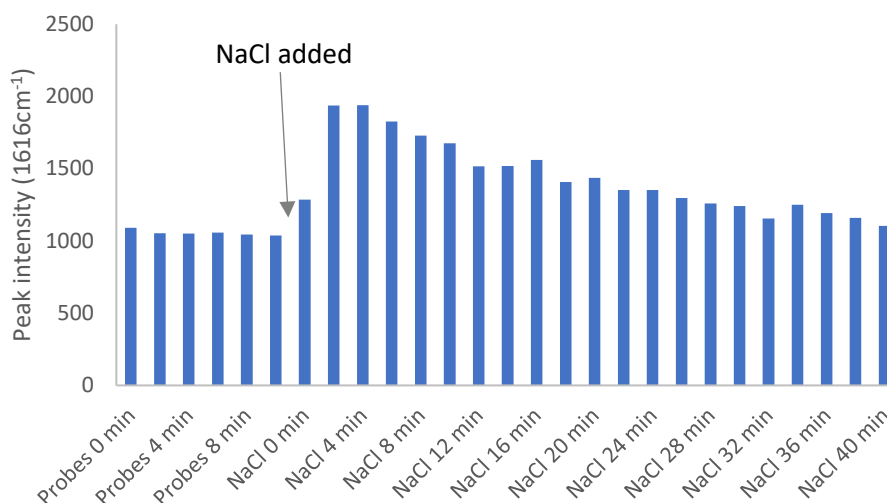
Figure 5.18 - Plot of peak intensity at 1616 cm^{-1} following addition of NaCl to aggregate probes.

Furthermore, the initial MGITC signal is already relatively high. By reducing this, possibly by only adding to MGITC to one set of probes, it may be possible to see a greater enhancement.

5.4.3 Cell Mapping

Similarly to in previous chapters the probes were incubated with PNT2 cells to determine whether any signal could be observed. Cells were incubated with AuNP functionalised with MGITC only, MGITC+probe A, MGITC+probe B, MGITC+combined probes (A+B). Samples were incubated for 2 hours or overnight before being fixed. Figure 5.19 and Figure 5.20 show the false colour images created using DCLS for 2 hours and 24 hours, respectively.

Compared to cells containing MGITC-AuNP, the oligonucleotide probes (individual or combined probes) showed a considerably higher signal. However, without comparison using random oligonucleotide sequences it is not possible to determine if this increased signal is a result of specific hybridisation. It is possible that adding

the oligonucleotide makes the AuNP more biocompatible, allowing them to stay in the cells for longer than the MGITC-AuNP.

For both timepoints, probe B shows higher signal than probe A. During probe functionalisation probe B appeared to be less stable so it is possible that aggregation occurred within the cells causing this increased signal.

If the probes were hybridising inside cells as expected, and causing specific aggregation of the nanoparticles, it would be expected that the combined probes would result in higher signal than the individual probes. However, this is not the case.

Comparing the timepoints, considerably higher signal can be seen at 2 hours, compared to overnight incubation. This may indicate that the probes are entering the cells but being removed again within 24 hours.

It is worth noting that this is in contrast to the thiol probes assessed in chapter 2, which showed low signal at 2 hours and higher signal at 24 hours. The main difference between the two sets of probes is the oligonucleotide sequence.
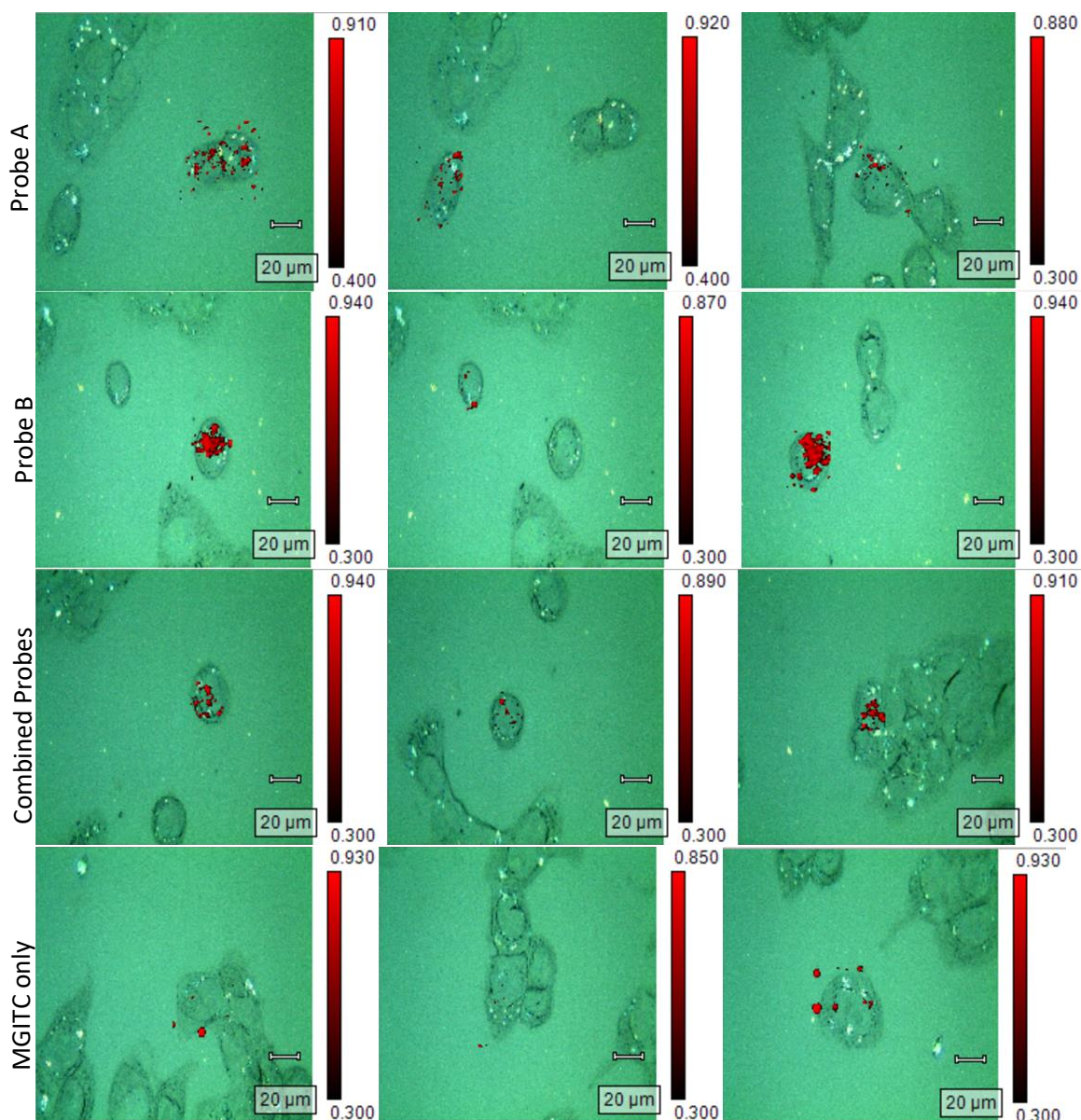
Figure 5.19 - False colour images for PNT2 cells incubated with Probe A, Probe B, combined probes and MGITC-AuNP for 2 hours in triplicate. After incubation cells were fixed and mapped using a 633 nm laser at 10 % power and 0.2 second acquisition.
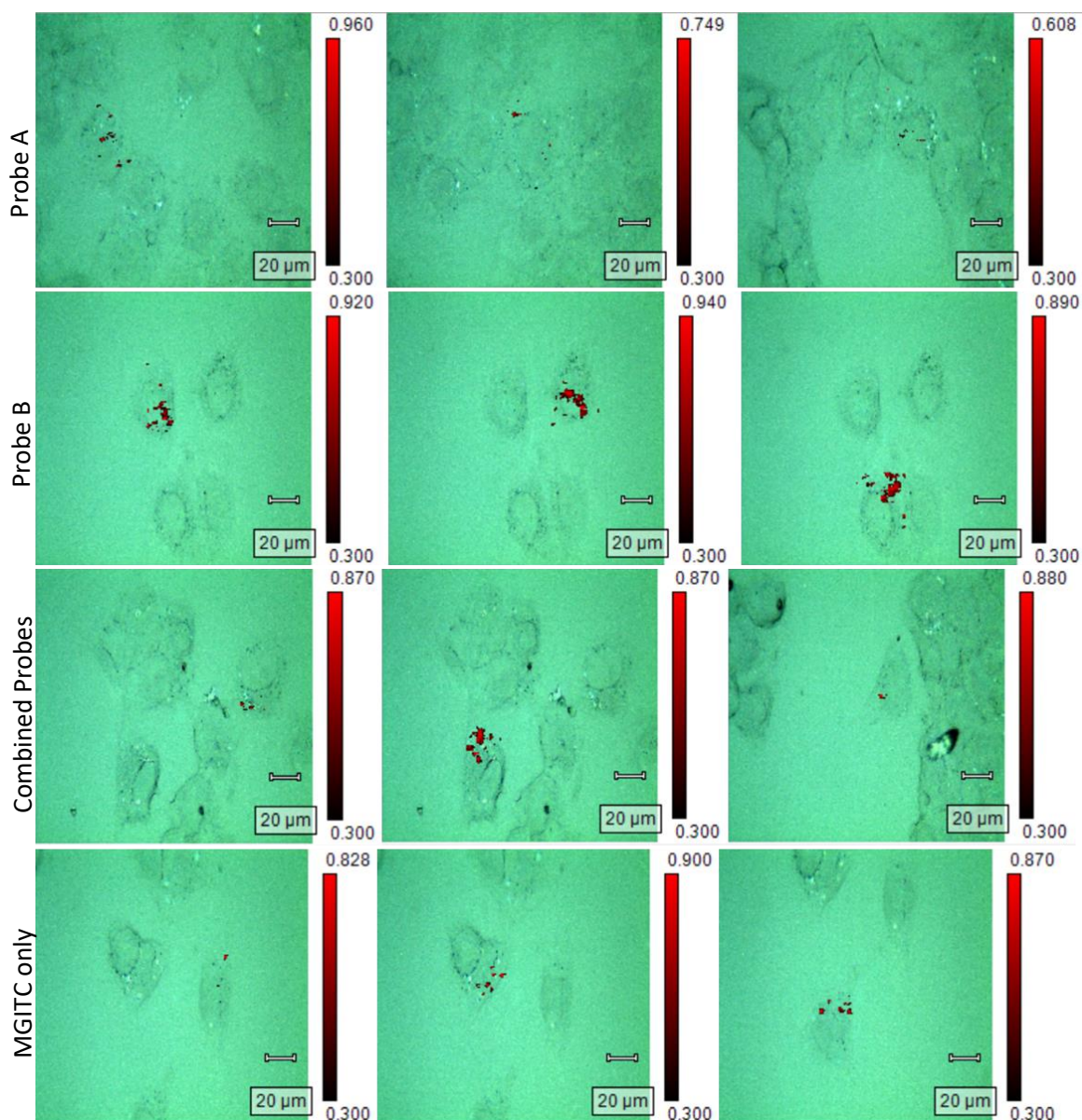
Figure 5.20 - False colour images for PNT2 cells incubated with Probe A, Probe B, combined probes and MGITC-AuNP for 24 hours in triplicate. After incubation cells were fixed and mapped using a 633 nm laser at 10 % power and 0.2 second acquisition.

5.4.4 Cell Toxicity

Cell counting was used to assess the toxicity of the probes in cells. In order to be accurate the cells were washed before performing the count, therefore removing dead cells, meaning that only the live cells are counted.

Figure 5.21 gives the calculated viability for PNT2 cells. Cells were incubated overnight with i) nothing added to serve as a control for comparison, ii) 1% DMSO to show the effect of toxicity on the cell count, iii) MGITC AuNP and iv) AuNP coated with MGITC and oligonucleotide (probes A and B combined).
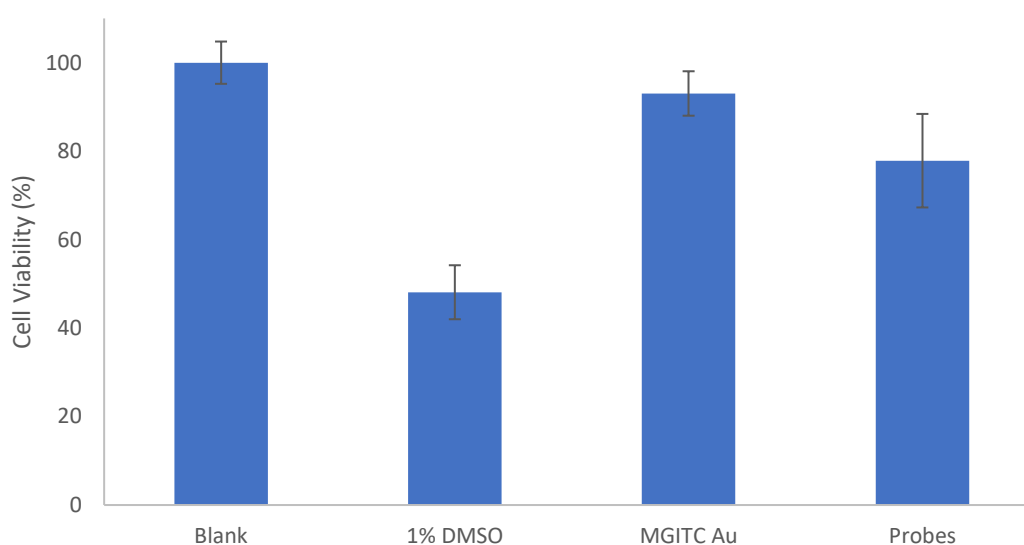
Figure 5.21 - Cell viability for PNT2 cells incubated with AuNP probes.

Cell counts were compared to the blank to determine the percentage viability. Approximately half of the cells incubated with DMSO were killed due to its known cytotoxic effect. MGITC-AuNP did not have a significant effect on cell viability with approximately 93 % of cells remaining after 24 hour incubation. Probes consisting of AuNP functionalised with both MGITC and oligonucleotide had a slightly lower viability of approximately 78 %. Since cell mapping shows that AuNP appear to enter the cells whether they contain only MGITC or MGITC and oligonucleotide, it is possible that the addition of the oligonucleotide caused the probes to disrupt cellular processes. However, the exact mechanism of this disruption cannot be determined

at this point. Possibly the oligonucleotides are binding to other sequences within the cells, either specifically or non-specifically, preventing them from carrying out their function.

5.7 Conclusions

The asymmetric y-shaped dimer gave positive results, however it has not been possible to repeat the duplex dimer formation experimentally. This difficulty in replicating the experiment may explain the limited number of published papers on the area. [86,87]

Using the same oligonucleotide sequences but fully coating the particles, as opposed to asymmetrically coating them, showed limited success. Extinction spectroscopy indicated clear aggregation of the particles on addition of the target, as expected, and the reversibility of this aggregation confirms that it is a result of hybridisation. Therefore, the target is detectable by extinction spectroscopy in solution. However, the expected, SERS enhancement was not observed. This may be due to sub-optimal distances between the nanoparticles.

Although the specificity of the probes was shown by the DNA melting curve, in order to confirm this, a random control probe would have to be assessed in place of the target oligonucleotide.

Following probe incubation with cells the SERS signal of the probes was observed, indicating that they are able to enter the cells. However, it is not possible to determine whether or not hybridisation has occurred without future investigations. Comparison with random control probes would be required to determine whether the probe signal is specific to GAPDH. Comparison of images with FISH probes could also be used to determine whether probes co-localise. Furthermore, TEM could be used in order to determine the localisation of the probes within the cells.

6. Conclusions & Further Work

The aim of this project was to develop a novel, reliable method of detecting mRNA in cells using Raman spectroscopy with the ultimate goal being disease diagnosis. Three main avenues were explored: i) a 'Raman *in situ* hybridisation', or RISH, approach where labelled oligos hybridised to the target mRNA *in situ* allowing localisation of signal, ii) a Raman beacon approach which provides a change in signal based on whether or not the target is present, and iii) a nanoparticle dimer system where SERRS response should 'turn on' in the presence of the target due to the formation of hot spots in the dimers. Each method has its own strengths and weaknesses, however all three methods would require extensive further work to reliably allow mRNA detection.

RISH is, in theory, the simplest concept – comparable to the widely used FISH. An oligonucleotide, complementary to the target, was attached to gold nanoparticles, with a Raman active dye for detection. Inside the cells, the oligonucleotide should bind to its counterpart allowing localisation when mapped using Raman microscopy. Two probe systems were assessed.

The first used spermine to electrostatically attach the oligonucleotide to the nanoparticle, whilst the second method used a thiol modification on the oligonucleotide for nanoparticle attachment. For both sets, the probes were incubated with cells overnight before cell fixation. Fixed cells were then mapped and false colour images were generated to represent the localisation of the probes.

Neither method showed any significant discrimination between probes containing oligonucleotide complementary to the target and those containing a random sequence, despite only the complementary probes showing hybridisation to the target in solution. 3D mapping indicated that both sets of probes entered the cells, although it was not possible to determine whether they were free in the cytoplasm or trapped in vesicles.

One possible theory is that the particles are entering the cells but are too large to be removed. This means that, whether hybridisation occurs or not, the probes remain inside the cell giving rise to signal.

In order to progress the RISH concept further, one method would be to synthesise the probes using smaller nanoparticles. Smaller particles may be able to be removed from the cell more readily if not hybridised to the target, allowing specificity to be achieved.

Towards the end of the project a new method was introduced. The oligonucleotide was modified to contain EdU in place of two thymine bases. However, Raman spectroscopy was not sensitive enough to detect these probes on their own due to the signal from the alkyne being too weak. To progress this method further, nanoparticles could be added to the assay to improve sensitivity. Alkyne-modified oligonucleotide would be added to the cells separately from nanoparticles in the hope that by having nanoparticles within the cell, although not attached to the oligonucleotide, the Raman signal would be enhanced.

Furthermore, SRS imaging, which has improved sensitivity could be assessed. By using a stronger alkyne label, it is possible that SRS could be used without using nanoparticles, simplifying the analysis.

The second probe design showed the greatest potential. Molecular beacons are already commonly used for fluorescence detection and the aim here was to investigate a similar method using SERS. A gold nanoparticle was functionalised with a dye and a dye-labelled hairpin loop oligonucleotide. In the closed position signal was obtained from both dyes, but in the open position the signal changed as the beacon opened removing the second dye from the surface. This allowed a ratiometric detection of the target.

Due to issues with supply of the labelled hairpin oligonucleotide, a limited number of experiments were performed. However, AuNP were successfully functionalised and a proof-of-concept experiment in solution proved successful. On addition to cells it

was possible to detect signal from the probes, however the intensity was too low for ratiometric analysis. Overall, the Raman beacon would need further investigation but has shown potential to be progressed further.

Comparison with a random control sequence would be necessary to ensure the response is specific to the target sequence. Furthermore, whether the probe can quantitatively measure the amount of target in a sample would have to be assessed. Further probe optimisation may be required to improve the signal strength in cells in order to allow the ratio to be measured, or SRS may be an alternative method to achieve greater sensitivity.

Lastly, a dimerization approach was explored. The aim was to create asymmetrically functionalised AuNP, however, despite promising extinction spectra, the nanoparticles did not dimerise as expected when incubated with the target. It was therefore not possible to determine if the asymmetric functionalisation had been successful. When the same oligonucleotides were used to fully coat the particles extinction spectra showed that aggregation did occur on addition of the target oligonucleotide, however the SERS response was limited. These probes could be detected in cells but it was not possible to determine whether they had hybridised to the target or were in the cytoplasm. In order to confirm whether the probes were hybridised inside the cells a second set of random control probes would need to be assessed for comparison. Comparison with known FISH probes would also be useful.

To progress this method further the oligonucleotide lengths may need optimisation to control the distance between the nanoparticles and optimise the SERS response. This could be done by using linkers of differing length to assess which gives the best response.

Overall, the probes with a switchable signal show the most promise for specific mRNA detection, however further work is required to create a reliable assay. With further optimisation and the use of SRS, both the SERS beacon and the fully coated probes have the potential to be useful in disease diagnosis.

References

1.   Cardiovascular Disease. Available at: https://www.bhf.org.uk/heart-health/conditions/cardiovascular-disease. (Accessed: 1st November 2015)

2.   CVD Statistics - UK Factsheet. Available at: https://www.bhf.org.uk/what-we-do/our-research/heart-statistics/heart-statistics-publications.

3.   Ferrari, P. & Krozowski, Z. Role of the 11beta-hydroxysteroid dehydrogenase type 2 in blood pressure regulation. *Kidney Int.* **57,** 1374–81 (2000).

4.   Fuller, P. J. & Young, M. J. Mechanisms of mineralocorticoid action. *Hypertension* **46,** 1227–1235 (2005).

5.   Stewart, P. M., Corrie, J. E. T., Shackleton, C. H. L. & Edwards, C. R. W. Syndrome of apparent mineralocorticoid excess. A defect in the cortisol-cortisone shuttle. *J. Clin. Invest.* **82,** 340–349 (1988).

6.   Craigie, E., Evans, L. C., Mullins, J. J. & Bailey, M. a. Failure to Downregulate the Epithelial Sodium Channel Causes Salt Sensitivity in Hsd11b2 Heterozygote Mice. *Hypertension* **60,** 684–690 (2012).

7.   Dahm, R. Friedrich Miescher and the discovery of DNA. *Dev. Biol.* **2,** 274–288 (2005).

8.   Watson, J. D. & Crick, F. H. C. Molecular Structure of Nucleic Acids: A Structure for Deoxyribose Nucleic Acid. *Nature1* **171,** 737–738 (1953).

9.   Franklin, R. E. & Gosling, R. G. The structure of sodium thymonucleate fibres. I. The influence of water content. *Acta Crystallogr.* **6,** 673–677 (1853).

10.   Wilkins, M. H., Stokes, a R. & Wilson, H. R. Molecular structure of nucleic acids. Molecular structure of deoxypentose nucleic acids. 1953. *Ann. N. Y. Acad. Sci.* **758,** 13–16 (1995).

11.   Goodwin, W., Linacre, A. & Hadi, S. *An Introduction to Forensic Genetics*. (John Wiley & Sons, 2011).

12.   Bruice, P. Y. *Organic Chemistry*. (Pearson, 2011).

13.   Butler, J. M. *Fundamentals of Forensic DNA Typing*. (Academic Press, 2010).

14.   Cooper, G. M. *The Cell: A Molecular Approach*. (Sinauer Associates, 2000).

15.   Wetmur, J. G. Hybridization and Renaturation Kinetics of Nucleic Acids. *Annu. Rev. Biophys. Bioeng.* **5,** 337–361 (1976).

16.   Lodish, H., Berk, A. & Zipursky, S. L. *Molecular Cell Biology*. (W. H. Freeman, 2000).

17.   Lander, E. S., Linton, L. M. & Birren, B. Initial sequencing and analysis of the human genome. *Nature* **409,** 860–921 (2001).

18.   Clancy, S. & Brown, W. Translation: DNA to mRNA to Protein. *Nat. Educ.* **1,** 171 (2008).

19.   Elliot, D. & Ladomery, M. *Molecular Biology of RNA*. (Oxford University Press, 2011).

20.   Mullis, K., Faloone, F. & Scharf, S. Specific Enzymatic Amplification of DNA in Vitro: The Polymerase Chain Reaction. *Cold Spring Harbous Symp. Quant. Biol.* **51,** 263–273 (1986).

21.   Ginzinger, D. G. Gene quantification using real-time quantitative PCR : An emerging technology hits the mainstream. **30,** 503–512 (2002).

22.   Mcneil, N. & Ried, T. Novel molecular cytogenetic techniques for identifying complex chromosomal rearrangements : technology and applications in molecular medicine. *Expert Rev. Mol. Med.* **2,** 1–14 (2000).

23.   Gall, J. G. & Pardue, M. L. Formation and detection of RNA-DNA hybrid molecules in cytological preparations. *Proc. Natl. Acad. Sci. U. S. A.* **63,** 378–383 (1969).

24.   Gall, J. G. The Origin of In Situ Hybridisation - a Personal History. *Methods* **98,**

4–9 (2016).

25. H. A. John, M. L. Birnstiel & K. W. Jones. RNA-DNA Hybrids at the Cytological Level. *Nature* **223,** 582–587 (1969).

26. Buongiorno-Nardelli, M. & Amaldi, F. Autoradiographic detection of molecular hybrids between rRNA and DNA in tissue sections. *Nature* **225,** 946–948 (1970).

27. Rudkin, G. T. & Stollar, B. D. High resolution detection of DNA-RNA hybrids in situ by indirect immunofluorescence [29]. *Nature* **265,** 472–473 (1977).

28. O'Connor, C. Fluorescence In Situ Hybridization (FISH). *Nat. Educ.* **171,** 1 (2008).

29. Bauman, J. G. J., Wiegant, J., Borst, P. & van Duijn, P. A new method for fluorescence microscopical localization of specific DNA sequences by in situ hybridization of fluorochrome-labelled RNA. *Exp. Cell. Res.* **128,** 485–490 (1980).

30. Femino, a M., Fay, F. S., Fogarty, K. & Singer, R. H. Visualization of single RNA transcripts in situ. *Science* **280,** 585–590 (1998).

31. Raj, A., van den Bogaard, P., Rifkin, S. a, van Oudenaarden, A. & Tyagi, S. Imaging individual mRNA molecules using multiple singly labeled probes. *Nat. Methods* **5,** 877–879 (2008).

32. Raman, C. V. & Krishnan, K. S. A New Type of Secondary Radiation. *Nature* **121,** 501–502 (1928).

33. Ewen Smith and Geoffrey Dent. *Modern Raman Spectroscopy - A Practical Approach*. (John Wiley & sons Ltd., 2005).

34. Robert, B. Resonance Raman Spectroscopy. *Photosynth. Res.* **101,** 147–55 (2009).

35. Albrecht, M. G. & Creighton, J. A. Anomalously Intense Raman Spectra of

Pyridine at a Silver Electrode. *J. Am. Chem. Soc.* **99,** 5215–5217 (1977).

36. Wustholz, K. L. *et al.* Structure-activity relationships in gold nanoparticle dimers and trimers for surface-enhanced raman spectroscopy. *J. Am. Chem. Soc.* **132,** 10903–10910 (2010).

37. Dubertret, B., Calame, M. & Libchaber, a J. Single-mismatch detection using gold-quenched fluorescent oligonucleotides. *Nat. Biotechnol.* **19,** 365–70 (2001).

38. Shimron, S., Cecconello, A., Lu, C. H. & Willner, I. Metal nanoparticle-functionalized DNA tweezers: From mechanically programmed nanostructures to switchable fluorescence properties. *Nano Lett.* **13,** 3791–3795 (2013).

39. Dougan, J. a & Faulds, K. Surface enhanced Raman scattering for multiplexed detection. *Analyst* **137,** 545–54 (2012).

40. Kneipp, K., Wang, Y., Kneipp, H., Perelman, L. T. & Itzkan, I. Single molecule detection using surface-enhanced Raman scattering (SERS). *Phys. Rev. …* **78,** 1667–1670 (1997).

41. Nie, S. & Emory, S. R. Probing single molecules and single nanoparticles by surface enhanced raman scattering. *Science (80-.).* **275,** 1102–1106 (1997).

42. Kneipp, K., Kneipp, H. & Kneipp, J. Surface-enhanced raman scattering in local optical fields of silver and gold nanoaggregates - From single-molecule raman spectroscopy to ultrasensitive probing in live cells. *Acc. Chem. Res.* **39,** 443–450 (2006).

43. Faulds, K., Barbagallo, R. P., Keer, J. T., Smith, W. E. & Graham, D. SERRS as a more sensitive technique for the detection of labelled oligonucleotides compared to fluorescence. *Analyst* **129,** 567–568 (2004).

44. Gracie, K. *et al.* Simultaneous detection and quantification of three bacterial

meningitis pathogens by SERS. *Chem. Sci.* **5,** 1030 (2014).

45. Gracie, K., Lindsay, D., Graham, D. & Faulds, K. Bacterial meningitis pathogens identified in clinical samples using a SERS DNA detection assay. *Anal. Methods* **7,** 1269–1272 (2015).

46. Faulds, K. *et al.* A new approach for DNA detection by SERRS. *Faraday Discuss.* **132,** 261-268-319 (2006).

47. Kneipp, J., Kneipp, H., Mclaughlin, M., Brown, D. & Kneipp, K. In Vivo Molecular Probing of Cellular Compartments with Gold Nanoparticles and Nanoggregates. *Nano Lett.* **6,** 2225–2231 (2006).

48. Stokes, R. J. *et al.* Rapid cell mapping using nanoparticles and SERRS. *Analyst* **134,** 170–175 (2009).

49. Ye, S., Li, X., Wang, M. & Tang, B. Fluorescence and SERS Imaging for the Simultaneous Absolute Quantification of Multiple miRNAs in Living Cells. *Anal. Chem.* **89,** 5124–5130 (2017).

50. Ye, S., Li, X., Wang, M. & Tang, B. Fluorescence and SERS Imaging for the Simultaneous Absolute Quantification of Multiple miRNAs in Living Cells. *Anal. Chem.* **89,** 5124–5130 (2017).

51. Tipping, W. J., Lee, M., Serrels, A., Brunton, V. G. & Hulme, A. N. Stimulated Raman scattering microscopy: an emerging tool for drug discovery. *Chem. Soc. Rev.* **45,** (2016).

52. Butler, H. J. *et al.* Using Raman spectroscopy to characterize biological materials. *Nat. Protoc.* **11,** 664–687 (2016).

53. Turkevich, J., Stevenson, P. C. & Hiller, J. a Study of the Nucleation and Growth Processes I N the Synthesis of Colloidal Gold. *Discuss. Faraday Soc.* **11,** 55–75 (1951).

54. Lee, P. C. & Meisel, D. Adsorption and surface-enhanced Raman of dyes on

silver and gold sols. *J. Phys. Chem.* **86,** 3391–3395 (1982).

55. Bigall, N. C. *et al.* Monodisperse platinum nanospheres with adjustable diameters from 10 to 100 nm: Synthesis and distinct optical properties. *Nano Lett.* **8,** 4588–4592 (2008).

56. Qiao, R., Yang, C. & Gao, M. Superparamagnetic iron oxide nanoparticles: From preparations to in vivo MRI applications. *J. Mater. Chem.* **19,** 6274–6293 (2009).

57. Freestone, I., Meeks, N., Sax, M. & Higgitt, C. The Lycurgus Cup - A Roman Nanotechnology. *Gold Bull.* **40,** 270–277 (2007).

58. Rojanathanes, R. *et al.* Gold nanoparticle as an alternative tool for a urine pregnancy test. *Taiwan. J. Obstet. Gynecol.* **47,** 296–299 (2008).

59. Zhao, W., Brook, M. A. & Li, Y. Design of gold nanoparticle-based colorimetric biosensing assays. *ChemBioChem* **9,** 2363–2371 (2008).

60. Huang, X. & El-Sayed, M. A. Gold nanoparticles: Optical properties and implementations in cancer diagnosis and photothermal therapy. *J. Adv. Res.* **1,** 13–28 (2010).

61. Eustis, S. & el-Sayed, M. a. Why gold nanoparticles are more precious than pretty gold: noble metal surface plasmon resonance and its enhancement of the radiative and nonradiative properties of nanocrystals of different shapes. *Chem. Soc. Rev.* **35,** 209–217 (2006).

62. Faraday, M. The Bakerian Lecture: Experimental Relations of Gold (and Other Metals) to Light. *Philos. Trans. R. Soc. London* **147,** 145–181 (1857).

63. Frens, G. Controlled Nucleation for the Regulation of the Particle Size in Monodisperse Gold Suspensions. *Nat. Phys. Sci.* **241,** 20–22 (1973).

64. Perrault, S. D. & Chan, W. C. W. Synthesis and surface modification of highly monodispersed, spherical gold nanoparticles of 50-200 nm. *J. Am. Chem. Soc.*

131, 17042–17043 (2009).

65. Ahner, T. T. *et al.* Mechanism of gold nanoparticle formation in the classical citrate synthesis method derived from coupled in situ XANES and SAXS evaluation. *J. Am. Chem. Soc.* **132,** 1296–1301 (2010).

66. Mie, G. On the optics of turbid media, especially colloidal metal solutions. *Ann. Phys. Berlin* **25,** 377–445 (1908).

67. Ghosh, S. K. & Pal, T. Interparticle Coupling Effect on the Surface Plasmon Resonance of Gold Nanoparticles: From Theory to Applications. *Chem. Rev.* **107,** 4797–4862 (2007).

68. Orendorff, C. J., Sau, T. K. & Murphy, C. J. Shape-dependent plasmon-resonant gold nanoparticles. *Small* **2,** 636–639 (2006).

69. Mirkin, C. a, Letsinger, R. L., Mucic, R. C. & Storhoff, J. J. A DNA-based method for rationally assembling nanoparticles into macroscopic materials. *Nature* **382,** 607–609 (1996).

70. Ap, A. *et al.* Organization Of Nanocrystal Molecules Using Dna. *Nature* **382,** 609–611 (1996).

71. Graham, D., Thompson, D. G., Smith, W. E. & Faulds, K. Control of enhanced Raman scattering using a DNA-based assembly process of dye-coded nanoparticles. *Nat. Nanotechnol.* **3,** 548–551 (2008).

72. Graham, D. *et al.* Selective detection of deoxyribonucleic acid at ultralow concentrations by SERRS. *Anal. Chem.* **69,** 4703–4707 (1997).

73. Pan, W. *et al.* Multiplexed detection and imaging of intracellular mRNAs using a four-color nanoprobe. *Anal. Chem.* **85,** 10581–10588 (2013).

74. Seferos, D. S., Giljohann, D. A., Hill, H. D., Prigodich, A. E. & Mirkin, C. A. Nano-flares: Probes for transfection and mRNA detection in living cells. *J. Am. Chem. Soc.* **129,** 15477–15479 (2007).

75. Prigodich, A. E. *et al.* Nano-flares for mRNA regulation and Detection. **3,** 2147–2152 (2010).

76. Prigodich, A. E. *et al.* Multiplexed Nanoflares : mRNA Detection in Live Cells. 2062–2066 (2012).

77. Czarnek, M. & Bereta, J. SmartFlares fail to reflect their target transcripts levels. *Sci. Rep.* **7,** 1–10 (2017).

78. Alkilany, A. M. & Murphy, C. J. Toxicity and cellular uptake of gold nanoparticles: What we have learned so far? *J. Nanoparticle Res.* **12,** 2313–2333 (2010).

79. Chithrani, B. D., Ghazani, A. A. & Chan, W. C. W. Determining the Size and Shape Dependence of Gold Nanoparticle Uptake into Mammalian Cells. *Nano Lett.* **6,** 662–668 (2006).

80. Arnida, Malugin, A. & Ghandehari, H. Cellular uptake and toxicity of gold nanoparticles in prostate cancer cells: A comparative study of rods and spheres. *J. Appl. Toxicol.* **30,** 212–217 (2010).

81. Rosi, N. L. *et al.* Oligonucleotide-modified gold nanoparticles for infracellular gene regulation. *Science (80-.).* **312,** 1027–1030 (2006).

82. Schoof, E. *et al.* Dehydrogenase in Human Placenta of Patients with Preeclampsia. *J. Clin. Endocrinol. Metab.* **86,** 3–7 (2014).

83. Engeli, S. *et al.* Regulation of 11beta-HSD genes in human adipose tissue: influence of central obesity and weight loss. *Obes. Res.* **12,** 9–17 (2004).

84. Nitin, N., Santangelo, P. J., Kim, G., Nie, S. & Bao, G. Peptide-linked molecular beacons for efficient delivery and rapid mRNA detection in living cells. *Nucleic Acids Res.* **32,** e58 (2004).

85. Hadjidemetriou, M. & Kostarelos, K. Nanomedicine: Evolution of the nanoparticle corona. *Nat. Nanotechnol.* **12,** 288–290 (2017).

86.   Zhou, W., Li, Q., Liu, H., Yang, J. & Liu, D. Building Electromagnetic Hot Spots in Living Cells via Target-Triggered Nanoparticle Dimerization. *ACS Nano* **11,** 3532–3541 (2017).

87.   Guo, L., Xu, Y., Ferhan, A. R., Chen, G. & Kim, D. H. Oriented gold nanoparticle aggregation for colorimetric sensors with surprisingly high analytical figures of merit. *J. Am. Chem. Soc.* **135,** 12338–12345 (2013).

88.   Regnima, G.-O. *et al.* Quantitative measurements of turbid liquids via structured laser illumination planar imaging where absorption spectrophotometry fails. *Appl. Opt.* **56,** 3929 (2017).

89.   Haiss, W., Thanh, N. T. K., Aveyard, J. & Fernig, D. G. Determination of size and concentration of gold nanoparticles from UV-Vis spectra. *Anal. Chem.* **79,** 4215–4221 (2007).

90.   Kamińska, A. *et al.* Highly reproducible, stable and multiply regenerated surface-enhanced Raman scattering substrate for biomedical applications. *J. Mater. Chem.* **21,** 8662–8669 (2011).

91.   Babendure, J. R., Adams, S. R. & Tsien, R. Y. Aptamers Switch on Fluorescence of Triphenylmethane Dyes. **647,** 14716–14717 (2003).

92.   Harper, M. M., Dougan, J. a, Shand, N. C., Graham, D. & Faulds, K. Detection of SERS active labelled DNA based on surface affinity to silver nanoparticles. *Analyst* **137,** 2063–8 (2012).

93.   Caradec, J. *et al.* 'Desperate house genes': the dramatic example of hypoxia. *Br. J. Cancer* **102,** 1037–1043 (2010).

94.   Rumsby, M. *et al.* Human prostate cell lines from normal and tumourigenic epithelia differ in the pattern and control of choline lipid headgroups released into the medium on stimulation of protein kinase C. *Br. J. Cancer* **104,** 673–684 (2011).

95.   Tang, F., Ma, N., Tong, L., He, F. & Li, L. Control of metal-enhanced fluorescence with pH- and thermoresponsive hybrid microgels. *Langmuir* **28,** 883–888 (2012).

96.   Mosmann, T. Rapid colorimetric assay for cellular growth and survival: Application to proliferation and cytotoxicity assays. *J. Immunol. Methods* **65,** 55–63 (1983).

97.   Aula, S. *et al.* Biophysical, biopharmaceutical and toxicological significance of biomedical nanoparticles. *RSC Adv.* **5,** 47830–47859 (2015).

98.   Häkkinen, H. The gold-sulfur interface at the nanoscale. *Nat. Chem.* **4,** 443–455 (2012).

99.   Yamakoshi, H. *et al.* Imaging of EdU, an alkyne-tagged cell proliferation probe, by Raman microscopy. *J. Am. Chem. Soc.* **133,** 6102–6105 (2011).

100.   Yamakoshi, H. *et al.* Alkyne-tag Raman imaging for visualization of mobile small molecules in live cells. *J. Am. Chem. Soc.* **134,** 20681–20689 (2012).

101.   Zhang, J. *et al.* In situ, accurate, surface-enhanced Raman scattering detection of cancer cell nucleus with synchronous location by an alkyne-labeled biomolecular probe. *Anal. Bioanal. Chem.* **410,** 585–594 (2018).

102.   Tyagi, S. & Kramer, F. R. Molecular beacon probes that fluoresce on hybridiztion. *Nat. Publ. Gr.* **14,** 303–308 (1996).

103.   Jaworska, A. *et al.* SERS-based monitoring of the intracellular pH in endothelial cells: the influence of the extracellular environment and tumour necrosis factor-α. *Analyst* **0,** 1–9 (2014).

104.   Talley, C. E., Jusinski, L., Hollars, C. W., Lane, S. M. & Huser, T. Intracellular pH sensors based on surface-enhanced raman scattering. *Anal. Chem.* **76,** 7064–7068 (2004).

105.   Michota, a. & Bukowska, J. Surface-enhanced Raman scattering (SERS) of 4-

mercaptobenzoic acid on silver and gold substrates. *J. Raman Spectrosc.* **34,** 21–25 (2003).

106. Casey, J. R., Grinstein, S. & Orlowski, J. Sensors and regulators of intracellular pH. *Nat. Rev. Mol. Cell Biol.* **11,** 50–61 (2010).

107. Mandl, A., Filbrun, S. L. & Driskell, J. D. Asymmetrically Functionalized Antibody–Gold Nanoparticle Conjugates to Form Stable Antigen-Assembled Dimers. *Bioconjug. Chem.* **28,** 38–42 (2017).